Emission Characteristics of Projectile Fragments in ^{24}Mg-Em interactions at 4.5 AGeV

A THESIS

SUBMITTED TO GAUHATI UNIVERSITY FOR THE DEGREE OF DOCTOR OF PHILOSOPHY IN PHYSICS IN THE FACULTY OF SCIENCE

SUBMITTED BY
RUPALIM TALUKDAR

DEPARTMENT OF PHYSICS
GAUHATI UNIVERSITY, GUWAHATI-781014
ASSAM: (INDIA)

2012

To

My Parents

Dr. Buddhadeb Bhattacharjee
Associate Professor of Physics
Phone : +91-361-2670968
Fax : +91-361-2670968
e-mail: bb_22@rediffmail.com

Department of Physics
Gauhati University
Guwahati-781014
Assam, India

Certificate

This is to certify that Ms. Rupalim Talukdar; M.Sc. B.Ed, has completed her works on this thesis entitled, "Emission Characteristics of Projectile Fragments in ^{24}Mg-Em interaction at 4.5 AGeV", under my supervision and guidance. The work is worthy of consideration for the award of Ph.D. degree of the Gauhati University. Ms. Talukdar has fulfilled all the requirements prescribed under Ph. D. regulations of the Gauhati University. The thesis, she has submitted, is the result of her own investigations and to the best of my knowledge this work as a whole or part thereof has not been submitted to any other universities for any research degree.

B. Bhattacharjee
22/3/2012

(Buddhadeb Bhattacharjee)

Associate Professor
Department of Physics
Gauhati University

DECLARATION

I do hereby declare that the thesis entitled "Emission Characteristics of Projectile Fragments in ^{24}Mg-Em interaction at 4.5 AGeV", embodies my original work that have been carried out by me under the supervision of my research guide Dr. Buddhadeb Bhattacharjee, Associate Professor, Department of Physics, Gauhati University, Guwahati. I declare that I have not submitted this thesis as a whole or any part of the works described in this thesis for any higher degree of this University or any other Universities / Institutions.

Rupalim Talukdar

(Rupalim Talukdar)

Acknowledgement

Recalling the years of my research will always be momentous for me and words will always fall short to express my gratitude for what I received in those precious years of my life. It has certainly shaped me as a person in the world and a sincere learner in the area of my research. I would like to express my thanks and gratitude to all the wonderful people around me without whom the completion of this thesis would have been out of question.

First and foremost, I would like to offer my sincerest gratitude to my supervisor, Dr. Buddhadeb Bhattacharjee, Associate Professor, Department of Physics, Gauhati University, for inspiring me with all the hopes and motivating me to undertake the research. With his able guidance, help and knowledge, he always encouraged me to tackle the difficulties I came across during my research and I am highly indebted to him for being a patient guide all through.

It is difficult to overstate my sincere gratitude to Prof. Kalyanee Baruah, Ex-Head of the of the Department of Physics and Prof. N.Nimai Singh, present Head of the Department of Physics, Gauhati University, for providing the adequate facilities to carry out my research successfully.

I further acknowledge the suggestions and support bestowed upon me by all my teachers of the Department of Physics, Gauhati University.

I also acknowledge the financial support provided to me by the University Grants Commission, New Delhi, in the form of RFSMS (Research fellowship in Science for Meritorious Students) fellowship.

I would also like to thank the supporting staff of the Computer Science section at the Department of Physics, Gauhati University, for their kind help and cooperation.

I take this opportunity to extend my sincere thanks to Prof. B.K, Srivastava of Purdue University (EOS Collaboration), West Lafayette, Indiana, USA, for his several important suggestions.

I wish to express my indebtedness to my co-workers, especially Dr. S.Sengupta and Dr. B. Debnath, for their cooperation and support which helped me immensely towards to complete this work. I also take this opportunity to thank Mr. C. Thakuria for his untiring help and technical support.

I express my whole hearted thanks to all my research scholar friends for providing a stimulating and an enjoyable environment where I could learn and grow. I am especially grateful to Dr. J. Bhadra, Dr. H.Z. Devi, Dr. S. Hazarika, Ms. J. Sharma, Ms. V.Baisya and Mr. K. Dey.

I would also like to thank Mrs. Mukta Biswas, Warden, Gandhi Bhawan research scholar hall, Gauhati University, for helping me in various ways throughout, during the tenure of my stay in the hostel. I also express my thanks to all my friends in the research scholar hostel for providing me an academic and peaceful environment in the hostel.

I wish to thank my all time friends Momee, Mrinalini and Dorie for helping me get through the difficult times, and for all the emotional support, comraderie, entertainment and care they provided.

I would also like to acknowledge the care, affection and unconditional support extended to me by my sisters, brother and brothers-in-law. They have been my backbone in all the difficult phases of my life. The smiling faces and tantrums of my niece Dona and nephew Jianshu have always been refreshing for me.

I bow my head, express my heartfelt and warm gratitude to my father Sri Gajendra Nath Talukdar and mother Sri Arati Talukdar for their blessings, enthusiastic moral support, love and believing me at every step of my life. To them I dedicate this thesis.

Last but not the least, the present endeavor couldn't have gleamed on the canvas of reality without the blessings of Almighty.

However, if I miss to mention any name that should have been properly thanked, he or she should consider it as a human error and pardon me for the same.

Rupalim Talukdar

(Rupalim Talukdar)

PREFACE

Nuclear fragmentation is one of the most active lines of research in contemporary nuclear physics and has been extensively investigated in proton-nucleus and nucleus-nucleus collisions at intermediate and high energies. Recent progress in experimental studies has produced considerable evidences concerning its statistical properties. At intermediate energy nucleus-nucleus collisions offer various possibilities to produce hot nuclei which undergo break-up into smaller pieces having charges $Z_{PF} \geq 3$, resulting nuclear multifragmentation. The presence of a power law for the quantity of fragments, as a function of fragment size (mass or charge), produced in certain ranges of beam energies in these collisions and from observation of the values of the exponents of various charge moments close to ordinary fluid, coupled with strong similarity of the nuclear and Van-der-Walls potentials, has stimulated the emergence of the idea that multifragmentation of nuclei might be analogous to a continuous phase transition associated with a critical point, in the vicinity of which a disorderness or fluctuation of the fragments charged distribution takes place. The occurrences of fluctuations which are large near a critical point are believed to be the signatures of a phase transition at that point. One of the most important challenges of heavy ion physics is the identification and characterization of nuclear liquid-gas phase transition believed to be the underlying mechanism of nuclear multifragmentation process.

Since nuclear emulsion is a global 4π detector and has the best spatial resolution (about 0.1 m rad) among all the detectors currently in use in high energy physics, this technique has been found to be an important tool particularly to study those properties which are related to the spatial distribution of the particles emitted in the extreme forward angle. Intermittency in the PF emission spectra of high energy A+A collision is one such property. Until now, only a very few investigations have been carried out on the studies of intermittency and fractal structure of the emission spectra of fast and slow target associated particles emerging from the target spectator. No results have so far reported on the studies of fluctuation in the spatial distribution of PFs. In the present investigation an attempt has therefore been made to study the fluctuations in the emission spectra as well as in the charge distribution of projectile fragments in terms of Scaled Factorial Moments (SFM) and generalized moments. Study of non-thermal phase transition has also been done in the light of intermittency.

For heavy ion collision, it is known that with the decrease of impact parameter, i.e., with the increase of centrality of the collision, more energy-momentum transfer takes place resulting more excitation energy (temperature). In A+A collisions, as the impact parameter decreases, the overlapping between the projectile and target increases resulting more nucleon-nucleon collisions which in turn increases the number of particles emitted from the collision centre i.e. multiplicity of collision. Multiplicity is therefore considered to be a linear function of temperature of the fragmenting system. Hence critical multiplicity and critical temperature are considered to be synonymous, as considered by most of the heavy ion workers. One of the prime intensions of the present investigation is to find if there exists any evidence of critical temperature for the multifragmentation of a smaller system like ^{24}Mg and if it exists at all then, by comparing the results of the present investigation with the results as reported by other workers, how this critical temperature depends on the size of the fragmenting system.

An attempt has also been made to study the emission characteristics of various charged secondaries emitted from projectile spectator part in the light of multiplicity distribution and their correlations.

Chapter I contains a brief history on high energy heavy ion collision and accelerator facilities available across the world to carry out researches in the field of experimental high energy physics. To get an insight into the dynamics of heavy ion collisions, different models of high energy nucleus-nucleus collisions that can explain various important features of such high energy collisions are discussed in chapter I. The importance of studying the spectator parts of the colliding nuclei at intermediate energy and the significance of the present investigation are narrated in this chapter.

Chapter II contains details about the experimental techniques. In this chapter a brief idea of nuclear emulsion, its advantages, limitations and uses are discussed.

The details about the scanning procedure of emulsion pellicles, classification of the tracks of different charged secondaries based upon their ionization measurement, selection criteria for the type of events, techniques of measurement of charge and emission angle of the different PFs are also discussed in this chapter.

Chapter III contains results on multiplicity distribution and angular distribution of different charged secondaries emitted from the projectile spectator. The correlations between the various charge secondaries are also presented in this chapter. The results obtained from the present investigation are compared with the results of Kr-Emulsion interactions at 0.95 AGeV and also with the results reported by other workers at similar energies for different systems.

Chapter IV is on the estimation of Scaled Factorial Moments and intermittency of the emission spectra of projectile fragments. To estimate Scaled Factorial Moments (SFM), the method proposed by Bialas and Peschanski has been adopted and discussed. The power law behaviour of Scaled Factorial Moments, popularly known as intermittency, has been studied in terms of the intermittency indices and anomalous dimensions to have an insight into the dynamics of nuclear collision. Attempt has also been made to study the non-thermal phase transition by studying the power law singularity.

The concept of intermittency is intimately related to the physics of fractal geometry. Intermittency is said to be a signal of the fractal nature of the source which emits the particles. A fractal or a self similar object has the characteristic property of satisfying a power law scaling behaviour, which reflects the underlying dynamics. An attempt to study the fractal properties in the spatial and charge distribution of projectile fragments is also made in this chapter.

Chapter V contains the details of the application of cluster approximation technique for analyzing multifragmentation data to realize the possible association of criticality with such processes. Various higher order of moments have been estimated with various PFs following the technique suggested by Campi and different observables such as fluctuation in the size of the largest cluster, rise and fall nature of reduced variance γ_2 peaking behaviour in mean value of second moment of charge distribution have been estimated to locate the critical temperature. Finite size effect has been found to have considerable influence on MF mechanism. It was found that finite size effect and Coulomb force lead to a considerable reduction in the critical temperature and the critical temperature decreases with the decrease of system size. In this chapter therefore an attempt has been made to examine the influence of system size on the critical behaviour of nuclear matter by studying the fragmentation of a smaller system such as ^{24}Mg at 4.5 AGeV. The results obtained from the present investigation have been compared with the results of earlier works of Kr-Em interaction of GU group and EOS collaboration respectively.

In chapter VI, the summary of the findings of the present study and concluding remarks about some interesting aspects of this investigation are narrated.

Rupalim Talukdar

CONTENTS

CERTIFICATE....................i
DECLARATION....................ii
ACKNOWLEDGMENTS....................iii
PREFACE....................v
CONTENTS....................ix
LIST OF FIGURES....................xiv
LIST OF TABLES....................xvii

CHAPTER I: GENERAL INTRODUCTION

1.1 Introduction....................1
1.2 Phase transition and critical phenomena....................3
1.2.1 The phase diagram of water....................3
1.2.2 The phase diagram of nuclear matter....................4
1.3 Nuclear fragmentation at various energy regimes....................6
1.4 Review of experimental attempts for multifragmentation studies....................7
1.5 Multifragmentation and critical behaviour....................9
1.6 Signatures of critical behavior in finite nuclear system....................11
1.6.1 Cluster Approximation Technique....................11
1.6.2 Scaled Factorial Moment Estimation....................12
1.7 System size effect on nuclear multifragmentation:
Role of Surface and Coulomb force....................13
1.8 Some models of nuclear multifragmentation....................14
1.8.1 Statistical Multifragmentation Model (SMM)....................14
1.8.2 Fisher Droplet Model (FDM)....................17
1.8.3 Cascade Evaporation Model (CEM)....................22
1.9 Motivation of the present work....................24
References....................29

CHAPTER II: EXPERIMENTAL TECHNIQUES AND GENERAL CHARACTERISTICS

2.1 Introduction..37

2.2 Some features and composition of nuclear emulsion..............................38

2.2.1 Advantages of using nuclear emulsion as a detector............................39

2.2.2 Disadvantages of nuclear emulsion..40

2.3 The characteristics of the photographic process....................................41

2.3.1 Formation of latent image...41

2.3.2 Processing of nuclear emulsion...42

2.3.2.1 Development...42

2.3.2.2 Stop bath..43

2.3.2.3 Fixation..43

2.3.2.4 Washing and Drying..43

2.3.3 Calibration of stack..44

2.3.4 Shrinkage factors...44

2.3.5 Emulsion stack and their exposure..44

2.4 Microscope..45

2.4.1 Scanning Procedure..45

2.5 Principle of identification of charged particles using emulsion...............46

2.6 Classification of secondaries..48

2.6.1 The classification of charged secondaries..48

2.6.2 The classification of projectile fragments..49

2.6.3 Selection criteria for electromagnetic dissociation events....................50

2.6.4 Selection criteria for the type of events..50

2.6.5 Charge estimation of Projectile Fragments...51

2.7 Measurement Methods...52

2.7.1 Measurement of grain density...52

2.7.2 Measurement of dip angle..52

2.7.3 Measurement of Space angle...53

2.8 Photo Plate of Mg Events in Emulsion...54

References...55

CHAPTER III: GENERAL CHARACTERISTICS OF Mg - PROJECTILE FRAGMENTS: MULTIPLICITY AND ANGULAR DISTRIBUTION

3.1 Introduction........57

3.2 Results and Discussion........60

3.2.1 Multiplicity Distribution........60

3.2.1.1 Dependence of mean multiplicity on A_p........60

3.2.1.2 Multiplicity distribution of projectile fragments........62

3.2.1.3 Multiplicity distribution of $Z_{PF} = 1, 2$ and ≥ 3 projectile fragments........63

3.2.2 Multiplicity correlations........66

3.2.3 Influence of mass of the fragmenting system on projectile Multifragmentation........73

3.2.4 Spatial distribution of projectile fragments........75

3.2.4.1 Angular distribution of $Z_{PF} = 1$ projectile fragments........76

3.2.4.2 Angular distribution of $Z_{PF} = 2$ projectile fragments........76

3.2.4.3 Angular distribution of $Z_{PF} \geq 3$ projectile fragments........76

References........80

CHAPTER IV: INTERMITTENCY AND MULTIFRACTALITY IN THE FRAGMENTATION OF Mg - PROJECTILE NUCLEI

4.1 Introduction........83

4.2 Mathematical formalism for intermittency analysis........87

4.2.1 Horizontally scaled factorial moment........88

4.2.2 Vertical scaled factorial moments........89

4.3 Mathematical formalism for fractal and multifractal analysis........90

4.4 Non-thermal phase transition for spatial and size distribution of projectile fragments........94

4.5 Results and discussion........95

Part A: On the spatial distribution of PFs........95

4.5.1 Angular distribution of charged projectile fragments........95

4.5.2 Scaled Factorial Moment Analysis for spatial distribution of projectile fragments........97

4.5.2.1 Variation of ln $<F_q>$ with ln M........97

4.5.2.2 Variation of ϕ_q with q....98
4.5.2.3 Variation of anomalous dimension d_q with q....99
4.5.2.4 Variation of λ_q with q....101
4.5.3. Fractal Analysis in the spatial distribution of projectile fragments....102
4.5.3.1 Variation of $\ln\langle G_q\rangle$ with ln M....102
4.5.3.2 Variation of τ_q^{exp} with q....103
4.5.3.3 Deviation of exponents from q-1....103
4.5.3.4. Variation of D_q^{dyn} with q....104

Part B: On the charge distribution of PFs....106

4.5.4 The Fragments multiplicity distribution....106
4.5.5 Scaled Factorial Moment Analysis for fragments charge(mass) distribution....107
4.5.5.1 Variation of $\ln\langle F_q\rangle_c$ with $-\ln \delta s$....108
4.5.5.2 Variation of ϕ_q with q....109
4.5.5.3 Variation of anomalous dimension d_q with q....110
4.5.5.4 Variation λ_q with q....111
4.5.6. Fractal Analysis of the charge distribution of projectile fragments....112
4.5.6.1 Variation of $\ln\langle G_q\rangle$ with $-\ln \delta s$....112
4.5.6.2 Variation of τ_q (exp) with q....114
4.5.6.3 Deviation of mass exponents from q-1....114
4.5.6.4 Variation of D_q^{dyn} with q....115
References....118

CHAPTER V: SYSTEM SIZE EFFECT AND CRITICAL BEHAVIOR IN NUCLEAR MULTIFRAGMENTATION

5.1 Introduction....121
5.2 Mathematical formalism....123
5.3 Charge moments and Conditional moments....124
5.4 Results and discussion....125
5.4.1 Frequency distribution of charged projectile fragments....125

5.4.2 Size effects on fluctuation in Z_{max} 127
5.4.3 Fluctuation in γ_2 128
5.4.4 Fluctuation in M_2 132
References 135

CHAPTER VI: SUMMARY AND CONCLUDING REMARKS

Summary and Concluding Remarks 137

List of Publications 141

List of Figures

Fig. 1.1 The phase diagram of water.. 4

Fig. 1.2 The phase diagram for nuclear matter, as predicted theoretically..........................5

Fig. 1.3 Equation of state relating the pressure (left) or the temperature (right) and the density (normalised to critical values) in nuclear matter. The curves represent isotherms (left) and isobars (right). The dashed-dotted lines are the coexistence lines and the dotted lines the spinodal lines..........................10

Fig. 2.1 Photo Plate of Mg Events in Emulsion 54

Fig. 3.1 The mean multiplicity of PFs <Ni> as a function of the projectile mass number A_p in the interactions of various projectile with Em nuclei..................61

Fig. 3.2 Variation of normalized multiplicity of projectile fragments for Mg-Em interactions at 4.5 AGeV...62

Fig. 3.3 Normalized multiplicity of $Z_{PF}=1$ projectile fragments...............................64

Fig. 3.4 Normalized multiplicity of $Z_{PF}=2$ projectile fragments...............................65

Fig. 3.5 Normalized multiplicity of $Z_{PF}\geq 3$ Projectile fragments...............................65

Fig. 3.6(a) Variation of $<N_s>$ with Q_{pf} for Mg-Em interactions..............................67

Fig. 3.6(b) Variation of $<N_s>$ with Q_{pf} for Mg-Em and Kr-Em interactions....................68

Fig. 3.7(a) Variation of $<N_g>$ with Q_{pf} for Mg-Em interactions..............................69

Fig. 3.7(b) Variation of $<N_g>$ with Q_{pf} for Mg-Em and Kr-Em interactions....................69

Fig. 3.8(a) Variation of $<N_b>$ with Q_{pf} for Mg-Em interactions..............................70

Fig. 3.8(b) Variation of $<N_b>$ with Q_{pf} for Mg-Em and Kr-Em interactions....................71

Fig. 3.9(a) Variation of $<N_h>$ with Q_{pf} for Mg-Em interactions..............................72

Fig. 3.9(b) Variation of $<N_h>$ with Q_{pf} for Mg-Em and Kr-Em interactions....................72

Fig. 3.10(a) Variation of $<N_{IMF}>$ with Z_b for Mg-Em interactions..........................74

Fig. 3.10(b) Variation of $<N_{IMF}>$ with Z_b for the works of different groups...........74

Fig. 3.10(c) Variation of $<N_{IMF}>$ on Z_b normalized with the projectile charge Z_p..........75

Fig. 3.11 Angular distribution of $Z_{PF}=1$...78

Fig. 3.12 Angular distribution of $Z_{PF}=2$...78

Fig. 3.13 Angular distribution of $Z_{PF}\geq 3$...79

Fig. 4.1 Angular distribution of projectile fragments in $\eta(\cos\theta)$ space..........................96

Fig. 4.2 Frequency distribution of projectile fragments in $\chi(\eta)$ space..........................97

Fig 4.3 Variation of $\ln \langle F_q \rangle$ with ln M for the spatial distribution of various PFs for Mg-Emulsion interactions at 4.5 AGeV.....98

Fig 4.4 Variation of the exponent ϕ_q with the order of the moments q for Mg - Em interactions at 4.5 AGeV.....99

Fig 4.5 Variation of anomalous dimension d_q with q for Mg Emulsion interactions at 4.5 AGeV.....100

Fig 4.6 Variation of λq with the order of the moment q for Mg-Em interactions at 4.5 AGeV.....101

Fig 4.7 Variation of $\ln \langle G_q \rangle$ with ln M for experimental and random number generated events.....102

Fig 4.8 Variation of τ_q^{exp} with q for Mg-Em interactions at 4.5 AGeV.....103

Fig 4.9 Deviation of exponents from q-1.....104

Fig. 4.10 Variation of D_q^{dyn} with q for Mg-Em interactions at 4.5 AGeV.....105

Fig. 4.11 Multiplicity distribution of projectile fragments.....107

Fig. 4.12 Variation of of $\ln \langle F_q \rangle_c$ with $-\ln \delta s$ for charge distribution in the interactions of Mg nuclei with emulsion targets at 4.5 AGeV.....108

Fig. 4.13 Variation of ϕ_q with q in the charge distribution of projectile fragments for Mg-Em interactions at 4.5 AGeV.....110

Fig. 4.14 Variation of anomalous dimension d_q with q for Mg-Em interactions at 4.5 AGeV.....111

Fig. 4.15 Variation of λq with q for size distribution of projectile fragments for Mg-Em interactions at 4.5 AGeV.....112

Fig. 4.16 Variation of $\ln \langle G_q \rangle$ with $-\ln \delta s$ for fragments charge distribution in 4.5 AGeV Mg nuclei with emulsion target.....113

Fig. 4.17 Variation of τ_q (exp) with q for fragments charge distribution in 4.5 AGeV Mg nuclei with emulsion target.....114

Fig. 4.18 Deviation of mass exponents from q-1.....115

Fig. 4.19 Variation of D_q^{dyn} with q for fragments charge distribution in 4.5 AGeV Mg nuclei with emulsion target.....116

Fig. 5.1(a) Frequency distribution of various charged projectile fragments with $Z_{PF} \geq 1$ for Mg- Em interactions at 4.5 AGeV..126

Fig. 5.1(b) Frequency distribution in log-log scale upto Z_{PF} = 1- 6 for Mg and 1-13 for Kr-Em interactions..127

Fig. 5.2 Standard deviation of normalized Z_{max} as a function of multiplicity m for Mg-Em and Kr-Em interactions..128

Fig. 5.3(a) Variation of γ_2 with total charged fragment multiplicity m for Mg-Em and Kr-Em interactions..129

Fig. 5.3(b) Variation of γ_2 with total charged fragment multiplicity m for Mg-Em and Au, La and Kr on C..130

Fig. 5.3(c) Variation of γ_2 against m/ Z_{proj}..131

Fig. 5.4(a) Average of second charge moments as a function of multiplicity m for Mg-Em and Kr-Em interactions..133

Fig. 5.4(b) Average of second charge moments as a function of multiplicity m for Mg-Em, Kr-Em and Au-C..134

List of Tables

Table. 2.1 Composition of standard nuclear emulsion 39

Table. 3.1 The average multiplicities of the different charged projectile fragments in ^{22}Ne, ^{24}Mg and ^{28}Si beams with the interaction of emulsion at 3.7 AGeV and 4.5 AGeV 60

Table 3.2 Standard deviations of projected angular distributions of projectile fragments for different systems in emulsion 77

Table 4.1 Values of the slope parameters ϕ_q for the collisions of 4.5 AGeV Mg nuclei with emulsion targets 101

Table 4.2 Values of τ_q for spatial distribution of projectile fragments 106

Table 4.3 Values of the slope parameters ϕ_q for charge distribution of projectile fragments in Mg-Em interaction at 4.5 AGeV. 109

Table 4.4 Values of τ_q for charge distribution of projectile fragments......................117

Table 5.1 Variation of peak height and peak position in γ_2 gamma with the system size 131

CHAPTER I

GENERAL INTRODUCTION

1.1 Introduction

Heavy ion physics deals with the phenomena that occur when two nuclei are brought into close contact with each other such that the strong and short range nuclear force of one nucleus is felt by the other. The study of heavy-ion collisions as a branch of nuclear physics concerns the properties of nuclear matter under the extreme conditions of density, pressure and temperature [1]. Such collisions in the relativistic energy regime may be viewed as an abrasion process where, depending on the impact parameter, few to majority of the nucleons from the interacting projectile and target nuclei are stripped off. Such processes often lead to the formation of target- and projectile-like primary fragments (spectators) that may be considerably excited and of the so called participant zone composed of the overlapping nucleons (participants). While the properties of a highly compressed and excited nuclear system may be accessed by studying the participant zone, the highly excited, normal to low density regimes may be accessed in the projectile-(target-) like spectators depending on the violence of the collision. Indeed, the properties of the highly excited nuclear systems formed in such collisions may considerably differ from the properties of cold nuclei observed in the nature and especially quite new and exotic phenomena may occur if the nucleus gets substantially excited [1-2]. It is a tempting task to access these phenomena and to learn more about their characteristics with the experimental and theoretical tools presently available.

The studies of the interactions of high energy nucleus-nucleus collisions have become much easier with the availability of beams of heavy ions from accelerators. Initially such studies either depended on examining the interactions of cosmic ray nuclei, which were essentially limited by the flux considerations and inclusive in nature or attempted to analyze the fragments provided from stationary target nuclei bombarded by high energy hadrons. When the nucleus whose disruption is being studied is moving, then the fragments produced will also be moving and can be more readily identified than if they are emitted from a stationary nucleus [3]. The experiment to be described in this work examines the break-up of relativistic ^{24}Mg nuclei when they interact with various target nuclei in nuclear emulsion. Specific attention in this work is directed towards the multiply charged fragments of projectile nucleus.

Three classes of particles are observed in the interactions occurred in emulsion : fragments of the target nucleus, fragments of the projectile nucleus with $Z_{PF} \geq 2$ and fast singly charged particles, which includes particles produced in nucleon-nucleon interactions mostly π-mesons and $Z_{PF} = 1$. Although it is not possible to separate the produced particles and the singly charged fragments from the projectile, which both appear as forwardly directed tracks having unchanged minimum ionization for a considerable length. The singly charged fragments from the projectile will include both spectator and participant particles. As a result, this experiment is unable to study the singly charged fragments on a particle by particle basis, although the number of such particles can be derived from charge conservation considerations.

The multiply charged fragments of the projectile must emerge from the interactions with essentially the same energy per nucleon as the incoming projectile. These multiply charged fragments can be readily identified and their charges can be determined from various track parameters.

In relatively peripheral(gentle) collisions between nuclei, the majority of the projectile and target nucleons are not directly involved in the interaction, but is left in a highly excited state. This excited piece of nuclear matter then loses its energy by breaking up into a few or many fragments.

The total number of alpha particles, N_{α} and of fragments with $Z_{PF} \geq 3$, N_z can be determined for each emulsion event. The total number of multiply charged projectile fragments (N_{α} + N_z) is then an indication of the degree of projectile multifragmentation occurring in an interaction.

The relative yields and the spatial distribution of different types of fragments and the relationship between them are measures of processes that occur during the break up of these excited nuclear remnants. This investigation has been carried out to study these relationships for even a smaller system like ^{24}Mg at 4.5 AGeV and compared the results with those observed for other heavier systems like ^{84}Kr and ^{197}Au.

1.2 Phase transition and critical phenomena

1.2.1 The phase diagram of water

The knowledge about the state of matter can be understood and correlated via phase diagram of water. The phase diagram of water basically shows the state of water depending on the pressure and temperature as depicted in Fig. 1.1. As seen in the figure, water can exist in three forms consisting of ice, liquid, or steam. Interestingly, when water reaches it's boiling point, additional heating does not yield higher temperatures. Even liquid-gas phase coexists together. This transformation of one state of matter into another state is called a phase transition. Out of the two main types of phase transitions, the first order and the second order phase transition, the order of the transition of the above mentioned transformation of liquid state to gaseous falls on the first order category, where the density of the fluid has a jump at the liquid-gas phase transition (evaporation) and all the physical quantities characterizing the material undergo a sudden change. Generally, the two phases are quite different at first order transitions and thus it takes a finite amount of energy to convert the substance from one phase to the other. This is the latent heat. It is interesting to note that the density jump at the liquid-gas transition decreases at higher pressures and temperatures. The first-order line ends at the liquid-gas critical point. The approach to this point is a second-order phase transition. In its vicinity, the fluid cannot seem to "decide" what to become: a liquid or a gas. The fluid is sufficiently hot and compressed that the distinction between the liquid and gaseous phases is almost non-existent. Large density fluctuations emerge leading to a "milky" appearance of the fluid called the critical opalescence. It is important to note that one can smoothly go from a liquid to a gas by traveling "around" the critical point (Fig. 1.1). Continuous phase transitions are easier to study than first-order transitions due to the absence of latent heat, and they are been found to have many interesting properties. The phenomena associated with continuous phase transitions are called critical phenomena, due to their association with critical points.

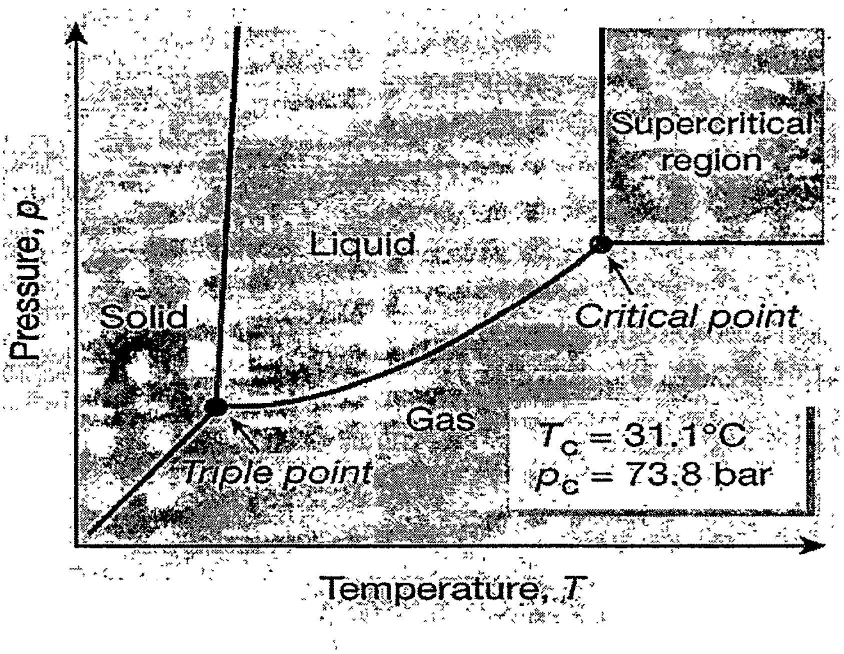

Fig. 1.1 The phase diagram of water

The importance of phase diagram lies in the fact that it can be used to predict the state of water at a given temperature and pressure. The mathematical relation inferred by this diagram is termed as "equation of state" for water.

1.2.2 The phase diagram of nuclear matter

In a similar fashion, the prediction of the equation of state for a nucleus is an important question. The phase diagram of nuclear matter (that has been predicted theoretically) is shown in Fig. 1.2 [4]. In their normal states of lowest energy, nuclei show liquid-like characteristics and have a density of 0.17 nucleons/fm3. In this low energy regime (i.e. $E/A \leq 20$ MeV/nucleon), basic interest is to look for the structure of nuclei. One can also study the phenomenon of fusion, fission [5-8], cluster-radioactivity [9-10] as well as halo nuclei [11-13]. When nucleus is heated to a temperature of a few MeV (1MeV = 1.2×10^{10} K), some of the nuclear liquid may evaporate. Just like water, it also has a latent heat of vaporization leading to a first order phase transition. This liquid-gas coexistence is expected to cease at a critical point.

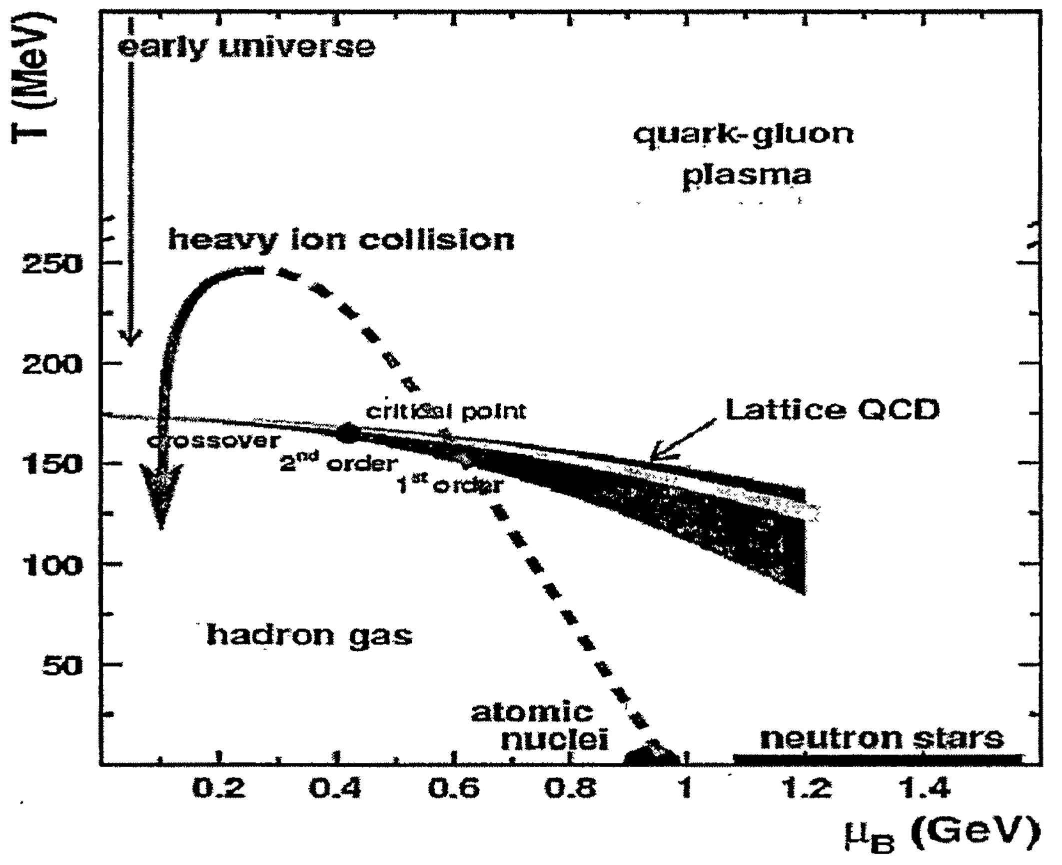

Fig. 1.2 The phase diagram for nuclear matter, as predicted theoretically.

The study of nuclear matter under the extreme conditions of temperature and density can be handled by a number of possible candidates such as finite nucleus, neutron star, supernova and heavy ion collisions at intermediate energies.

The best candidate that provides nuclear matter under the extreme conditions in a controlled fashion is the heavy-ion collision at intermediate energies (i.e. 20 MeV/nucleon $\leq$ E/A $\leq$ 2 GeV/nucleon) which will be discussed in later sections. Some of the observed phenomena in this energy domain are transverse flow, nuclear fragmentation and particle production etc. In recent years exploration of fragmentation in the intermediate energy has been carried out in an effort to understand the transition from the high energy fragmentation to the complex processes occurring in the low energy regime.

1.3 Nuclear fragmentation at various energy regimes

The bombarding energies used for heavy ion collisions have changed with technological advances. The processes which occur at the various energies differ tremendously. Low energy "fragmentation" was available for many years, and a large amount of data has been accumulated [14]. At low energies ($E/A \leq 20$ MeV/nucleon), several different reaction mechanisms contribute to the process. Reactions in these energy regimes are generally not considered "true" fragmentation and can not be described by Serber's [15] simple two–step process. The time of interaction is long, due to the slow relative velocity between the target and the projectile nuclei, and the Fermi momentum of the individual nucleon constituents of the target and the projectile is greater than the momentum of the nucleus itself. These factors can result in a combination of processes (dependent on the impact parameter of the collision) including Coulomb scattering, incomplete fusion, complete fusion and compound nucleus interaction. Reactions occurring at much higher energies ($E/A \geq 200$ MeV/nucleon) are considered to be "pure" fragmentation as was discussed by Serber. It should be noted that the energy limits are not exact since transitions between dominant processes occur gradually as a function of beam energy. In this situation the kinetic energy is of the order of magnitude of the rest mass of the constituent nucleons and the interaction time between the target and the projectile is very short. Central collisions will result in a "shattering" of the projectile into light particles and individual nucleons while distant interactions will undergo Coulomb scattering and excitation. Peripheral reactions will exhibit "pure" fragmentation in which the region of the projectile that overlaps the target during the interaction will be torn off. As accelerators improved over the past few decades, many high energy experiments using heavy nuclei were performed [16-17]. In recent years exploration of fragmentation in the intermediate energy regime (20 MeV/nucleon $\leq E/A \leq 2$ GeV/nucleon) has been carried out in an effort to understand the transition from the high energy fragmentation to the complex processes occurring in the low energy regime. The emission of intermediate mass fragments ($Z_{PF} \geq 2$) is an important probe of the dynamical evolution in intermediate energy regime heavy-ion collisions. At low energies (<20 MeV/nucleon) intermediate mass fragment (IMF) emission is a rare process while at high energies (> several AGeV) the reaction is so violant for central collisions that the system disassembles into nucleons, pions and light fragments like alpha (α) particles. In the transition region, multifragment emission, which is defined such that the final states involve two or more IMF's[18-19] has been experimentally observed [20-30]. This new phenomenon in the high excitation energies is called multifragmentation (multifragment break-up) and is presently under extensive experimental investigation. However the dominant mechanism of multifragment emission has not yet been unambiguously determined. On the other hand, the liquid-gas phase transition in nuclear matter has been predicted to occur at intermediate energy [31-32] and it may be related to multifragment emission. This intermediate energy regime has proven to be very interesting and challenging, to both the experimental procedures and theoretical models. Extensive experimental and theoretical efforts have been made during last 20 years to understand this mechanism. The factors affecting the multifragmentation and associated phenomena will be the main emphasis of the present work.

1.4 Review of experimental attempts for multifragmentation studies

Nuclear multifragmentation was discovered nearly seventy years ago [33-34] in cosmic rays studies as a puzzling phenomenon accompanying the collisions of relativistic protons with a target and consisted of the emission of slow nuclear fragments. Their masses were heavier than those of α particles, but lighter than those of fission fragments. As stated earlier in section 1.3, these are now known as intermediate mass fragments (IMF's). Using radiochemical methods, a total cross section for the fragmentation could not be determined and this process has been considered quite rare and exotic. In 1980's, the situation changed dramatically after Jakobsson et al. [35] observed multiple emissions of IMF's in emulsion irradiated by the carbon beam of 250 MeV/nucleon. In experiments involving large target nuclei and heavy ions, Warwick et al. [20] found that multifragmentation is a dominant reaction channel at beam energies higher than 35 MeV/nucleon. Observing that the mass yield curve approximately obeys a power law, Purdue group [36] conjectured that multifragmentation is a clear signature for the phase transition between a gaseous and liquid phase of nuclear matter. This transition is predicted to occur around a density of 0.4 ρ_0 ; ρ_0 is the normal nuclear matter density. Since then, the study of multifragmentation has been considered of such interest that special 4π detectors are designed to inspect this process in detail.

One of the earlier accelerators was the BEVALAC accelerator at the Lawrance Berkeley Laboratory that led way to high energy accelerators built at the Michigan State University (MSU)(USA). The EOS collaboration at BEVALAC lay emphasis in the exploration of phase transition in nuclear matter. Multifragmentation in fully reconstructed events from 1 GeV/nucleon ^{86}Kr, ^{139}La and ^{197}Au collisions with ^{12}C have been performed to extract the value of critical exponents [37-39]. Another major group INDRA at GANIL (Grand Accelerator National D'ions Lourds (GANIL) (France)), analyzed the influence of different parameters on multifragmentation. The main emphasis of their work is on entrance channel effects. The system size effects, role of system size in entrance channel as well as coulomb instabilities are studied in a variety of symmetric collisions like ^{36}Ar + ^{58}Ni, ^{129}Xe+^{nat}Sn and ^{155}Gd + ^{238}U (at 30-95 MeV/nucleon), ^{208}Pb + ^{197}Au at E=29 MeV/nucleon, ^{36}Ar+KCl (at 32-74 MeV/nucleon), ^{58}Ni+^{58}Ni (at 32-90 MeV/nucleon)[40-44]. Relativistic Heavy-Ion Collider (RHIC) and Superconducting Supercollider (SSC) at BNL (USA), NSF-Arizona accelerator at the University of Arizona (USA), Vivitron accelerator in Strasbourg (France), Superconducting cyclotron at Texas (USA), Superconducting cyclotron at INFN (Italy) and the Heavy-ion Synchrotron (SIS) accelerator at GSI (Germany) etc. are the major facilities where multifragmentation studies have been performed with different projectile at various energies. The two major groups at GSI i.e., FOPI and ALADIN have provided an important breakthrough on the experimental front to study the phenomena of multifragmentation. Incidently, the ALADIN group made the first measurements of the nuclear caloric curve [45]. They offered a wide coverage of masses between ^{12}C and ^{208}Pb with incident energy between 100 to 1000

MeV/nucleon [23, 46-62]. The ALADIN results are the most complete piece of data available for multifragmentation. In these collisions, energy depositions are reached which cover the range from the particle evaporation to multifragment emission and further to the total disassembly of the nuclear matter. These accelerators provide unique possibility to study the heavy-ion collisions in a laboratory under controlled fashion.

Apart from these, a large number of individual groups at different institutes have studied nuclear multifragmentation mechanism at relativistic energies using photo nuclear emulsion detector [39, 63-72]. All such studies have contributed significantly in understanding the multifragmentation mechanism of heavy nuclei at energies from 1 AGeV to 10 AGeV.

1.5 Multifragmentation and critical behaviour

As stated earlier, nuclear matter is an idealized macroscopic system with little excess of neutrons over the number of protons. The dominant mode of interaction is strong interaction; Coulomb interaction is relevant only for larger systems. Its density ρ_0 is spatially uniform. The nucleon-nucleon interaction is constituted by two components according to their radial inter-distance: a very short-range repulsive part which takes into account the compressibility of the medium and a long-range attractive part. Changed by five orders of magnitude the nuclear interaction is similar to Van der Waals forces acting in molecular medium. In a sense the phase transition in nuclear matter resembles the liquid–gas phase transition in classical fluids. However, as compared to classical fluids the main difference comes from the gas composition: for nuclear matter the gas phase is predicted to be composed not only of single nucleons, neutrons and protons, but also of complex particles and fragments depending on temperature conditions [73-74].

A set of isotherm for an equation of state (pressure versus density) corresponding to nuclear forces is shown in Fig. 1.3. It exhibits the maximum minimum structure typical of Van der Waals equation of state. Depending on the

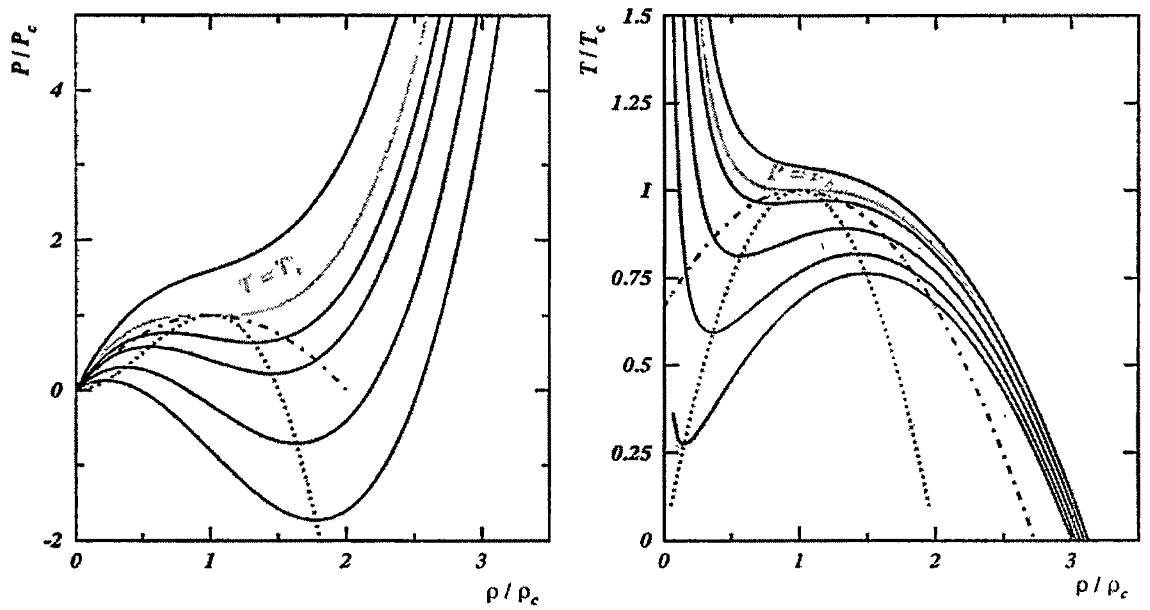

Fig. 1.3 Equation of state relating the pressure (left) or the temperature (right) and the density (normalised to critical values) in nuclear matter. The curves represent isotherms (left) and isobars (right). The dashed-dotted lines are the coexistence lines and the dotted lines the spinodal lines[75].

effective interaction chosen and on the model [76-78], the nuclear equation of state exhibits a critical point at $\rho_c \approx$ -0.3 - 0.4 ρ_0 and $T_c \approx$ 16 - 18 MeV. The region below the dotted line in Fig. 1.3 corresponds to a domain of negative compressibility: at constant temperature an increase of density is associated to a decrease of pressure. Therefore in this region a single homogeneous phase is unstable and the system breaks into a liquid phase and a gas phase in equilibrium. It is the so called spinodal region, and spinodal instability corresponds to the breaking into the two phases. Such instability has been proposed, for a long time, as a possible mechanism responsible for multifragmentation [79-81].

However to this point much uncertainty remains, regarding its nature, in particular whether multifragmentation is a phase transition and if so, whether it is associated with the liquid to vapour phase transition.

1.6 Signatures of critical behavior in finite nuclear system

One of the most important challenges of heavy ion physics is the identification and characterization of nuclear liquid-gas phase transition. As discussed earlier, a power law distribution of mass fragments is not enough to characterize the underlying physical process as a phase transition. The striking characteristics of the systems undergoing continuous phase transition that might have taken place in the final stage of fragmentation of heavy ion collisions is believed to be the occurrences of fluctuations of the fragments charge distribution, that exist on all length scales in a small range of the control parameter, which may diverse or even tend to vanish near some critical value of the control parameter.

Fluctuations are central to all critical phenomena and indeed, such fluctuation should be apparent in inclusive multifragmentation data. High statistics exclusive experiments in which the fragmenting system is characterized according to its nucleon number and excitation energy permit both the correlation of dynamical and statistical information and the study of fluctuation in experimental observables.

A number of techniques have been developed to realize fluctuation that might occur in certain experimental observables when the system is near to its critical point. Estimation of moments of cluster distribution as developed to study large percolation lattice and estimation of scaled factorial moments of fragments size are two well known techniques generally adopted in the study of fluctuation of nuclear data.

1.6.1 Cluster Approximation Technique

Campi [63-64] and Bauer et al. [65] showed that the methods of estimation of various moments of cluster size as used in percolation can be applied to analyze multifragmentation data to realize the possible association of criticality with such processes. Subsequently a large number of workers [39, 63-72] have applied the technique of cluster approximation in analyzing projectile fragmentation data for various systems at different energies. They proposed an event-by-event analysis of the moments of the cluster size distribution, where every event i produces a value $M_k^i(p)$ which is defined as,

$$M_k^i(p) = \sum_{A_f} (A_f)^k . n_i(A_f, p) \tag{1.1}$$

The advantage of this technique is that $M_k^i(p)$ can be computed without a prior knowledge of p for each event which is known as the percolation parameter. With this event-by-event technique it is possible to obtain valuable insight into the question whether phase transition occurs in nucleon-nucleus collisions and nucleus-nucleus collisions. In addition one should be able to make statements concerning the specific nature of the phase transition.

1.6.2 Scaled Factorial Moment Estimation

Many methods have been developed to analyze the fluctuations and the correlations for various physical quantities. In particular one of the most powerful and promising possibilities seems to be the analysis of event-by-event data in terms of intermittency which is a statistical concept initially developed to study turbulent flows [82-83]. Intermittency in physical systems is studied by examining the scaling properties of the moments of the distributions of relevant variables over a range of scales. To identify the intermittent pattern of fluctuations Bialas and Peschanski [82,84-86] first proposed the method of scaled factorial moments which has the advantage of measuring dynamical fluctuations in the density distributions of particles produced in high energy collisions without the spurious influence of statistical fluctuations. Satz and coworkers [87-88] studied the moments of the distribution of the size of spin clusters in the two-dimensional Ising model and found that intermittency occurs around and can be associated with the critical point of that system. These studies attest to the extent to which intermittency is cross-disciplinary in application. In particular, they point to the usefulness of the (factorial) moments as a method for studying fragmentation or decay mechanisms [89]. Later Płoszajčzak and Tucholski [90-93] first introduced the SFM analysis for the study of dynamical fluctuations in fragment size distributions following the break-up of high energy nuclei in the nuclear emulsion. They studied the break-up of

^{197}Au [94-95] nuclei at around 1 GeV/nucleon, and showed that the factorial moments of the charge distribution of the fragments increased like a power law with increasing charge resolution, thus exhibiting the property of self similarity or otherwise the intermittency and concluded that the study of intermittency in nuclear fragmentation is relevant in the search for critical phenomena [96]. A similar analysis, confirming the existence of intermittency in nuclear fragmentation, was later applied to the break-up of ^{238}U and ^{131}Xe nuclei with energy a few GeV/nucleon [71-72, 83, 97-98].

1.7 System size effect on nuclear multifragmentation: Role of Surface and Coulomb force

The effects of finite size [75-76, 99-105] and Coulomb force [106] on multifragmenation mechanism have been studied by several workers and it is found that these effects can lead to a sizeable reduction in the critical temperature of nuclear matter. Surface effects can reduce the temperature by 5-6 MeV while the Coulomb force is responsible for a further reduction of a few MeV. As the system size varies, the temperature (or otherwise the multiplicity) at which the critical singularity occurs also varies. This is believed to be due to the interplay of surface and Coulomb free energies [106] of the fragmenting system. Levit et al.[106] pointed out that nuclei becomes unstable at a much lower temperature $T' < T_c$ (or otherwise much lower multiplicity $m' < m_c$). This temperature was found to depend strongly on the charge to mass ratio of nuclei and on the choice of an effective interaction used in the H-F calculation. A qualitative explanation of the instability at T' was given based on the discussion of the balance between the Coulomb, the bulk and surface free energies of the compound nucleus. Since the surface tension decreases with temperature the Coulomb repulsion and the bulk inside pressure eventually prevail, giving rise to the instability. This is called Coulomb instability. The surface tension vanishes at T_c and therefore the instability temperature T' is below T_c. Different effective interactions in the H-F equations produce different bulk pressures and different dependences of the surface tension leading to different values of T'. For any nucleus the value of T' decreases significantly with larger A.

1.8 Some models of nuclear multifragmentation

The task of modeling multifragmentation from the initial collision phase of the reaction to freeze out has proven to be a daunting task. Models that adequately describe the initial stage of the reaction do not satisfactorily describe the fragment formation stage, in either statistical or dynamical aspects.

Competing models suggest different decay mechanisms and experiments have yet to discriminate between several theoretical scenarios [107-108] that ranged from the sequential decay of the compound nucleus [109-110] to statistical nuclear models [19,111-112], percolation models [32,63,113-117] and Ising models [118-123]. The liquid-gas phase transition in nuclear matter has well been described using cluster approximation technique by a phenomenological model [31,124] what is known as Fisher droplet model and will be described in details in Sec. 1.8.2 to establish the relationship between the various parameters of equation of state and the observables of multifragmentation experiments. Many of these models assume equilibrium thermodynamics and produce results often interpreted as evidence of a phase transition.

In the following sections, some of the models widely used to describe nuclear multifragmentation are briefly discussed.

1.8.1 Statistical Multifragmentation Model (SMM)

There are several statistical models that have been used to study multifragmentation [19, 109,112, 125-133] but the most widely used is the statistical multifragmentation model put forwarded by J. Bondorf et al. [112,125,127].

SMM is a statistical description of the simultaneous breakup of an expanded excited nucleus into nucleons and hot fragments [112,125,127,134]. The statistical multifragmentation model is based on the assumption of statistical equilibrium at a low-density freeze out stage of the nuclear system formed during the collision. At this stage, primary fragments are formed according to their equilibrium partitions. Equilibrium partitions are calculated according to the microcanonical ensemble of all breakup channels composed of nucleons and excited fragments of different masses. The model conserves total excitation energy, momentum, mass, and charge numbers. The statistical weight of decay channel j is given by $W_j \propto \exp[S_j(E_o, V, A_o, Z_o)]$, S_j is the entropy of the system in channel j and E_o, V, A_o and Z_o are the excitation energy, volume, mass, and charge numbers of the fragmenting source. Different breakup configurations are initialized according to their statistical weights. The fragments are then propagated in their mutual Coulomb field and allowed to undergo secondary decay [135]. In the model, successive particle emission from hot fragments with A > 16 is assumed the de-excitation mechanism. The de-excitation of these fragments is treated by means of the standard Weisskopf evaporation model. Light fragments (A < 16) de-excite via Fermi breakup. The lightest particles (A < 4) can be formed only in their ground states and undergo no secondary decay [136].

If the free energy F_f of a partition f is known, the entropy and the energy may be calculated using the conventional thermodynamical formulae. The free energy $F_f(T, V)$ of the system consisting of fragments of different kinds and being in thermal equilibrium with a common temperature, T may be conveniently expressed as [125]:

$$F_f = -T \ln Z_f \tag{1.2}$$

where the statistical sum for a given partition f is written as:

$$Z_f(T,V) = \sum_{\{r,p,\varepsilon\}} \exp(-E_F / T) . \tag{1.3}$$

The sum runs over all the coordinates, momenta and excitation energies of the fragments forming the partition f. Here E_F is the total energy of the configuration F in the quasiclassical approximation and given by

$$E_F = \sum_{i=1}^{M} \left(E_i^{gs} + \frac{p_i^2}{2m_i} + \frac{s_i^2}{2I_i} + \varepsilon_i \right) + U_F , \tag{1.4}$$

Here, M is the total number of fragments including nucleons. The terms in round brackets stand respectively for the ground state energy, translational, rotational and internal excitation energies of the i^th fragment. p_i, s_i are momenta and angular momenta and m_i is the effective mass of the i^th fragment with respect to translational motion. The last term is the fragment interaction energy. After calculating the statistical sum the free energy of the system may be written in the form:

$$F_f(T,V) = F_f^{tr}(T,V) + \sum_{A,Z} F_{AZ}(T,V)N_{AZ} + E_0^C(V). \qquad (1.5)$$

The first term corresponds to the translational motion of fragments. The second term contains the contributions from internal excitation energy and Coulomb energy of individual fragments. This additive representation becomes possible in the Wigner-Seitz approximation after subtracting the Coulomb energy of a total charge homogeneously distributed over the whole volume V (the last term in Eq. (1.5)).

The direct calculation of F_{AZ} for composite nuclear fragments in a hot nuclear medium is a very complicated task. They assume that all the fragments except the lightest one may be treated as drops of nuclear matter. Unlike nuclei in their ground states, these drops have nonzero temperature and are surrounded by nucleons and other clusters. It was also assumed that these drops have a spherical shape with radius $R_{AZ} = r_0 A^{1/3}$ corresponding to the normal nuclear density (r_0 = 1.2 fm).

The free energy F_{AZ} of an individual fragment of (A, Z) kind, ($Z_{PF} \geq 3$) is parameterized as follows:

$$F_{AZ} = F_{trans} + F_{vol} + F_{surf} + F_{sym} + F_{coul} \qquad (1.6)$$

The terms in the right hand side are, respectively, the translational, volume, surface, symmetry and Coulomb contributions. This free energy is used to determine the fragment formation probability.

This solution explicitly assumes the inhomogeneous nature of the hot MF final state. Light fragments $Z_{PF} < 3$ may also be present in the hot MF final state. For the $Z_{PF} \geq 3$ fragments, a quantum mechanical description is used for the temperature dependent volume, surface, and translational free energy of the fragments. The temperature independent parameters are based on the coefficients of the semi empirical mass formula. The critical temperature, at which the surface tension of neutral nuclear matter droplets would go to zero, is in the range suggested by infinite neutral nuclear matter calculations [137].

In SMM the translational free energy depends on the free volume. The free volume, V_f, can be expressed in terms of the volume of the multifragmenting system at normal nuclear density, V_{rem},

$$V_f = \chi V_{rem}, \tag{1.7}$$

where the free volume parameter χ depends on the SMM fragment multiplicity according to the relation

$$\chi = \left[1 + \frac{d}{R_0}(M^{1/3} - 1)\right]^3 - 1, \tag{1.8}$$

where $R_o = 1.17A_o^{1/3}$ fm and M is the charged plus neutral hot fragment multiplicity. The crack width parameter, *d*, scales the magnitude of the multiplicity dependent free volume. The breakup volume V_b, which includes the volume of the fragments, is $V_b = (1 + \kappa)V_{rem}$, where κ is the Coulomb reduction parameter.

Here the version of the model that incorporates only thermal degrees of freedom is given. Consequently, radial expansion or angular momentum is not included here.

1.8.2 Fisher Droplet Model (FDM)

The focal point of most of the phase transitions studies is to find out standard thermodynamical variables such as a system's temperature, density, compressibility, etc. But in present day nuclear multifragmentation (MF) experiment; these quantities are difficult or impossible to measure directly. Therefore a theory is considered necessary which deal with the accessible quantities of MF experiments. To that end Fisher's gas-to-liquid phase transition model that is called Fisher droplet model, based on Mayer's condensation theory, is followed [31, 138-139]. According to FDM, the free energy for the formation of clusters of size A_f can be given by:

$$\Delta G_{A_f} = -k_b T A_f \ln[g(\mu,T)] - k_b T \ln[f(A_f,T)] + k_b T \tau \ln(A_f) + \cdots \qquad (1.9)$$

where k_b is the Boltzmann constant and g is the bulk formation energy, or volume and can be written as

$$g(\mu,T) = \exp[(\mu - \mu_{coex}) / k_b T], \qquad (1.10)$$

here μ is the chemical potential and μ_{coex} is the chemical potential along the coexistence curve.

The surface free energy of cluster formation is represented by the f term where

$$f(A_f,T) = \exp[a_0 \omega A_f^{\sigma} \varepsilon T_c / k_b T] \qquad (1.11)$$

In the above equation,

$\sigma \rightarrow$ is a critical exponent and is related to the ratio of the dimensionality of the surface to the dimensionality of the volume

$a_0 \rightarrow$ is a constant of proportionality relating the average surface area of a droplet to its number of constituents and

$\omega \rightarrow$ is the surface entropy density

$\varepsilon \rightarrow$ is a measure of the distance from the critical point.

Generally for usual thermodynamic systems $\varepsilon = (T_c - T)/T_c$, in the percolation treatment $\varepsilon = (p_l - p_c)/p_c$ and for multifragmentation $\varepsilon = (m_c - m)/m_c$ is to be used. All formulations of ε are such that $\varepsilon > 0$ corresponds to the liquid region whereas $\varepsilon < 0$ is for gas region. This form of the surface free energy is applicable on only one side of the critical point, the single phase side. A more general form suggested by efforts from percolation theory [113, 140-142] that can be applied on both sides of the critical point and leads to a power law that describes the behavior of the order parameter is:

$$f(z) = A \exp[-(z - B)^2 / C], \qquad (1.12)$$

where the scaling variable z is

$$z = A_f^{\sigma}\varepsilon \tag{1.13}$$

The physical interpretation of the parameters A, B, and C is an open question.

Finally τ is another critical exponent depending principally on the dimensionality of the system and has its origins in considerations of a three dimensional random walk of a surface closing on itself, thus for three dimensions $2 \leq \tau \leq 3$ [70].

From the free energy of cluster formation the average cluster distribution normalized to the size of the system is

$$n_{A_f}(\varepsilon) = \exp(-\Delta G_{A_f} / k_b T) = q_0 A_f^{-\tau} f(z) g(\mu, T)^{A_f} \tag{1.14}$$

q_0 is normalization constant and dependent solely on the value of τ [143].

At the critical point $\varepsilon = 0$ both f and g are unity and the cluster distribution is given by a pure power law

$$n_{A_f}(\varepsilon) = q_0 A_f^{-\tau} \tag{1.15}$$

If the first moment of the normalized cluster distribution is considered at the critical point then [114]

$$M_1(\varepsilon = 0) = \sum_{A_f} n_{A_f}(\varepsilon) A_f = q_0 \sum_{A_f} A_f^{1-\tau} = 1.0 \tag{1.16}$$

where the sum runs over all clusters. From Eq. (1.16) it is obvious that the value of the overall cluster distribution normalization constant, q_0, is dependent on τ via a Riemann ζ function

$$q_0 = 1.0 / \sum_{A_f} A_f^{1-\tau} \tag{1.17}$$

The above is true only if the scaling assumptions in the FDM apply to all clusters. For finite size systems even at the critical point this is only approximately true. However, it will be seen that Eq. (1.17) holds reasonably well at the critical point for systems with a continuous phase transition over some range in cluster size.

In the FDM it is assumed that all clusters of size A_f can be treated as an ideal gas, so that the total pressure of the entire cluster distribution can be determined by summing all of the partial pressures.

$$P/(k_bT) = \sum_{A_f} n_{A_f}(\varepsilon) = q_0 \sum_{A_f} A_f^{-\tau} f(z) g(\mu,T)^{A_f}$$

$$= M_0(\varepsilon). \qquad (1.18)$$

It is clear from Eq. (1.18) that the pressure of the system is related to the zeroth moment of the cluster distribution.

The density is then

$$\rho = \frac{\delta P}{\delta\mu} = q_0 \sum_{A_f} A_f^{1-\tau} f(z) g(\mu,T)^{A_f}$$

$$= \sum_{A_f} n_{A_f}(\varepsilon) A_f = M_1(\varepsilon) \qquad (1.19)$$

The density is given by the first moment of the cluster distribution.

It is now a simple matter to derive the power law that describes the divergence of the isothermal compressibility κ_T. By definition:

$$\kappa_T = -\frac{1}{V}\left(\frac{\delta V}{\delta P}\right)_T = \frac{1}{\rho}\left(\frac{\delta\rho}{\delta P}\right)_T \qquad (1.20)$$

Noting that $k_bT\rho = g(\mu, T)[\delta P/\delta g(\mu, T)]$, Eq. (1.20) can be rewritten as:

$$\kappa_T = \frac{-1}{\rho^2}\left(g(\mu,T)\frac{\delta P}{\delta g(\mu,T)} + g(\mu,T)^2 \frac{\delta^2 P}{\delta g(\mu,T)^2}\right)_T \qquad (1.21)$$

that leads to

$$\kappa_T = (\rho k_b T)^{-1} + (\rho^2 k_b T)^{-1} \sum_{A_f} n_{A_f}(\varepsilon) A_f^2$$

$$= (\rho k_b T)^{-1} + (\rho^2 k_b T)^{-1} M_2(\varepsilon) \tag{1.22}$$

The sum in the second term illustrates the relation of the second moment of the cluster distribution $M_2(\varepsilon)$ to the isothermal compressibility. The sums in Eqs. (1.18), (1.19) and (1.22) run over all clusters in the gas and exclude the bulk liquid drop. In percolation and multifragmentation the largest cluster on the liquid side of the critical point will be considered as the liquid drop and will thus be excluded from the sum. On the gas side of the critical point, the sum runs over all clusters, as there is no longer a liquid drop.

In the thermodynamic limit, large A_f dominate the sum so that it may be treated as an integral giving:

$$\kappa_T = (\rho k_b T)^{-1} + (\rho^2 k_b T)^{-1} \int_0^\infty n_{A_f}(\varepsilon) A_f^2 dA_f \,. \tag{1.23}$$

Working along the liquid-gas coexistence curve so that $g(\mu, T) = 1$ Eq. (1.23) reduces to:

$$\kappa_T = (\rho k_b T)^{-1} + (\rho^2 k_b T)^{-1} \int_0^\infty A_f^{2-\tau} f(z) dA_f \tag{1.24}$$

A change of variables from A_f to z shows that near the critical point

$$\kappa_T \sim (\rho^2 k_b T)^{-1} \left| \frac{q_0}{\sigma} \int_0^{\pm\infty} dz f(z) |z|^{(3-\tau-\sigma)/\sigma} \right| |\varepsilon|^{(\tau-3)/\sigma}$$

$$= (\rho^2 k_b T)^{-1} \Gamma_\pm |\varepsilon|^{-\gamma} \tag{1.25}$$

This is the so-called γ-power law that describes the divergence of the isothermal compressibility and the second moment of the cluster distribution near the critical point. The scaling relation between the exponents γ, σ and τ is:

$$\gamma = \frac{3-\tau}{\sigma} \tag{1.26}$$

The absolute normalization constants of the $M_2(\varepsilon)$ power law depend on the scaling function f(z) the exponent σ and the overall normalization of the cluster distribution q_o which in turn depends on the exponent τ

$$\Gamma_{\pm} = \left| \frac{q_0}{\sigma} \int_0^{\pm\infty} dz f(z) |z|^{(3-\tau-\sigma)/\sigma} \right|. \tag{1.27}$$

The second moment is related to the isothermal compressibility by the temperature and density of the system.

The derivation of the γ-power law demonstrates one way to arrive at the scaling relations between the critical exponents. In addition it illustrates the existence of only two independent exponents and shows the relation of the moments of the cluster distribution to familiar thermodynamic quantities.

1.8.3 Cascade Evaporation Model (CEM)

The first such model has originally developed by Chen et al., [144] for nucleon-nucleus collisions and later generalized to high-energy heavy ion interactions [145-151].

In cascade evaporation model [152] each of the colliding nuclei in its coordinate system is considered as a Fermi gas of nucleons in a Wood-Saxon potential well, V(r) that may be written as:

$$V(r) = B + (P_F^2/2m) \tag{1.28}$$

where m is the mass of free nucleon, B is the average binding energy of a nucleon inside the nucleus and P_F is the local Fermi momentum. The momentum distribution inside the nucleus may approximately be given by the relation:

$W(P)dP \sim P^2dP$ with $0 \leq P \leq P_F(r)$, that is isotropic in the momentum space. The maximum value of local Fermi momentum $P_F(r)$ may be expressed in terms of nuclear density $\rho(r)$ as:

$$P_F(r) = h[3\pi^2 \rho(r)]^{1/3} \tag{1.29}$$

This is an approximation of two-parameter Fermi distribution; values of these parameters can be found from the electron elastic scattering experiments. Practically, this distribution is cut off at a distance R where $\rho(R)/\rho(0) = 0.01$.

The form of nuclear density is an oscillatory one for nuclei having mass number $A \leq 16$ and a Wood-Saxon one for $A > 16$. The distance between any two of the nucleons inside a nucleus is taken to be not less than $2r_c$ (~ 0.4 fm) where, r_c is the radius of the nucleon core.

It was assumed that a nucleon of the incident nucleus in the laboratory frame can be considered as independent particle and characterized by a four vector, space-time (**r**, t) and four vector momentum-energy (**p**, E) having an effective mass 'm_{eff}' as:

$$
\begin{aligned}
m_{eff} &= \sqrt{(E^2 - \mathbf{p}^2)} \\
&= m - V(r) \qquad (1.30)
\end{aligned}
$$

This consideration is also applicable for the nucleons of the target nucleus in the coordinate system connected with the projectile. The effect of the nuclear potential on a particle entering the nucleus may be increasing the particle kinetic energy by the quantity, V(r).

The approximation of independent particle with effective mass allows one to use the relativistic kinematics, taking into consideration in particular the effect of relativistic compression and the symmetry, of the problem with respect to the colliding nuclei. In this model, the collision is assumed to be made up of a superposition of individual binary collisions.

The dynamics of the interaction are followed in time by using Monte-Carlo method with the probability of scattering on another particle given by free particle cross-section. The incident particle can interact with any target nucleon lying in the path with a cylindrical cut of cross-section area $\pi(r_{int} + \lambda_D)^2$, where λ_D is the de-broglie wavelength and r_{int} is nothing but the quantity which is nearly double the value of the strong interactions range and taken to be 1.3 fm [153].

Thus the probability of scattering of n^{th} nucleon after traversing without any interaction with (n^{th} - 1) nucleons is given by the binomial distribution

$$W_n = \sum_{i=1}^{n-1}(1-q_i)q_n \tag{1.31}$$

where q_i, i = 1, 2, 3....(n - 1) is the partial probability. This partial probability may be expressed in the terms of interaction cross-section for the i^{th} nucleon, σ_i as

$$q_i = [\, \sigma_i/(r_{int}+\lambda_D)^2] \tag{1.32}$$

Tracing the time evolution of the interacting system, at a fixed time t, all possible collisions are considered and the one which is realized before the others is chosen, i.e. D_t = min (t_i). Thus for two particle collisions chosen in this way, the reaction characteristics are selected at random, demanding that the Pauli principle holds.

The cascading stage ends when the colliding projectile and target nuclei are separated at such a distance where the potential wells of these nuclei do not overlap further and all cascading particles are emitted from nuclei. In this model, the Coulomb force acting between the projectile and the target is taken into account. Effectively this corresponds to an increase in the impact parameter and a rotation of all the coordinate system by a particular angle [154].

1.9 Motivation of the present work

In the complex scheme of high energy nucleus-nucleus collision, the overlapping parts of the two colliding nuclei are considered as participants, which disintegrate totally, producing various particles, with velocity ranging from zero to the projectile velocity, while the non interacting parts of the projectile and target are called spectators. It is expected that a quark-gluon-plasma (quark matter)[155] may be formed in the participant at very high incident energies, and a liquid-gas phase transition [156] might occur in the spectators. Both the participant and spectator are relevant for studying the nuclear reaction mechanism.

The Dubna energy (a few A GeV) is a special energy, at which the nuclear limiting fragmentation applies initially. The constituents of the spectator part of the projectile as well as the spectator part of the target can be well separated at this energy. But the experimental work on high energy A-A collisions carried out with electronic detector have limited coverage in the pseudorapidity range. Nuclear emulsion, on the other hand, is a global 4π detector and has the best spatial resolution (0.1mrad) among all the detectors currently in use in experimental high energy physics [157-158]. Even the largest collaborative detector [50, 159-163] that has been formed to study various characteristics of projectile fragments is found to have limitation over the angular acceptance. Because of this advantage nuclear emulsion has been found to be a useful tool to study those properties which are related to the spatial distribution of emitted particles.

The properties of high energy nucleus-nucleus collision vary significantly with collision geometry as the energy and momentum transferred in such collision is different for different impact parameters. More central collisions involve more number of nucleons of both projectile and target nuclei participating in the collision resulting in large transfer of energy and momentum from projectile to target nucleus. Considering the total charge of the projectile spectator fragments Q_{pf} as a measure of the degree of centrality of the collision [107,164-166], in the present investigation an attempt has been made to find the correlation between Q_{pf} and other multiplicity parameters of charged secondaries such as N_s, N_h etc. that are generally taken as a measure of collision geometry. It is expected that such studies may throw some light on the effect of collision geometry on the multiplicities of secondary charged particles emitted from ^{24}Mg-Em interactions at 4.5 AGeV.

In projectile fragmentation process, a projectile spectator, on excitation, often splits into several pieces of intermediate mass fragments (IMFs) which span the mass-range between alpha particle and fission fragments. It is believed that studies on the decay of such excited nuclear system may provide information of the nuclear collision dynamics. The sum of all projectile fragments (PFs) with charge $Z_{PF} \geq 2$, which is also known as bound charge Z_b, is related to the size of the excited projectile spectator and gives the measure of the mass of the fragmenting system

[45, 167]. Therefore it should reflect the centrality of the collision and can be used as a measure of the impact parameter. Larger Z_b values correspond to larger impact parameters and to more peripheral collisions. For a given collision system, the size of the projectile spectator remnant should be independent of the beam energy [3,167]. Different projectile energies lead to different excitations of the spectator remnant, and thus, influence its decay, but not the size. It also gives an idea about the energy-momentum transferred to the participant part of the colliding nuclei [3,23,46,50,167-168]. Correlation between mean number of intermediate mass fragments (IMFs) and the mass of the fragmenting system is one of the most interesting aspects of studying projectile fragmentation which is studied by different workers for various systems at different energies. To have more insight into the role of centrality of collisions, in this work an attempt has therefore made to study the correlation between $<N_{IMF}>$ and mass of the fragmenting system, Z_b

Białas and Peschanski [82,84-86], introduced the technique of scaled factorial moments (SFM), in analyzing heavy ion collision data to extract the dynamical fluctuations in the density distributions of particles produced in high energy collisions. An increase in the value of SFM with the decrease of width of the phase space bin, implies the power law behaviour indicating self-similarity of the emission spectrum, which is often termed as intermittency.

The concept of intermittency is in turn intimately connected to the fractal geometry of the object under investigation and hence the dynamics of the underlying physical process [169]. Fractal geometry allows us to mathematically describe systems that are intrinsically irregular at all scales. A fractal structure has the property that, if one magnifies a small portion of it, it still shows the same complexity as the entire system. Usually the term fractal is used to characterize systems with properties of self-similarity in general. If these properties can be described by a single exponent, one has a simple or homogeneous fractal, a monofractal. In a more complex case, the term multi-fractality is used when discussing generalized scaling.

To understand the underlying physics of hadronization in QGP type phase transition, several works have been carried out to study the dynamical fluctuation of the produced particle [170-172]. However, only a very few investigations have been carried out on the studies of intermittency and fractal structure of the emission spectra of fast and slow target associated particles emerging from the target spectator [173-175]. No such studies have been so far reported on the studies of fluctuation in the spatial distribution of PFs. Projectile fragments have the momentum per nucleon almost equal to that of the parent nucleus, so they are essentially emitted inside a narrow forward angle around the direction of the beam and remain relativistic. Hence unlike the target fragments the heavy fragments of the projectile nucleus are very closely spaced having a very small angular separation. It has therefore always been a challenging task to study those properties of the projectile fragments that are related to the spatial distribution of the fragments. In the present investigation an attempt has been made to study the fluctuations in the spatial as well as in the size distribution of the projectile fragments in terms of Scaled Factorial Moments (SFM) and generalized moments. The results of SFM analysis have been extended further to study the non-thermal phase transition in nuclear fragmentation.

The occurrence of a first order phase transition in nuclear matter has been the subject of numerous investigations that study the transition from the liquid like phase of ordinary nuclear matter to a gaseous phase where the average interparticle distance is much larger than the range of interparticle interaction. Associated with such a phase transition is a critical temperature above which only the gaseous phase can exist. This critical temperature is very interesting in view of experimental results from relativistic to ultra relativistic heavy ion reactions. In a finite system like a nucleus the contribution of Coulomb and surface energy not only lowers the critical point but might even change the order of the phase transition [69-70,75-76]. In the multifragmentation of finite nuclei which one of these plays the dominant role is not clearly understood yet. A dominant surface energy contribution might make the liquid gas phase transition a first order type while the dominant Coulomb energy contribution might make the phase transition a 2nd order type.

In the present investigation an attempt has also been made to realize the effect of finite size on the multifragmentation mechanism by studying the 'rise and fall' pattern of a few traditionally accepted signatures of critical behavior.

References

1. H. F. Liu et al., *Phys. Rev.* **C 75** (2007) 054613.
2. Y. G . Ma et al., *Phys. Rev.* **C 71** (2005) 054606
3. M. L. Cherry et al., *Phys. Rev.* **C 52** (1995) 2652
4. Accelerator and Fusion Research Division, Summary of Activities, LBNL Image Library-Collection, Dec. (1991) 7.
5. J. R. Birkelund et al, *Phys. Rev. Lett.* **40** (1978) 1123.
6. A. Bonasera, *Phys. Rev.* **C 34** (1986) 740.
7. J. N. De and W. Stocker, *Phys. Rev.* **C 42** (1990) R819.
8. M. M. Majumdar et al., *Phys. Rev.* **C 48** (1993) 2093.
9. P. B. Price et al., *Phys. Rev.* **C 46** (1992) 1939.
10. Z. Ren et al., *Phys.Rev.* **C 70** (2004) 034304.
11. C. Yanhuang, A. Smerzi and M. D. Toro, *Phys. Rev.* **C 50** (1994) 2809.
12. Z. H. Liu et al., *Phys. Rev.* **C 68** (2003) 024305.
13. C. Beck et al., *Phys. Rev.* **C 75** (2007) 054605.
14. A. Fleury and J. M. Alexander, *Annu. Rev. Nucl. Part. Sci.* **24** (1974) 279.
15. R. Serber, *Phys. Rev.* **72** (1947) 1114.
16. L. M. Bollinger, Annu. Rev. *Nucl. Part. Sci.* **36** (1986) 475.
17. A. S. Goldhaber and H. H. Heckman, Annu. Rev. *Nucl. Part. Sci.* **38** (1978) 161.
18. W.G.Lynch, Annu. *Rev. Nucl. Part. Sci.* **37** (1987) 493.
19. D.H.E. Gross, *Rep. Prog. Phys.* **53** (1990) 605.
20. A.I. Warwick et al., *Phys. Rev.* **C 27** (1983) 1083.
21. Y.D kim at al., *Phys. Rev. Lett.* **63** (1989) 494,
22. S.J. Yellenno et al., *Phys. Rev.* **C 48** (1993) 1092.

23. C.A. Ogilive et al., *Phys. Rev. Lett.* **67** (1991) 1214.

24. D. R. Browmin et al., *Phys. Rev. Lett.* **67** 1527(1991).

25. R.T. de. Souza et al., *Phys. Lett.* **B 268** (1991) 6.

26. K. Hagel et al., *Phys. Rev. Lett.* **68** (1992) 214.

27. J. B. Natowitz et al., *Nucl.Phys.***A 538** (1992) 263.

28. T. Li et al., *Phys. Rev. Lett.***70** (1993) 1924.

29. M. B. Tsang et al., *Phys. Rev. Lett.***71** (1993) 1502.

30. V.Lips et al., *Phys. Rev. Lett.***72** (1994) 1604.

31. M.E. Fisher, *Ann. Phys. (N.Y.)* **3.** (1967) 255.

32. W. Bauer, *Phys.Rev.***C 38** (1988) 1297.

33. E. Schopper, *Naturwissenschaftler* **5** (1937) 557.

34. I. I. Gurevich et al., *Dokl. Akad. Nauk SSSR* **18** (1938) 169.

35. B. Jakobsson et al., *Z. Phys.* **A 307** (1982) 293.

36. J. E. Finn et al., *Phys. Rev. Lett.* **49** (1982) 1321.

37. N. T. Porlie, *Nucl. Phys.* **A 681** (2001) 253.

38. B. K. Srivastva *et al.*, *Phys. Rev.* **C 65** (2002) 054617.

39. J. B. Elliott et al., *Phys. Rev.* **C 71** (2005) 024607.

40. N. Marie et al., *Phys. Rev.* **C 58** (1998) 256.

41. W. Loveland et al., *Phys. Rev.* **C 59** (1999) 1472.

42. J. D. Frankland et al., *Nucl. Phys.* **A 689** (2001) 940.

43. S. Hudan et al., *Phys. Rev.* **C 67** (2003) 064613.

44. J. D. Frankland et al., *Phys. Rev.* **C 71** (2005) 034607.

45. J. Hubele et al., *Z. Phys.* **A 340** (1991) 263.

46. J. Hubele et al., *Phys. Rev.***C 46** (1992) R1577.

47. M. Begemann-Blaich et al., *Phys. Rev.* **C 48** (1993) 610.

48 G.F. Peaslee et al., *Phys. Rev.* **C 49** (1994) R2271.

49. A. S. Botvina et al., *Nucl. Phys.* **A 584** (1995) 737.

50. A. SchÄuttauf et al., *Nucl. Phys.* **A 607** (1996) 457.

51. N. T. B. Stone et al., *Phys. Rev. Lett.* **78** (1997) 2084.

52. A. S. Botvina et al., *Phys. Rev.* **C 74** (2006) 044609.

53. B. de Schauenburg et al., *GSI Rep.* **98-1** (1997) 56.

54. W. Reisdorf, *Nucl. Phys.* **A 630** (1998) 15.

55. W. Reisdorf et al., *ibid.* **2000-1** (1999) 45.

56. W. Reisdorf, *Hirschegg* (1999) p. 82;

57. B. Hong et al., *Phys. Rev.* **C 66** (2002) 034901.

58. G. Poggi et al., *Nucl. Phys.* **A 586** (1995) 755.

59. J. Konopka et al., GSI Rep. **96-1** (1995) 65.

60. J. P. Alard et al., *ibid.* **97-1** (1996) 54.

61. N. Bastid et al., *ibid.* **98-1** (1997) 54.

62. A. Andronic et al., *ibid.* **98-1** (1997) 55.

63. X. Campi, *J. Phys.* **A 19** (1986) L917 .

64. X. Campi, *Phys. Lett.* **B 208** (1988) 351 .

65. W. Bauer et al., *Nucl. Phys.* **A 452** (1986) 699 .

66. X. Campi, *Nucl. Phys.* **A 495** (1989) 259 .

67. J. Pochodzalla et al., *Phys. Rev. Lett.* **75** (1995) 1040.

68. D. Kudzia et al., *Phys. Rev.* **C 68** (2003) 054903-1.

69. B. Bhattacharjee and B.Debnath, *Nucl. Phys.* **A 829** (2009) 210.

70. J. B. Elliott et al, *Phys. Rev.* **C 62** (2000) 064603-1.

71. P. L. Jain and G. Singh, *Phys. Rev.* **C 46** (1992) R10.

72. G. Singh et al., *Mod. Phys. Lett.* **A 7** (1992) 1113.

73. K. A. Bugaev et al., *Phys. Rev.* **C 62** (2000) 044320.

74. K. A. Bugaev et al., *Phys. Lett.* **B 498** (2001) 144.

75. B. Borderie, *J. Phys. G: Nucl. Part. Phys.* **28** (2002) R217.

76. H. Jaqaman et al., *Phys. Rev.* **C 29** (1984) 2067 and ref. no. 8 therein.

77. L. P. Csernai et al., *Phys. Rep.* **131** (1986) 223.

78. H. Muller et al., *Phys. Rev.* **C 52** (1995) 2072.

79. G. F. Bertsch et al., *Phys. Lett.* **B 126** (1983) 9.

80. H. Heiselberg et al., *Phys. Rev. Lett.* **61** (1988) 818.

81. J. Lopez et al., *Phys. Lett.* **B 219** (1989) 215.

82. A. Bialas and R. Peschanski, *Nucl. Phys.* **B 273** (1986) 703.

83. P.L. Jain et al., *Phys. Rev.* **C 47** (1993) 342.

84. A. Bialas and R. Peschanski, *Nucl. Phys.* **B 308** (1988) 857.

85. A. Bialas et al., *Euro. Phys. Lett.* **7** (1988) 125.

86. R. Peschanski, *New Results in hadronic interaction. Proc. of the 24th Rencontre de Moriond.* Les Ares. Savoie, French, March 12-18, 1989 ed. J. Tran Thanh Van (Editions Frontiesse) p. 247.

87. H . Satz, *Nucl. Phys.* **B 326** (1989) 613.

88. B. Bambah et al., *Nucl. Phys.* **B 332** (1990) 629.

89. A.R. DeA̕NGELIS et al., *Nucl. Phys.* **A 537** (1992) 606.

90. M. PloszaJczak and A. Tucholski, *Nucl. Phys.* **A 523** (1991) 651.

91. P.Bozek et al., *Nucl. Phys.* **A 539** (1992) 693.

92. M. Ploszajczak and A. Tucholski, *Phys. Rev.Lett.* **65** (1990) 1539.

93. M. PloszaJczak et al., *Phys. Lett.* **B 262** (1991) 383.

94. C. J. Waddington and P.S. Freier, *Phys. Rev.* **C 31** (1985) 888.

95. P.L Jain and G. Singh, *Nucl. Phys.* **A 591** (1995) 711.

96. Yu. Murin et al., *Phys. Rev.* C **55** (1997) 528

97. P.L. Jain et al., *Phys. Rev. Lett.* **68** (1992) 1656.

98. G. Singh et al., *Euro. Phys. Lett.* **21** (1993) 527 and references therein.

99. B.K. Srivastava (EOS Collaboration), *Pramana-J. Phys*. **57** (2001) 301.

100. B.K. Srivastava et al, *Phys. Rev.* C **64** (2001) 041605(R)-1.

101. Y. Imry, *Phys. Rev.* **B 21** (1980) 2042.

102. P. Labastic and R. L. Whatten, *Phys. Rev. Lett.* **65** (1990) 1567.

103. D. H.Boal and J. N. Glosli, *Phys. Rev.* C **42** (1990) R502.

104. Wang Neng-ping et al., *J. Phys.* **G 20** (1994) 101.

105. G. T. Zheng, *Phys. Rev.* **C 50** (1994) 771.

106. S. Levit and P. Bonche, *Nucl. Phys.* **A 437** (1985) 426.

107. M. A. Jilany, *Phys. Rev.* **C 70** (2004) 014901.

108 M. I. Adamovich, *Eur. Phys. J.* **A 5** (1999) 429.

109. W. A. Friedman, *Phys. Rev.* **C 42** (1990) 667.

110. R. J. Charity *et al.*, *Nucl. Phys.* A **483** (1988) 371.

111. H. R. Jaqaman and D. H. E. Gross, *Nucl. Phys.* **A 524** (1991) 321.

112. J. Bondorf et al., *Nucl. Phys.* **A 444** (1985) 460.

113. D. Stauffer, *Phys. Rep.* **54** (1979) 1.

114. W. Bauer et al., *Annu. Rev. Nucl. Sci.* **42** (1992) 77.

115. W. Bauer et al., *Nucl. Phys.* **A 152** (1986) 600.

116. J. D. Desbois, *Nucl. Phys.* **A 466** (1987) 724.

117. X. Campi and H. Krivine, *Z. Phys.* **A 344** (1992) 81.

118. S. Das Gupta et al., *Nucl. Phys.* **A 621** (1997) 897.

119. J. M. Carmona et al., *Nucl. Phys.* **A 643** (1998) 115.

120. J. Pan and S. Das Gupta, *Phys. Rev.* **C 51** (1995) 1384.

121. J. Pan and S. Das Gupta, *Phys. Rev.Lett.* **80** (1998) 1182.

122. X. Campi and H. Krivine, *Nucl. Phys.* **A 620** (1997) 46.

123. F. Gulminelli and Ph. Chomaz, *Phys. Rev. Lett.* **82** (1999) 1402.

124. A. L. Goodman et al., *Phys. Rev.* **C 30** (1984) 851.

125. J. Bondorf et al., *Phys. Rep.* **257** (1995) 133.

126. D. H. E. Gross, *Phys. Rep.* **279** (1997) 119.

127. J. Bondorf et al., *Nucl. Phys.* **A 443** (1985) 321.

128. A. S. Botvina et al., *Nucl. Phys.* **A 475** (1987) 663.

129. D. Durand, *Nucl. Phys.* **A 541** (1992) 266.

130. K. C. Chase and A. Z. Mekjian, *Phys. Rev.* **C 49** (1994) 2164

131. K. C. Chase et al., *Phys. Rev.* **C 55** (1997) 1410.

132. S. J. Lee and A. Z. Mekjian, *Phys. Rev.* **C 56** (1997) 2621

133. S. Das Gupta and A. Z. Mekjian, *Phys. Rev.* **C 57** (1998) 1361.

134. J. Bondorf et al., *Phys. Lett..* **B 150** (1985) 57.

135. P. F. Mastinu et al., *Phys. Rev.* **C 57(2)** (1998) 831

136. R. P. Scharenberg et al., *Phys. Rev.* **C 64** (2001) 054602

137. D. G. Ravenhall et al., *Nucl. Phys.* **A 407** (1983) 572.

138. D. Stauffer and C. S. Kiang, *Adv. Colloid Interface Sci.* **7** (1977) 103.

139. D. Stauffer and A. Aharony, *Introduction to Percolation Theory*, 2nd ed. (Taylor and Francis, London, 1992).

140. J. Hoshen et al., *J. Phys.* **A 12** (1979) 1285.

141. P. L. Leath, *Phys. Rev. Lett.* **36** (1976) 921.

142. P. L. Leath, *Phys. Rev.* B **14** (1976) 5046.

143. H. Nakanishi and H. E. Stanley, *Phys. Rev.* **B 22** (1980) 2466.

144. K. Chen et al., *Phys. Rev.* **166** (1968) 949.

145. Y. Yarik and Z. Fraenkel, *Phys. Rev.* **C 20** (1979) 2227.

146. A. Capella et al., *Nucl. Phys.* **B 241** (1984) 75.

147. A. Capella et al., *Z Phys.* **C 10** (1981) 249.

148. I. Otterlund et al., *Z. Phys.* **C 20** (1983) 281.

149. Y. Yariv and Z. Fraenkel, *Weizmann Institute Preprint WIS*-**18/80** (1980).

150. K. K. Gudima and V. D. Toneev, *Yad. Fiz.* **27** (1978) 658

151. K. K. Gudima and V. D. Toneev, *Yad. Fiz.* **31** (1980) 1455.

152. K. K. Gudima and V. D. Toneev, Preprint R2-10431 JINR, Dubna (1977).

153. V. S. Barashenkov et al., *Ups. Fiz. Nauk.* **103** (1973) 93.

154. V. Singh, *Ph. D. Thesis*, Banaras Hindu University, Varanasi (1998).

155. G. Odyniec, *Int. J. Mod. Phys.* **A 17** (2002) 3107.

156. Y.G. Ma, *Phys. Rev. Lett.* **83** (1999) 3617 and references therein.

157. V. Bradnova et al., JINR-LHE-0983-2.

158. M. Aggarwal, Physics and Astrophysics of Quark–Gluon Plasma, Narosa Publishing House, New Delhi

159. J. Pouthas et al., *Nucl. Inst. and Meth.* **A 357**(1995) 418.

160. J. Lukasik et al., *Phys. Lett.* **B 566** (2003) 76.

161. C. Volant et al., *Nucl. Phys.* **A 734** (2004) 545.

162. M. Pichon et al., *Nucl. Phys.* **A 779** (2006) 267.

163. E. Bonnet et al., *Phys. Rev. Lett.* **105** (2010) 142701.

164. M. A. Jilany et al., *Int. J. Mod. Phys.* **E 4(4)** (1995) 815.

165. S. A. Keasnov et al., *Czechoslovak Journal of Phys.* **46 (6)** (1996) 513.

166. N. N. Abd Allah et al., *Int. J. Mod.Phys.* **E 10 (1)** (2001) 55.

167. A. Dabrowska et al., *Acta Physica Polonica* **B 31(3)** (2000) 725.

168. P. L. Jain et al., *Phys. Rev. Lett.* **74** (1995) 1534.

169. B. Chiu and R. C. Hwa, *Phys. Rev.* **D 45** (1992) 2276.

170. R. Holynski et al., *Phys. Rev.Lett.* **62** (1989) 733.

171. R. Holynski et al., *Phys. Rev.* **C 40** (1989) R2449.

172. M. I. Adamovich et al., *Phys. Rev. Lett.* **65** (1990) 412.

173. D. Ghosh et al., *Phys. Rev.* **C 58** (1998) 3553.

174. D. Ghosh et al., *Z. Phys.* **C 73** (1996) 269.

175. D. Ghosh et al., *Int. J. Mod. Phys.* **E 12** (2003) 407.

CHAPTER II

EXPERIMENTAL TECHNIQUES AND GENERAL CHARACTERISTICS

2.1 Introduction

Detector plays a very important role in the studies of high energy nucleus-nucleus collisions and hence this field of experimental nuclear physics has made considerable progress since the time of Rutherford's alpha particle scattering experiment with gold. With the availability of more energetic beams the complexity of nuclear reaction has been increased manifold with more number of ejectiles and hence need for better and better detector system has been felt over the period of time. Nuclear emulsion is one such detector. Developed by CF Powel [1], the emulsion has been a standard tool to study high energy h-A and A+A collisions since 1950s.

Nuclear emulsions are photographic emulsions of very high silver concentration that are thickly coated on glass backings. Ionizing particles which happen to pass through such emulsions leave behind a number of silver bromide crystals that have been so altered that, upon development, they appear as rows of black grains of colloidal silver and identify the trajectories of the particles. The more strongly ionizing the particles, the more numerous are these grains; and the greater their initial energies, the longer the resulting track. Nuclear emulsion was connected to many major discoveries in the early days of nuclear and particle physics. It was in an emulsion stack brought to high altitude that the pion[2] was discovered. Stacks of 0.5 mm thick emulsions were also lifted with balloons to very high altitudes to study the cosmic radiation. It still remains the detection technique with the best known three-dimensional spatial resolution, and zero intrinsic dead time. However its uses have gradually been decreased after the development of electronic detectors. Contrary to emulsion, electronic detectors offer immediate time correlated readout, and digitized output storable to computer accessible media. They serve therefore better the needs of most present experiments, which require large statistics of accumulated data for prompt and accurate physics result. Recent developments in automatic emulsion scanning, have given a renaissance to emulsion as a particle detector. Automatic scanning allows for fast extraction of digital information from emulsion sheets, after they have been exposed to particle radiation. Not only does it make handling of large data sets possible, it also ensures that physics results can be produced shortly after the running of the experiment.

2.2 Some features and composition of nuclear emulsion

The nuclear emulsion technique of studying high energy h-A and A+A collisions rely mostly on the studies of various parameters of tracks produced along the trajectory of charged secondaries. The various information that can be gathered from the analysis of such tracks are enlisted herewith:

1. Curvature of a track to measure mass and charge of the charged particle.
2. Counting of the individual tracks is a measure of the number of charged nuclear particles produced in a collision.
3. The study of scattering interaction and production cross-section.
4. An extensive study on the structure of the tracks can lead to the determination of the momentum and hence the energy of the particles.
5. The investigation of lifetime and decay gives the characteristics of unstable particles.
6. A detailed study of charge and angular distribution of particles leads to the identification of some exotic phenomena namely criticality and liquid-gas phase transition.

The composition of a standard nuclear research emulsion is presented in the table 2.1.

Table 2.1 Composition of standard nuclear emulsion

Element	Atomic Number	Atomic Weight	No. of atoms x 10^{22}			
			Per cc of halide	Per g of halide	Per g of gelatin % R.H	Per g of water
Ag	47	107.88	2.071	0.32		
Br	35	79.916	2.06	0.318		
I	53	126.93	4.57	0.018		
H	1	1.008			4.58	6.70
C	6	12.00			2.48	
N	7	14.008			0.55	
O	8	16.000			1.137	3.35
S	16	32.06			0.032	

2.2.1 Advantages of using nuclear emulsion as a detector

The distinctive advantages of nuclear emulsion are :

i) Versatile activity

Nuclear emulsion has the ability to serve the purpose of both detector and target in high energy interactions. This advantage of nuclear emulsion increases its acceptability over many other detectors. In high energy collision studies, it is often instructive to use target nuclei differing immensely in their mass number. Nuclear emulsions provide such targets since they contain a light group (H,C,O,N) and a heavy group (Ag, Br) of nuclei. Although the separation of events into these two group are not, by any means, exact, but still one can get information regarding the dependence of the production mechanism on the mass of the target nucleus.

ii) 4π Detectibility

Emulsion covers 4π geometry. It can recognize all the charged particles emitted in space in the final state of the high energy nuclear interactions. This advantage of emulsion has made it very much useful in studying charged secondaries mainly produced particles and projectile fragments which are emitted mostly in the extreme forward angle.

iii) The stopping power

Because of the differences in the densities of the media, the stopping power in nuclear emulsion is several times higher than that of the cloud-chamber or bubble-chamber medium. The times of elapse of the charged particles are higher in emulsion compared to that of the other detectors and hence found to be suitable to study the decay of various elementary particles.

iv) Sensitivity

The emulsion detector has the sensitivity of registering all the charged particles having energies very low upto the relativistic regime. Further the sensitivity of the emulsion lasts for more than a week, which helps to record all the charged particles within this time span. Hence it is the only tool to study the cosmic ray events where the incident beam can be hardly found.

v) Mechanical features

It is most easy to handle because of its size and weight. One of the greatest advantages of using this type of detector is that it can record permanently the trajectories of the charged particles until and unless it is destroyed completely.

vi) Operating range

Nuclear emulsion has the large operation range with regard to temperature. It may be used successively in the temperature ranging from the temperature of the liquid helium upto the boiling point of the water [3].

2.2.2 Disadvantages of nuclear emulsion

Though nuclear research emulsions have great advantages of detecting various charged particles, yet it has few drawbacks:

1) The sensitivity and thickness are affected by factors like temperature, humidity, age of the emulsion, the conditions under which they are developed etc.

2) The tracks are relatively short, at best few mm in length and they must have to be studied only under a high power microscope.

4) The manual analysis at the microscope is painstaking and time-consuming. Further there is no way to identify the exact target atom in an event; one can at best conclude that the target could be a H or C, N, O or Ag, Br nucleus.

5) Another disadvantage is that they remain always sensitive to ionizing particles and there is no method to trigger them by the particles one wishes to study, unlike the cloud chambers.

2.3 The characteristics of the photographic process

2.3.1 Formation of latent image

A photographic emulsion is essentially a dispersion of silver halide crystals in a gelatin matrix [1,3-4]. The elements present in the gelatine medium (along with plasticizer i.e glycerine) are carbon, nitrogen, oxygen, hydrogen and sulphur. The nuclear emulsions are fundamentally the same as general purpose photographic emulsions, but have several distinguishing features:

- The silver halide crystals are very uniform in size and sensitivity.
- There are very few crystals that may be developed without exposure to a charged particle (very low chemical fog).
- The silver to gelatin ratio is much higher than in a conventional emulsion.

When such an emulsion is exposed to relativistic hadron or heavy ion beam the incident particle while passing through emulsion may collide one of the nucleus of the atom it consisted of. As a result of such collision, a number of charged secondaries and radiation will come out of the interaction centre. These ionizing charged particles (radiation) on passing through the emulsion modify the silver ion of AgBr crystals along its trajectory. These are known as latent image centres, as they are not visible until the emulsion is developed. On development all the crystals containing a latent image centre are reduced to metallic silver which are easily distinguishable because of their black colour. Thus, as a charged particle advances through emulsion, it leaves behind a trail of black grains called track. By investigating the characteristics of these tracks, ionization produced may be determined and information about their charges and velocities can be obtained. The tracks in an interaction appear to come out from a single vertex. The recorded interaction in emulsion is thus called a star due to its characteristic appearance.

2.3.2 Processing of nuclear emulsion

2.3.2.1 Development

Photographic development is the process by which the latent image contained in an emulsion is made visible by the reduction of silver ions in the silver halide crystal to metallic silver. When developing nuclear emulsions, a developer is usually chosen which reduces those crystals containing a latent image centre completely and leaves those unchanged, not containing a centre. The development time used for processing material should be sufficient for those crystals with a latent image centre be reduced completely, but not so long that unexposed crystals are developed. In practice, a certain number of crystals will be developed even though they do not contain a latent image centre. These grains, when developed, constitute what is known as fog or background. Developing agents may be divided into two main groups, depending on the source of silver ions for reduction. In practice, most developers give a combination of the two sorts of development. The first group is known as physical developing agents. In physical development, silver ions are provided from the solution in the form of a soluble complex. These are deposited on the latent image centre and are reduced to metallic silver. This produces spherical particles, the precise shape of which is affected by pH. Chemical developing agents make up the second group and are more usually chosen when processing nuclear emulsions. However, the choice between a physical developer and a chemical developer will largely depend on the grain structure required in the processed image. In chemical development, silver ions are provided from the silver halide crystal containing the latent image centre. The action of a chemical developer produces a mass of filaments bearing little resemblance to the original crystal. If silver halide solvents such as sulphite are present in a chemical developer, an opportunity exists for some physical development to occur. In this case, the filaments in the processed plate will be shorter and thicker. Chemical development, like many other chemical reactions, is dependent on temperature. In general, development occurs more rapidly at higher temperatures - below 10°C development virtually stops. For this reason it is important to keep the processing temperature constant during the development, otherwise it will not be possible to assess the correct development time. Chemical developers are also dependent on pH and will only maintain a given activity within a narrow pH range. In general, the less alkaline the environment, the less active the developer will be. For this reason, the use of an acid stop bath is often recommended at the end of the development. This stops development immediately so that the development time can be controlled precisely.

2.3.2.2 Stop bath

After development, the material is transferred to an acid stop bath. This may be made up with 0.2-2% acetic acid solution. Like development, stop bath times vary with layer thickness. A time of 1 minute will suffice for thinner layers, rising to around 10 minutes for a 100 micron layer.

2.3.2.3 Fixation

The purpose of fixation is to remove all the residual silver halide, leaving the metallic silver to form the image. If the silver halide is left in the emulsion, it will slowly go brown and degrade the image. The fixing agents most widely used are sodium or ammonium thiosulphate, which form thiosulphate complexes with the silver halide. Silver thiosulphate is soluble in water and so may be removed from the emulsion by washing. It is important to use a fixer which has not been exhausted when processing nuclear emulsions; otherwise some silver halide will remain in the emulsion. To ensure that it is all removed a fixing time should be used which is twice the time it takes for the emulsion to clear [1].

2.3.2.4 Washing and Drying

After fixation, the emulsion must be washed very thoroughly. This is to remove all the silver thiosulphate complexes in the emulsion. If any do remain, they will eventually break down, forming silver sulphide which is brown and will obscure the image.

After washing, the plates are soaked in a solution of glycerine of strength 2 to 5% and dried. The glycerine solution is used to prevent the stripping of dried emulsion from the glass. The final drying of processed plates may be carried out by placing them with the emulsion surface horizontal in a gentle current of air [1].

2.3.3 Calibration of stack

When the emulsion is processed, there occurs a reduction in its volume as the silver halide crystals are dissolved by fixer. The ratio of the thickness of the emulsion before and after processing is called the shrinkage factor (S) [1]. This factor determines the relationship between the geometrical conditions during exposure and during observations.

2.3.4 Shrinkage factors

Gelatine and glycerine, both being hygroscopic, the actual equilibrium thickness and index of refraction of both the processed and unprocessed emulsion depends on the surrounding humidity. Consequently, we defined the shrinkage factor[1], S as:

$$S = \frac{\text{Thickness of emulsion layer during exposure}}{\text{Thickness of emulsion layer during scanning}} \tag{2.1}$$

Thus for any quantitative measurement of track densities, range and angles in emulsion, the original thickness of the emulsion is to be known. The shrinkage factor is generally supplied by the manufacturer of the emulsion plates [5-6].

2.3.5 Emulsion stack and their exposure

Nuclear emulsion pellicles of the type NIKFI-BR-2 and dimensions $20 \times 10 \times 0.06$ cm^3 were irradiated parallel to their lengths by a 4.5 A GeV ^{24}Mg beam from the JINR synchrophasotron at Dubna.

2.4 Microscope

In this work, a high magnifying power optical trinocular research microscope (Olympus BH-2) was used to magnify and study the particle tracks in nuclear emulsion. In general, these microscopes consist of a set of objectives (including an oil-immersion one) of different magnifications. A pair of eyepiece (15 ×) was used to magnify the real image formed by the objective. Disintegration centre's were scrutinized and different parameters of various tracks were recorded under higher magnification (1500 × oil immersion) using the same microscope.

2.4.1 Scanning Procedure

The scanning of the emulsion plates are carried out as a part of a planned programme in which minimum biased events are identified in a systematic way. The two different methods of scanning are generally employed:

i) Area Scanning

In area scanning, the focal surface in the emulsion is swept up and down, from the surface of the emulsion to the supporting glass. This is done by rolling the fine focus control while observing the events successfully coming into and going out of view. Each field of view is scanned through out its depth, from one surface of the emulsion to the other. Thus, a definite area (infact the volume) of the plate is covered.

Area scanning is employed if the following situations arise:

a) When all the events of certain type in a given volume of emulsion are to be found.

b) When a sample of a particular kind of event is required.

c) If the situation demands a representative sample of events.

d) When the number and an unbiased spectrum of events in a given volume are to be found.

But the area scanning will not be a favorable process, for single diffractive dissociation events or interactions with H-nuclei.

ii) Along the Track Scanning

If a stack of emulsion is exposed to a beam of particles entering one face in a perpendicular direction, and if one intends to study the density and distribution of the beam entering the stack, then the procedure for finding tracking of a specified type is to traverse each plate parallel to the leading edge and perpendicular to the incoming tracks. This type of scanning is known as along the track scanning.

In the present investigation along the track scanning method has been employed for identifying the Mg-Em interaction.

2.5 Principle of identification of charged particles using emulsion

A charged particle passing through a photographic emulsion slows down as a result of interactions with the atoms of the emulsion along its path. These interactions result in a loss of energy of the incident charged particle. The forces responsible for this energy loss are electromagnetic involving the electrons of the atoms of the emulsion medium. The energy transfer to the medium takes place as a result of interactions, which may be elastic (the atom is displaced but its internal state remains unchanged) or inelastic (the atom is both displaced as well as excited internally). The total rate of loss of energy of a particle of charge Ze moving with a velocity β due to interactions while it travels through a medium is given by [4,7-8]:

$$-\frac{dE}{dx}=\frac{2\pi nZ\,2r_o^2}{\beta^2}\left(\ln\frac{2m_ec^2\beta^2\gamma^2W_{max}}{I_0^2}-2\beta^2-2C\right) \tag{2.2}$$

Here, $r_o = \frac{e^2}{m_ec^2}$, the classical radius of electron

m_e = mass of electron

I_o = mean ionization potential

β = relative particle velocity

$$\gamma = \frac{1}{\sqrt{(1-\beta^2)}}$$

W_{max} = maximum energy imparted to the electron.

C = correction term to be applied at high velocity of the projectile.

The development of grains in the emulsion takes place by the loss of energy of a charged particle through the process of ionization while passing through nuclear emulsion. The number of grains deposited per unit length of track is defined as grain density (dn/dx). The grain density has been found to be proportional to to $|\frac{dE}{dx}|$, which in turn is related to Z and E (or β) of the charged particle. Experiments have shown that as the velocity of a charged particle approaches 'c', the grain or blob-density in its track reaches a minimum value for $\beta = 0.95$ and then rises again to a nearly constant value for $\beta > 0.995$ [9-12]. The rise of grain density (g*) above the minimum value (g_o) as the energy of particle increases due to the longitudinal contraction and lateral extension of the field of the moving particle [1] . This leads to the excitation and ionization of atoms at increasing distances from the trajectory of the particles. In association with the above, the rate of loss of energy (E) increases with ~ log E. This increased rate of loss is not reflected in a corresponding increase in the grain density, because much of it is dissipated at points outside the core of the track. Some of the additional energy loss leads however, to the formation of relatively low energy, δ rays which contributes to the observed limited increase in the grain density.

This minimum grain density 'g_o' plays an important role in the identification of different charged secondaries emitted from the target nucleus.

Another important parameter for the measurement of charge of particles traversing the emulsion medium is the delta rays, which are electrons knocked free from atoms by the primary ionizing particle. Delta rays of energy < 5 KeV have their tracks so contracted that the mean distance between the origin of δ-rays and its point of arrest is covered in such a manner that the δ-ray tracks are tied into knots by scattering and are closely confined to a region near the trajectory of the charged particle. When the energy of δ-rays increases slightly, their effective range increases and the δ-ray electrons escape from the trajectory of parent particle. They make the neighboring grains develop in the form of spurs to the particle track and give a clearly distinguishable δ-ray track. Thus, the δ-rays having energy < 5 KeV are retained in the grains and have a contribution towards ionization but those having a greater energy are excluded. For a constant velocity, the δ-ray density is directly proportional to the square of the charge of the particle whose track is formed [5].

2.6 Classification of secondaries

2.6.1 The classification of charged secondaries

All the charged secondaries emitted or produced in an interaction are classified into the following categories in accordance with their normalized grain density g^*, defined as $g^* = g / g_o$, where g is the observed grain density and g_o is the minimum number of grains per unit length developed due to a singly charged particle, ionaization etc.

(i) Black track producing particles (N_b)

These are mainly the evaporation products (protons) of the remnant of the target nucleus and the fragments emitted at the final stage of the nuclear collision from the excited target nuclei. They have range L < 3mm from interaction vertex from which they originates and $g^* > 6.0$. This ionization range corresponds to protons with kinetic energy < 30 MeV and velocity less than 0.3c. Their multiplicity is denoted by N_b.

(ii) Grey track producing particles (N_g)

These are the particles having grain density $1.4 < g^* \leq 6.8$ and a range $L > 3$ mm in emulsion. These tracks are mostly due to recoil target protons with kinetic energies in the range 30–400 MeV and in the velocity range $0.3 \leq \beta \leq 0.7$ with a small admixture of slow pions, deuterons, tritons and helium nuclei. Their multiplicity is denoted by N_g.

The black and/or grey tracks together are called the heavily ionizing particles (N_h), their multiplicity of which is denoted by $N_h = N_b + N_g$.

(iii) Shower track producing particles (N_s)

These are the singly charged relativistic particles with grain density g* <1.4, corresponding to pion energies above 70 MeV and proton energies above 400 MeV. Most of these tracks belong to pions contaminated with small proportions of fast protons and *k*-mesons and having $\beta > 0.7$.

2.6.2 The classification of projectile fragments

The noninteracting (spectator) fragments of the projectile nucleus having charge $Z_{PF} \geq 1$ and having velocity close to the beam velocity, are the tracks which lie within the narrow forward narrow cone around the beam direction and their ionization remains constant for at least 20 mm from the interaction point.

The forward angle is the angle whose tangent is the ratio between the average transverse momentum of the projectile fragments to the longitudinal momentum (P_l) of the beam. Taking P_l as the beam momentum in AGeV itself, i.e.

$$\theta_f = \tan^{-1}(P_t / P_{beam}) \qquad (2.3)$$

for the present study, θ_f is found to be equal to $0.2/P_{beam} = 3^{\circ}$

The PFs are further classified into three categories

a) Heavy projectile fragments (N_f): PFs with charge $Z \geq 3$

b) Alpha projectile fragments (N_α): PFs with charge Z=2

c) Singly charged ($N_z = 1$) relativistic projectile fragments

Since these projectile fragments have velocities nearly equal to the initial beam velocity, their specific ionization may be used directly to estimate their charge.

The total multiplicity of the secondary charged particles (N_{ch}) [13-14] for an emulsion event is the sum of all the charged particles that are emitted or produced in an interaction.

$$N_{ch} = N_s + N_g + N_b + N_{pf} \qquad (2.4)$$

2.6.3 Selection criteria for electromagnetic dissociation events

Each event was very carefully examined and qualitatively classified into four principal categories [14-15]: (i) central events, (ii) semi-central events, (iii) peripheral events and (iv) electromagnetic events. The electromagnetic dissociation (ED) events, as described in ref.[14,16], were picked up among the peripheral ones with no visible excitation of the target nucleus (N_h = 0) and with an additional constraint that the sum of charges of all the PFs with $Z_{PF} \geq 1$ inside the fragmentation cone are always 12 for the ^{24}Mg beam. The contribution of the nuclear peripheral events in these samples of the electromagnetic events is effectively minimized subject to the requirement that the number of produced shower particles (N_s) in ED events ≤ 1. According to these stringent selection criteria, the numbers of ED events corresponding to the incident beams ^{24}Mg at 4.5 AGeV are estimated to be 77 out of the entire sample of data.

The accuracy of the Z determination was always better than 1 unit. This was verified by summing up the charge of fragments in events of electromagnetic dissociation type [17].

2.6.4 Selection criteria for the type of events

For the present study, we have used the following selection criteria for determining the type of events [18-21].

a) $N_h \leq 1$:	Mg- H interaction
b) $2 \leq N_h \leq 5$:	Mg-CNO interaction (having no short track)
	Mg-AgBr interaction (at least one short track)
c) $N_h > 8$:	Mg-AgBr interaction

d) $6 \leq N_h \leq 8$: Mg-CNO/AgBr interaction (CNO for no heavy short track and AgBr for heavy short track)

2.6.5 Charge estimation of Projectile Fragments

The charges of the projectile fragments were estimated by adopting the method of ionization measurement. Although different methods are employed to estimate the charge of PF's [1], the fundamental principle is related to ionization in some way or the other. For emulsion technique this ionization is related with the grain density, i.e., the number of developed grains per unit length. With low ionization there is no significant error in the estimation of the grain density. But with the increase in grain density, it is not possible to resolve the adjacent grains even under a high magnification microscope. In the tracks of heavily charged fragments, the grains get clogged to each other to form blobs and thus the counting of individual grains become impossible. One then counts the number of developed blobs and the gaps between them per unit length as the measure of PF charge

The charge of various PF's can be measured by adopting a number of methods of measurement which are listed below :

a) Grain density.

b) Blob and hole density.

c) lacunarity and opacity [22]

d) δ-ray density and

e) Relative track width measurement.

Since each method has its own limitations, therefore a single method cannot be applied to estimate the charge of the PF's over the entire range. Also, to estimate the charge of PF's with better accuracy, one should not measure a single parameter related to the ionization of the track. For the present study therefore, in most of the cases, more than one parameter of a particular projectile fragment's track has been measured and made a cross examination of their values before finally assigning the charge to that particular PF. Suitable track parameters are being measured for different charge range of the PF's.

2.7 Measurement Methods

2.7.1 Measurement of grain density

Grain density depends on the particle velocity. So the grain density provides means for the estimation of particle velocity.

To measure the developed grains in a track of a charged particle, the most obvious method is to count the developed grains in the measured length of the track. At low grain densities, the error in such measurements may not be great. But as the grain density increases, adjacent grains become irresolvable under the microscope, the error in this case is certainly high. Another counting procedure is merely to determine the mean linear density B, of resolvable clumps, known as blobs consisting of one or more grains. The estimation of the number of blobs in a track is equivalent to measuring the number of gaps. So that gap counting and blob counting are equivalent terms.

2.7.2 Measurement of dip angle

The dip angle of a particular track 'δ' can be calculated using the relation:

$$\tan\delta = \frac{\Delta Z}{L} \tag{2.5}$$

where, ΔZ = the true difference of depth between any two points in the track.

L = length of the projection of the track between these two points.

Since the index of refraction of the emulsion may not be same as the oil used for an immersion objective (and certainly will not be same as air when an air objective is used), the depth measurement, even using a microscope with linear, accurately calibrated focusing motion, may not be correct. If dry objectives are used, the apparent depth d_a will be less than the true depth d_t:

$$d_t = \mu_e . d_a \tag{2.6}$$

with oil-immersion objectives, however, the d_a and d_t are more or less equal because of the close approach of equality of the refractive indices of the immersion oils commonly employed (μ_o = 1.52) and the emulsion

$$d_t = \mu_e^o d_a \; ; \; \mu^o \approx 1 \qquad (2.7)$$

The true angle of dip, Δ, at the time of the parent particle is given by:

$$\tan \Delta = S \tan\delta = S \, \Delta z / L = S\mu \, . \, \Delta z / L \qquad (2.8)$$

S being the shrinkage factor.

2.7.3 Measurement of Space angle

The space angle θ between two tracks can be estimated by the simple co-ordinate method. If the direction cosines of the tracks are (l_1, m_1, n_1) and (l_2, m_2, n_2) then:

$$\text{Cos } \theta = l_1 l_2 + m_1 m_2 + n_1 n_2 \qquad (2.9)$$

Direction cosines of a track can be easily obtained by taking space co-ordinates (x,y,z) of any two points on the track. If (x_1, y_1, z_1) and (x_2, y_2, z_2) are the readings of the space coordinates, the directions cosines are given by:

$$l = \frac{(x_1 - x_2)}{[(x_1 - x_2)^2 + (y_1 - y_2)^2 + (z_1 - z_2)^2]^{1/2}} \qquad (2.10)$$

$$m = \frac{(y_1 - y_2)}{[(x_1 - x_2)^2 + (y_1 - y_2)^2 + (z_1 + z_2)^2]^{1/2}} \qquad (2.11)$$

$$n = \frac{(z_1 - z_2)}{[(x_1 - x_2)^2 + (y_1 - y_2)^2 + (z_1 - z_2)^2]^{1/2}} \qquad (2.12)$$

2.8 Photo Plate of Mg Events in Emulsion

Few Images of various interactions of ^{24}Mg nuclei with Emulsion targets

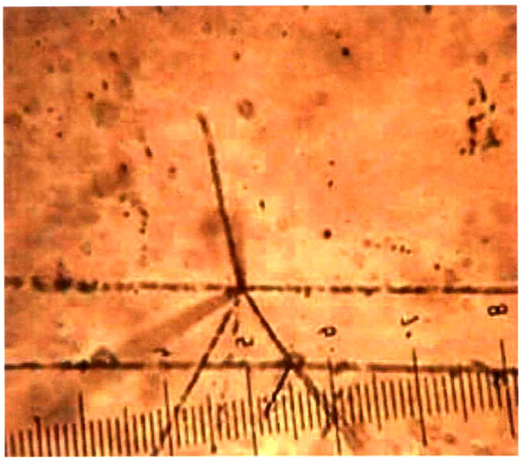

Mg-AgBr (Peripheral Collision)

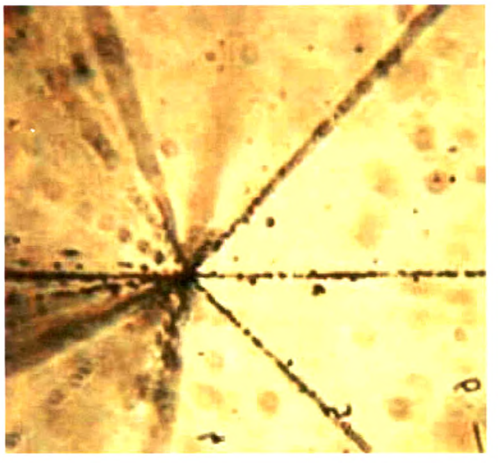

Mg-CNO (Peripheral Collision)

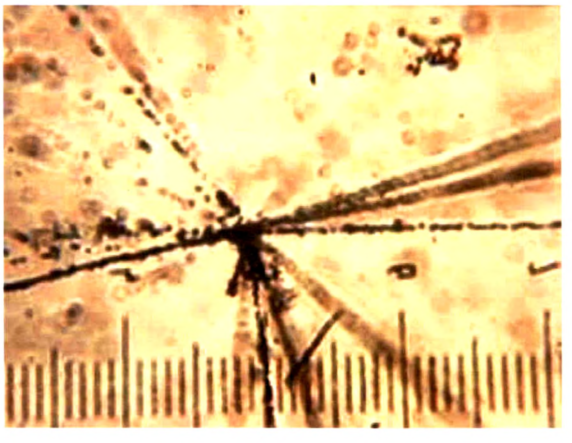

Mg-AgBr (Central Collision)

References

1. C. F. Powell, P. H. Fowler and D. H. Perkins: *The study of elementary particles by the photographic method*, Pergamon Press, London (1959).
2. C. M. G. Lattes et al., *Nature* **159** (1947) 694.
3. W. H. Barkas, *Nuclear Research Emulsions*, Academic press, NY & London, Vol **1.** (1963).
4. S. Nagamiya, *Proc. of Int. Conference on Nuclear Physics*, Bombay (1984); U. Nantes, IRES Strasbourg and LEPSI Strasbourg *"Proposal for a Silicon Strip Detector for STAR"* (1997); VECC, Calcutta; Inst. Physics, Bhubaneshwar; Rajasthan Univ., -Jaipur; Punjab Univ., -Chandigarh, and Jammu Univ., -Jammu *"Proposal for a Photon Multiplicity Detector in STAR"* (1996).
5. V. Singh, *Ph.D. Thesis*, Banaras Hindu University, Varanasi, India (1998).
6. K. Chattopadhyay, *Ph.D Thesis*, Jadavpur University, Kolkata, India (2004).
7. H. Bethe, *Z. f. Physik* **76** (1932) 293.
8. F. Block, *Z. f. Physik* **81** (1933) 363.
9. R. R. Daniel et al., *Phil. Mag.* **43** (1952) 154.
10. A. H. Morrish, *Phil. Mag.* **43** (1952) 533.
11. L. Voyvodic, *Bristol conf. Rep.* Dec (1951).
12. L. Voyvodic and E. Pickup, *Phys. Rev.* **85** (1952) 91.
13. M.A. Jilany, *Nucl. Phys.* **A 705** (2002) 477.
14. G. Singh and P.L. Jain, *Z. Phys.* **A 344** (1992) 73.
15. G. Singh et al., *Phys. Rev.* **C 41** (1990) 999.
16. G. Baroni et al., *Nucl. Phys.* **A 516** (1990) 673.
17. M. I. Adomovich et al., *Z . Phys.* **A 351** (1995) 311.
18. B. Bhattacharjee, *Nucl. Phys.* **A 748** (2005) 641.

19. R. K. Shivpuri and V. K. Verma, *Phys. Rev.* **D 47**(1) (1993) 123.

20. N. N. Abd-Allah, *J. Phys. Soc. Jpn.* **69** (2000) 1068 and references therein.

21. M. El-Nadi et al., *Nouvo Cimento* **A 107** (1994) 1.

22. M. A. Bloomer et al., *Nuclear Instruments and Methods in Physics Research,* **215** (1983) 247 and the references therein.

CHAPTER III

GENERAL CHARACTERISTICS OF Mg PROJECTILE FRAGMENTS: MULTIPLICITY & ANGULAR DISTRIBUTION

3.1 Introduction

According to participant spectator model [1] the interacting system in high energy nucleus-nucleus collision can be divided into three parts: a target spectator, a participant and a projectile spectator. The overlapping part of the two colliding nuclei is called the participant, and the non overlapping portions of target and projectile nuclei are respectively called the target and projectile spectators. The model predicts that violent nucleon-nucleon collisions take place in the participant region and weak excitation and cascade collision take place in the spectator parts. The participants produce many mesons, nucleons, photons, lepton pairs etc., and the spectators break into many nucleons and nuclei. While the produced particles from the participant portion are believed to be emitted during the early stage of A+A collision, the knocked out protons from the participant portion are supposed to be emitted at some later stage. At the last stage of the collision, the spectator portions of both the nuclei are de-excited through evaporation or/and fragmentation resulting another stage of particle emission. Thus in time scale a relativistic heavy ion collision may be viewed as consisting of three different stages of particle production and it is therefore quite rational to believe that there might exists some correlation between the charged secondaries emitted at different stages from both the participant and spectators parts of heavy ion collisions.

The size of the projectile spectator produced in collisions at all energies depends strongly on the impact parameter [2]. It is thus essential to sort out the collisions according to their centrality. The impact parameter that determines if a particular collision would be of central, quasi central or peripheral in nature is not a directly measurable quantity; it is thus necessary to find an observable intimately correlated with it. The number of particles produced in an interaction, called the particle multiplicity is often considered as a good measure of impact parameter. Studies on particle multiplicity are important from the point of view that such studies are expected to yield significant information about the collision dynamics [1,3] and help us to check the predictions of different phenomenological and theoretical models used to describe high energy nuclear collisions. Particle multiplicity is often used as an important tool for understanding the multiparticle production mechanism and the nuclear fragmentation process and also for investigating the correlation between the two processes [4]. The Intranuclear cascade (INC) calculations [5] confirmed this hypothesis of strong correlation between impact parameter and multiplicity of emitted participant nucleons; no better correlation could be achieved even with more complicated observables. Even though this selection of the centrality by means of the multiplicity gives only a qualitative ordering of the collision according to their impact parameter, exclusive measurements of relativistic nucleus-nucleus collisions have been most often presented as a function of the multiplicity, without trying to get the impact parameter.

A number of workers have taken various particle multiplicities such as average number of shower tracks $<N_s>$, average number of heavily ionizing track $<N_h>$ or the total charge of the projectile spectator fragments Q_{pf} as a measure of the degree of centrality of the collision or otherwise the impact parameters [6-9]. It has also been observed that the number of various charged secondaries produced in an interaction depends strongly on the system size and energy of the incident nuclei. It would therefore be interesting to look for the correlation between the various experimentally observable quantities such as $<N_s>$, $<N_h>$, Q_{pf} etc., that are often taken as a measure of collision geometry and how these correlations, if any, vary on system sizes.

In the present investigation an attempt has been made to find the correlation between Q_{pf} and other multiplicity parameters such as N_s, N_h, N_g etc..for ^{24}Mg-Em interactions at 4.5 AGeV. The results obtained from ^{24}Mg-Em interaction have been compared with the ^{84}Kr-Em interaction at nearly the same energy (0.95A GeV).

In the complex scheme of high energy nucleus-nucleus collisions, projectile fragmentation, in general, is a relatively well isolated phenomenon. The fragmentation parameters of relativistic heavy ion nuclei provide vital information for the solution of many problems in astrophysics, radiation physics and associated applications [10]. Projectile fragmentation at high energies has proven to be a powerful tool in the production and study of new exotic nuclei [11]. It has become a widely used technique for production of Radioactive Ion beams (RIBs) at many existing facilities [12].

In projectile fragmentation process, a projectile spectator, on excitation, often splits into several pieces of intermediate mass fragments (IMFs) which span the mass-range between alpha particle and fission fragments. It is believed that studies on the decay of such excited nuclear system may provide information of the nuclear collision dynamics. The sum of all projectile fragments (PFs) with charge $Z_{PF} \geq 2$, which is also known as bound charge Z_b, is related to the size of the excited projectile spectator and gives the measure of the mass of the fragmenting system [13-14]. Therefore it should reflect the centrality of the collision and can be used as a measure of the impact parameter. Larger Z_b values correspond to larger impact parameters and to more peripheral collisions. The size of the projectile spectator remnant is a measure of the geometry of the collision, and therefore, for a given collision system, it should be independent of the beam energy [14-15]. Different projectile energies lead to different excitations of the spectator remnant, and thus, influence its decay, but not the size. It also gives an idea about the energy-momentum transferred to the participant part of the colliding nuclei [13-21]. Correlation between mean number of intermediate mass fragments (IMFs) and the mass of the fragmenting system is one of the most interesting aspects of studying projectile fragmentation and is being studied by different workers for various systems at different energies. To have more insight into the role played by size of the projectile remnant on the production of intermediate mass fragments, in this work an attempt is therefore made to study the correlation between $\langle N_{IMF} \rangle$ and mass of the fragmenting system, Z_b of incident Mg nuclei.

Further, studies on the angular distributions of projectile and target fragments are also important to understand the various collective effects such as side splash, bounce-off effect, transverse flow, etc. [22-26]. In this work, an attempt has also been made to study the angular distribution of various projectile fragments emitted from ^{24}Mg-Em interactions at 4.5 AGeV.

3.2 Results and Discussion

3.2.1 Multiplicity Distribution

3.2.1.1 Dependence of mean multiplicity on A_p

The mean multiplicity of all the projectile fragments for the entire data sample of present investigation on ^{24}Mg-Em interactions at 4.5 AGeV is found to be 2.76 ± 0.37. The mean multiplicities of projectile fragments with $Z_{PF} = 1$, $Z_{PF} = 2$ and $Z_{PF} \geq 3$ are found to be 1.57 ± 0.1, 0.89 ± 0.09 and 0.47 ± 0.11 respectively. Table 3.1 presents the mean multiplicities of different charged projectile fragments for the present work and compares the results with the results of other workers. It can be readily seen from this table that at about same energy the multiplicity of various charged projectile fragments increases with increase of size of the projectile. The results obtained from the present investigation are found to be consistent with such observations.

Table. 3.1 The average multiplicities of the different charged projectile fragments in ^{22}Ne, ^{24}Mg and ^{28}Si beams with the interaction of emulsion at 3.7 AGeV and 4.5 AGeV.

Fragments charge Z	Projectile nucleus	Em	Reference
	^{22}Ne	1.36±0.02	[27]
1	^{24}Mg	1.61±0.04	[6]
	^{24}Mg (4.5 AGeV)	1.57±0.01	[Pw]
	^{28}Si	1.53±0.05	[28]
	^{22}Ne	0.82±0.02	[27]
2	^{24}Mg	0.86±0.03	[6]
	^{24}Mg (4.5 AGeV)	0.89±0.09	[Pw]
	^{28}Si	1.06±0.03	[28]
	^{22}Ne		
≥3	^{24}Mg	0.48±0.01	[27]
	^{24}Mg (4.5 AGeV)	0.49±0.03	[6]
	^{28}Si	0.47±0.11	[Pw]
		0.49±0.02	[28]

As the mean multiplicities of various charged projectile fragments are found to vary with the mass (size) of the incident nucleus, in Fig. 3.1 the mean multiplicities of the various charged projectile fragments are therefore plotted as a function of projectile mass number A_P. The mean multiplicities of projectile fragments having $Z_{PF} = 1$, $Z_{PF} = 2$ and $Z_{PF} \geq 3$ are denoted by $<N_p>$, $<N_\alpha>$ and $<N_f>$ respectively.

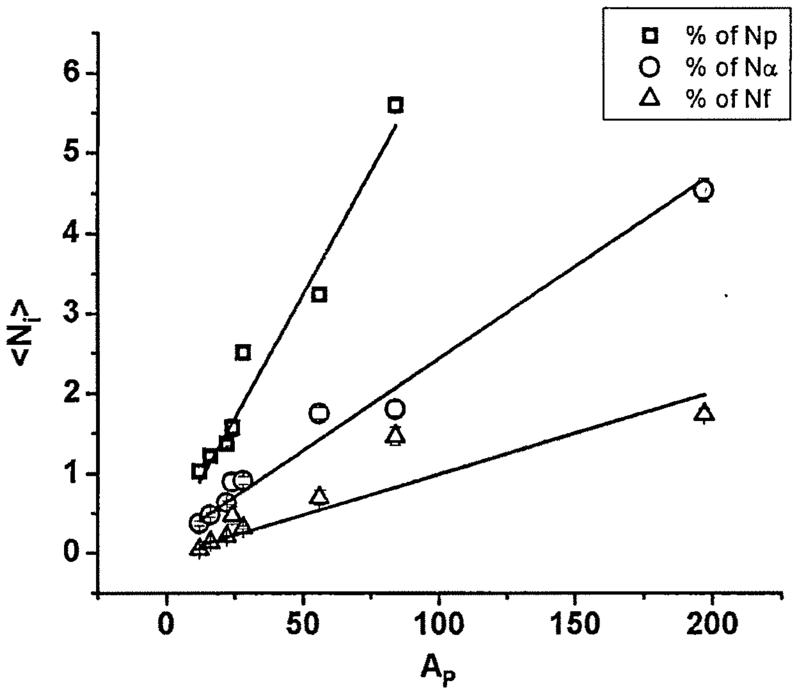

Fig. 3.1 The mean multiplicity of PFs $<N_i>$ as a function of the projectile mass number A_p in the interactions of various projectile with Em nuclei

The straight lines shown in the figure are the best fitted lines for the experimental data points with R^2 values equal to 0.986, 0.969 and 0.994 for the variations of $< N_p>$, $< N_\alpha>$ and $<N_f>$ respectively. It could be readily seen from this plot that the correlation between the yield of $< N_\alpha>$ and $< N_f>$ with A_P is weaker than that of $<N_p>$, thereby indicating a stronger dependence of the mean multiplicity of the singly charged projectile fragments on the projectile mass. This observation supports the result obtained by S. Fakhraddin and M. A. Rahim [29] for the interactions of different projectiles with emulsion at 4.1-4.5 AGeV. Such observations have also been supported by M.A. Jilany [6] for the studies on ^{24}Mg-

AgBr interactions at 3.7A GeV and for ^{16}O-AgBr interactions at 3.7A GeV by C. R. Meng et al. [30].

The increase in the mean multiplicity of $Z_{PF} = 2$ with the increase of projectile mass may be due to the fact that in case of a large projectile, on the average a large portion of the incident nucleus remains out side the overlapping region resulting a large projectile spectator to disintegrate.

3.2.1.2 Multiplicity distribution of projectile fragments

The multiplicity distribution of various projectile fragments emitted from ^{24}Mg-Em interactions at 4.5 AGeV is shown in Fig. 3.2. The black line is the fitted curve of the distribution with a Poisson function. The calculated standard deviation of the distribution is found to be 1.306 ± 0.46.

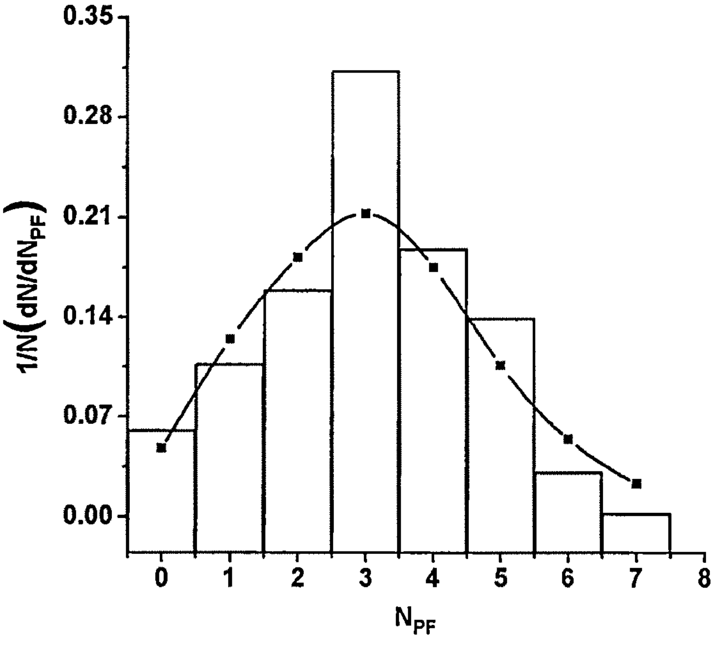

Fig. 3.2 Variation of normalized multiplicity of projectile fragments for Mg-Em interactions at 4.5 AGeV.

The width of the distribution at half maximum is 3.5 ± 0.30 with the tail extending up to 7. The figure indicates that most of the events in the data sample have 3 to 4 projectile fragments. On the other hand, the results obtained by Jain et al. [31] in case of ^{238}U-Em interactions at 0.96 AGeV showed that most of the events have multiplicity equal to 9. In comparison to present results on ^{24}Mg-Em interaction, the distribution of ^{84}Kr-AgBr [32], ^{238}U-Em interactions has longer tail and a larger width. This is probably due to the fact that a heavier beam breaks up into a large number of fragments with various charges resulting in increased multiplicity of projectile fragments.

3.2.1.3 Multiplicity distribution of $Z_{PF} = 1, 2$ and ≥ 3 projectile fragments

The studies of multiplicity distribution of projectile fragments are important for investigating the underlying mechanism of nuclear fragmentation [25]. Most significantly, the helium projectile fragments produced from various heavy ion beams at different energies have been studied extensively during the last one and half decade [25, 33-40]. These studies have revealed that the multiplicity distributions of alpha fragments obey a universal scaling law and that the transverse momenta distributions can be explained by two or three different emission sources at different temperatures. Present studies on ^{24}Mg-Em interactions are expected to provide some more information on the fragmentation mechanism of the projectile nucleus into helium fragments at Dubna energy.

The distributions of $Z_{PF} = 1, 2$ and ≥ 3 projectile fragments are shown in Figs. 3.3 to 3.5 taking the total ensemble of minimum biased events. Multiplicities for projectile $N_z > 1$ with $Z_{PF} \geq 5$ were not observed, i.e. the cross-section for fragmentation of ^{24}Mg in emulsion into two pieces each of $Z_{PF} = 5$ or 6 is smaller than 5.8×10^{-4} of the total inelastic cross-section [41].

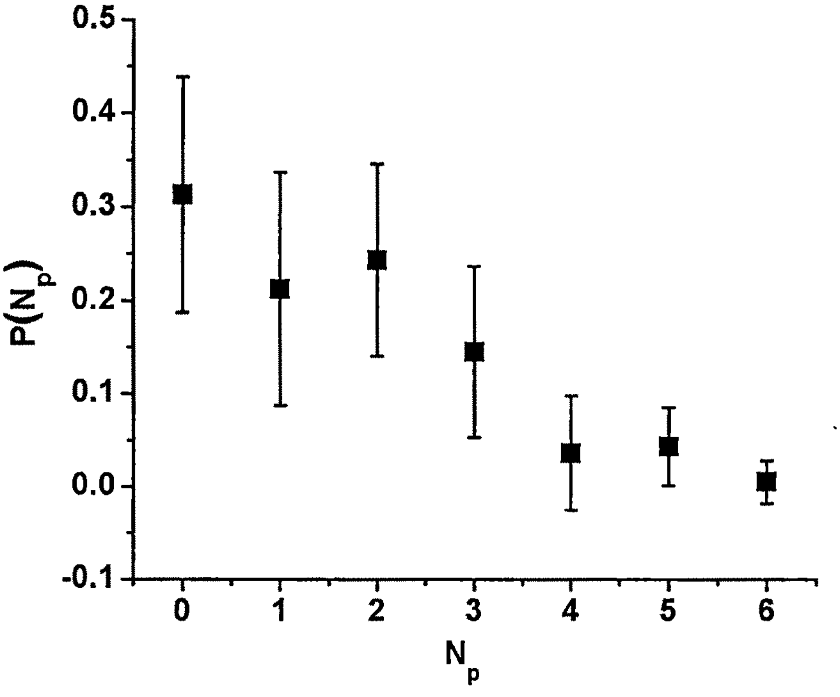

Fig. 3.3 Normalized multiplicity of Z_{PF} =1 projectile fragments.

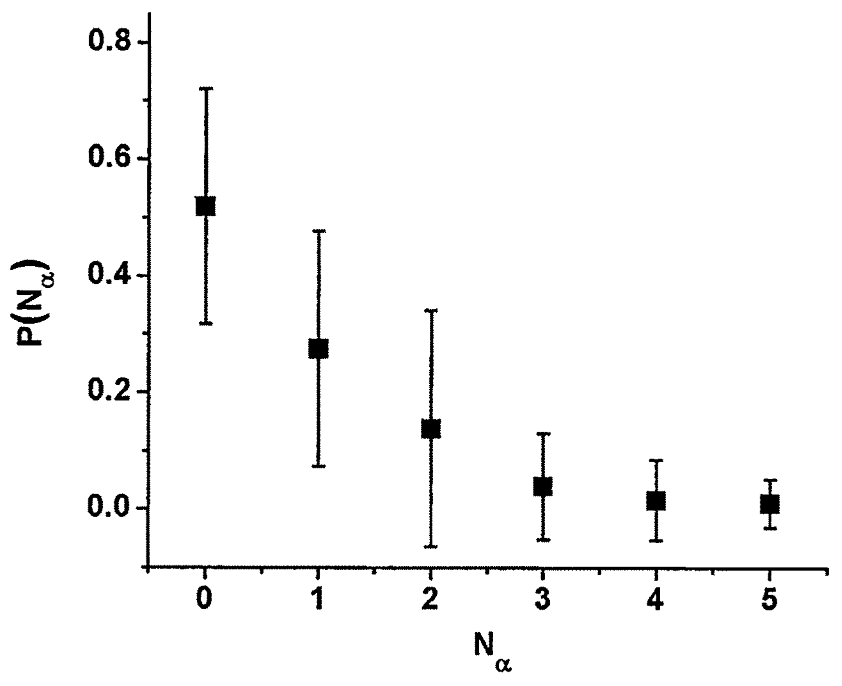

Fig. 3.4 Normalized multiplicity of $Z_{PF}=2$ projectile fragments.

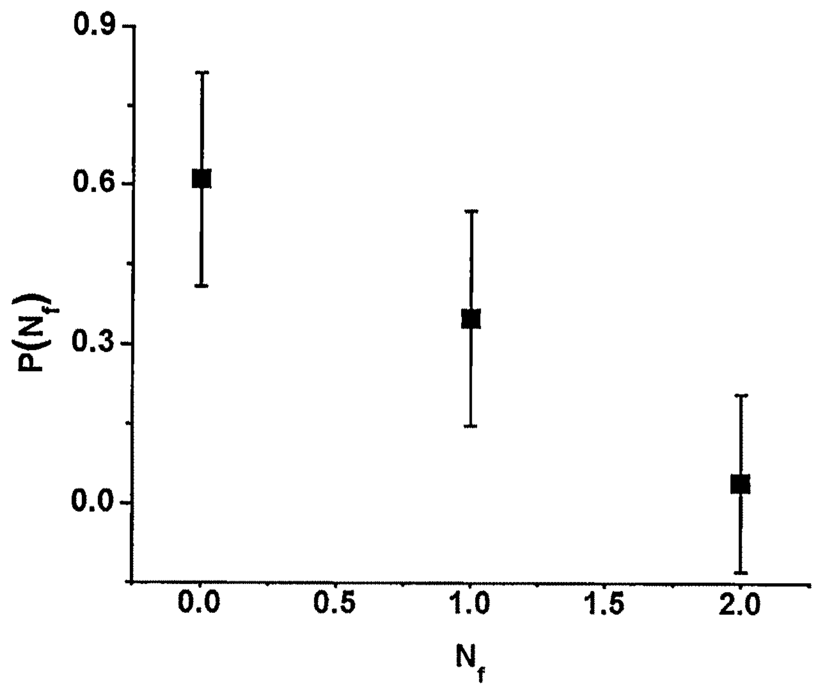

Fig. 3.5 Normalized multiplicity of $Z_{PF} \geq 3$ projectile fragments.

It is quite evident from the Fig. 3.4 that, for the present study, most of the events in the data sample have no $Z_{PF} = 2$ projectile. In case of interactions of 4.5 A GeV ^{12}C, ^{16}O and ^{28}Si and 4.1 AGeV ^{22}Ne projectiles with AgBr nuclei also, most of the events in the data sample were found to have no $Z_{PF} = 2$ projectile fragments [29]. Similar results were also reported by other workers where most of the events do not have any $Z_{PF} = 2$ projectile fragments [29, 36, 42-44]. On the other hand, the results obtained by M.L. Cherry et al. [45] on ^{197}Au-AgBr interactions at 10.7 AGeV reveal that most of the events in the data sample have four $Z_{PF} = 2$ projectile fragments. Thus, it appears that a larger mass of the projectile nucleus results in the emission of a larger number of $Z_{PF} = 2$ projectile fragments. It is therefore evident that the fragmentation mechanism differs considerably in smaller and larger mass systems.

In a similar way, from the Fig. 3.5 it is clear that the occurrence of $Z_{PF} \geq 3$ projectile fragments is zero in most of the events of the entire sample of data of this work. M.L. Cherry et al. [45] and P.L. Jain et al. [46] have found the mode of the multiplicity distribution of $Z_{PF} \geq 3$ projectile fragments at 1 for 10.6 AGeV ^{197}Au-AgBr and 1 AGeV ^{238}U-Em interactions respectively. It is also interesting to note that the probability of occurrence of events having $N_f = 0$ decreases with increasing mass number of the projectile. Similar results were also reported by other workers such as A.El-Naghy et al. [47] and also by T.Ahmed and M. Irfan [48] in case of ^{28}Si-Em interactions at 4.5 AGeV and comparing their results with the corresponding distributions for ^{24}Mg-Em interactions and ^{12}C-Em interactions [49] respectively at the same incident energy. Such studies show that heavy beams rarely yield events having no heavier fragments.

Thus the probability of projectile multifragmentation (events having two or more fragments with $Z_{PF} \geq 3$) has been found to increase as we go from ^{24}Mg to ^{238}U.

3.2.2 Multiplicity correlations

As mentioned earlier, the total charge Q_{pf} of the projectile spectator fragments can be related to the impact parameter or the degree of centrality of the collisions. The events with small Q_{pf} (i.e. $Q_{pf} \leq 2$) are considered as central collisions, where the participant part is large and large numbers of projectile and target nucleons actually take part in the reaction. On the other hand, events having large Q_{pf} (i.e. $Q_{pf} \sim Q_{beam}$) are considered as peripheral collisions with very few nucleons participating in the reaction. Those collisions lying in between central & peripheral collisions are called quasi-central collisions.

The variation of multiplicity distribution of produced particles, which is also considered as the degree of centrality of collision, with Q_{pf} is presented in Fig. 3.6(a) for ^{24}Mg-Em interactions at 4.5 AGeV. The results obtained are compared with the results of ^{84}Kr-Em interaction at 0.95 A GeV (GU Group) [32] and is shown in Fig. 3.6(b). From these plots it is found that, for both the systems, the mean number of produced particles decreases exponentially with the increase of Q_{pf} showing strong correlation between $\langle N_s \rangle$ and Q_{pf}. Similar results have been reported by M El-Nadi et al. [50] for ^{28}Si-Em interactions at 14.6 AGeV.

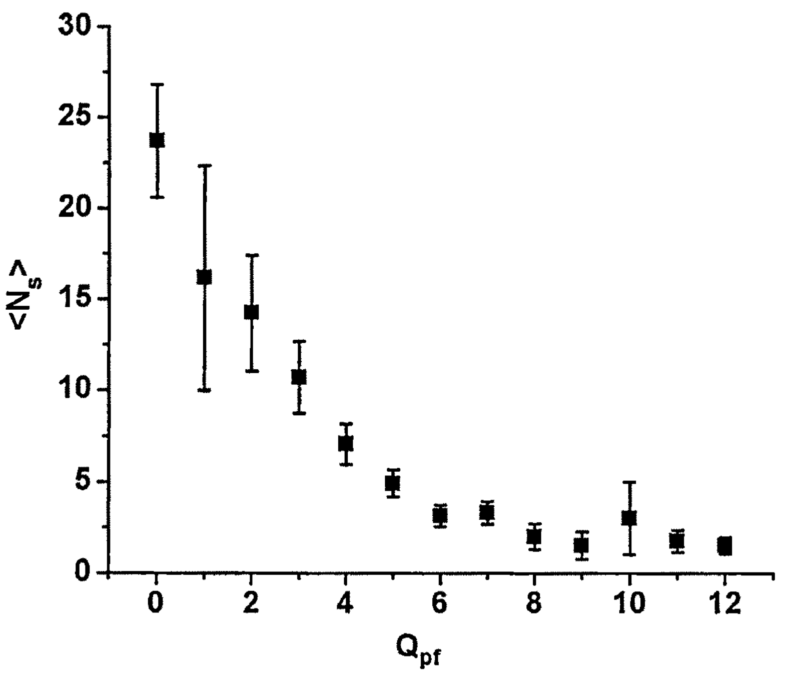

Fig. 3.6(a) Variation of $\langle N_s \rangle$ with Q_{pf} for Mg-Em interactions.

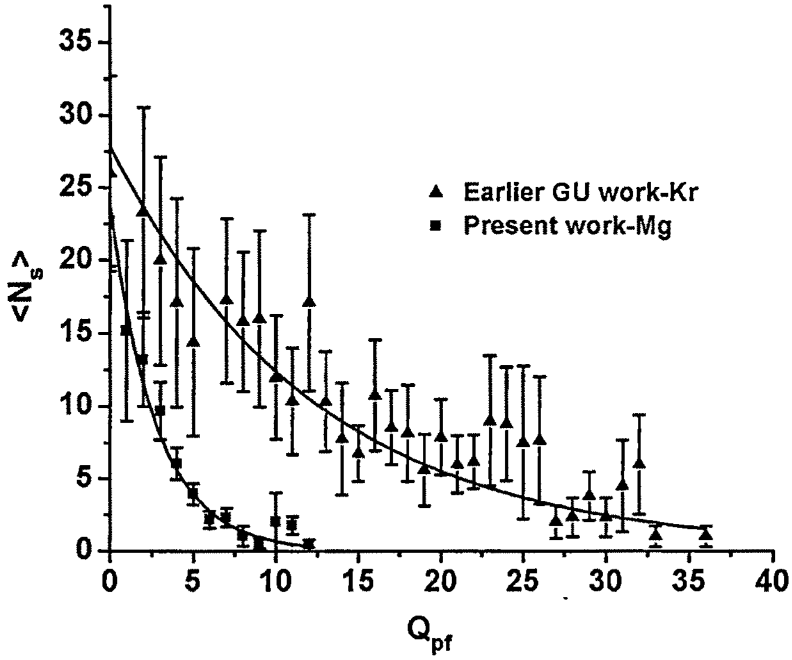

Fig. 3.6(b) Variation of $<N_s>$ with Q_{pf} for Mg-Em and Kr-Em interactions.

The number of grey tracks N_g produced by the knocked out proton is often considered as a measure of violent nucleon-nucleon collision.

In Fig. 3.7(a), the variation of $<N_g>$ is plotted as a function of Q_{pf} for ^{24}Mg-Em interactions. From this plot it is observed that the yield of fast target associated protons decreases exponentially with Q_{pf}. However a linear variation of $<N_g>$ with Q_{pf} for ^{84}Kr-Em interactions [32] at 0.95 AGeV is readily evident from Fig. 3.7(b). Similar linear negative correlation have been reported by M.I Adomovich et al. [51] and Fu Hu Liu [52] for ^{16}O-Em and ^{28}Si-Em interaction respectively at 3.7 AGeV and also by Keasnov et al. [8] for ^{84}Kr-Em interactions at 0.95 AGeV. M EI- Nadi et al. have also reported a decrease in the mean number of fast protons with the increase of Q_{pf} for ^{28}Si-Em interaction at 14.6 AGeV [50].

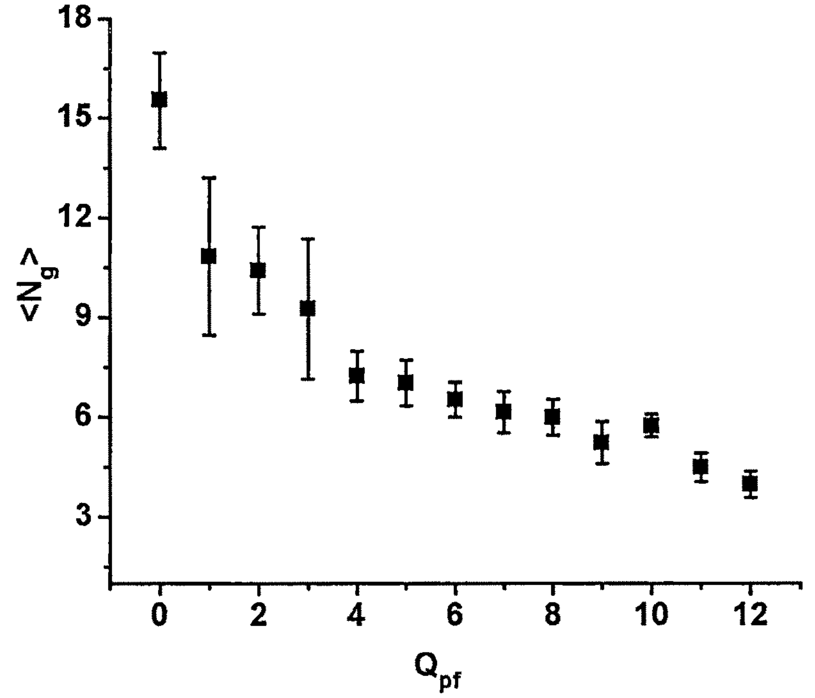

Fig. 3.7(a) Variation of $\langle N_g \rangle$ with Q_{pf} for Mg-Em interactions.

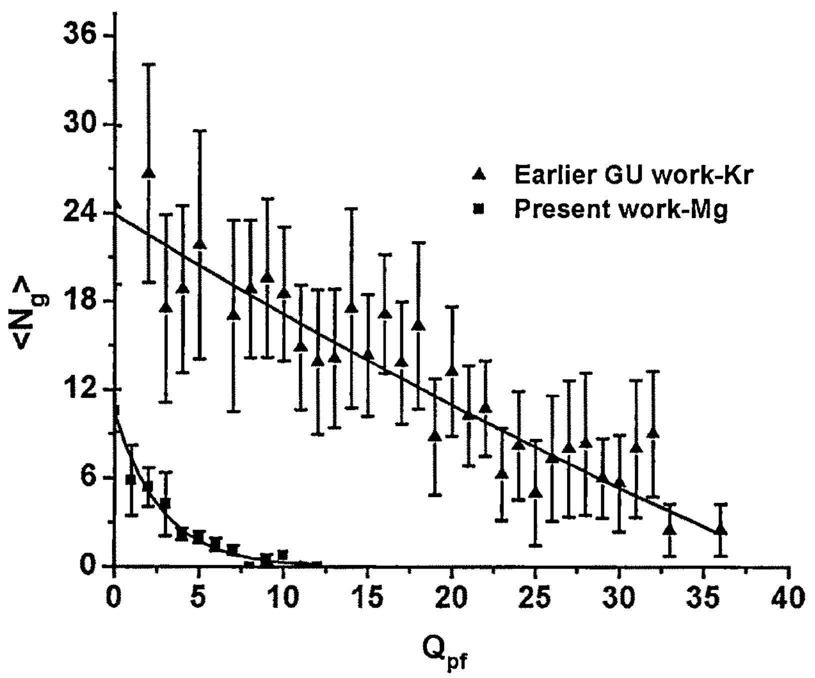

Fig. 3.7(b) Variation of $\langle N_g \rangle$ with Q_{pf} for Mg-Em and Kr-Em interactions.

The number of black tracks N_b produced by evaporated particles or fragments emitted at the last stage of heavy ion collision are considered to be measure of excitation energy of the target spectator.

The dependence of $\langle N_b \rangle$ on Q_{pf} for Mg-Em interaction of the present work and for Kr-Em interaction of earlier GU group [32] work have been presented in Figs. 3.8(a) and 3.8(b) respectively. It is interesting to note from these plots that while in case of Mg-Em interactions there exists a strong negative correlation between $\langle N_b \rangle$ and Q_{pf}, for Kr-Em interaction the correlation is absent or extremely weak indicating that nearly same amount of excitation energy was deposited to the residual target nucleus, irrespective of the degree of centrality of collision. The excess energy that might have been pumped into the system due to increased nucleon-nucleon interactions in central collision of heavy projectile is being used up in the production of new particles [8, 51-53].

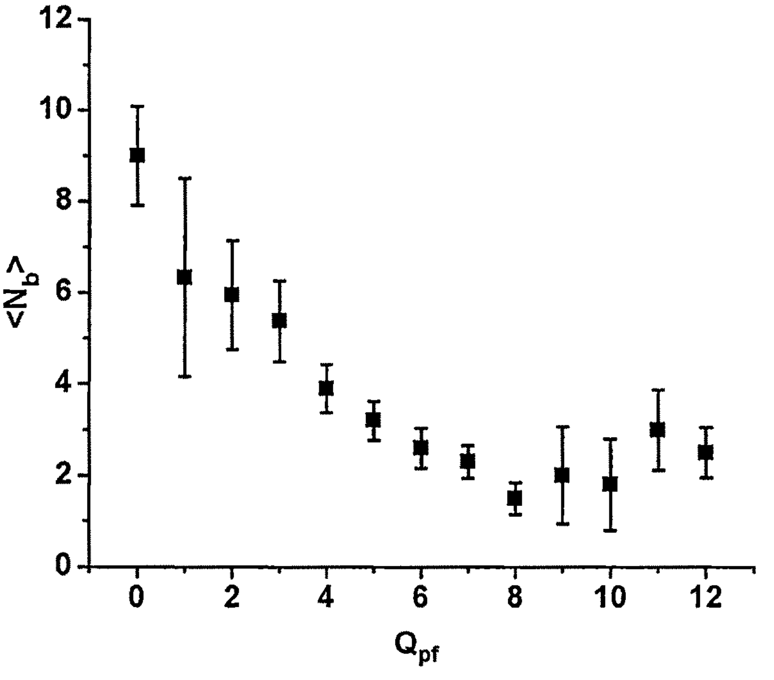

Fig. 3.8(a) Variation of $\langle N_b \rangle$ with Q_{pf} for Mg-Em interactions.

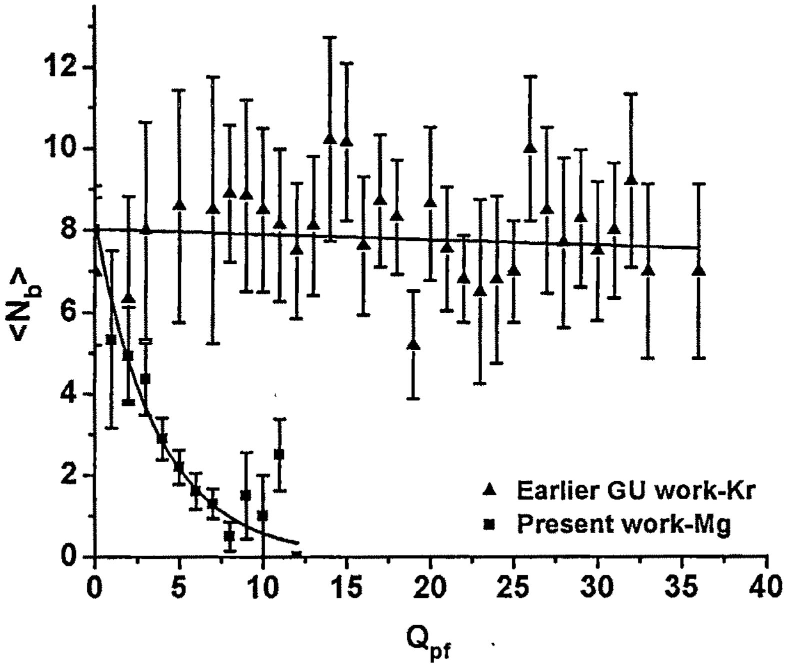

Fig. 3.8(b) Variation of $\langle N_b \rangle$ with Q_{pf} for Mg-Em and Kr-Em interactions.

The number of heavily ionizing tracks N_h ($=N_g+N_b$) produced mostly by fast and slow protons and fragments of target spectator is often considered as a measure of degree of centrality of collision. Thus it is expected that there should exists some correlation between N_h and Q_{pf}.

The correlation between $\langle N_h \rangle$ and Q_{pf} for the present investigation is shown in Fig. 3.9(a). It is observed that with the increase of Q_{pf}, the mean number of heavily ionizing particles decreases exponentially in case of ^{24}Mg-Em showing strong co-relation with Q_{pf}. A linear dependence of $\langle N_h \rangle$ on Q_{pf} that has been observed for ^{84}Kr-Em interaction at 0.95 AGeV is shown in Fig. 3.9(b). Similar results have been reported by M. E. Solite et al. [53] for ^{24}Mg-Em and Fu Hu Liu [52] for ^{84}Kr-Em interactions.

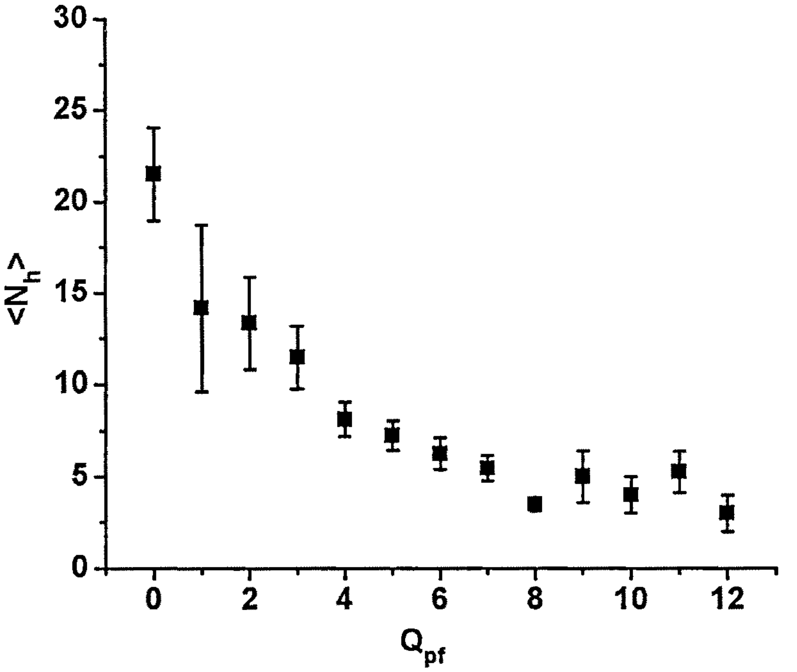

Fig. 3.9(a) Variation of <N_h> with Q_{pf} for Mg-Em interactions.

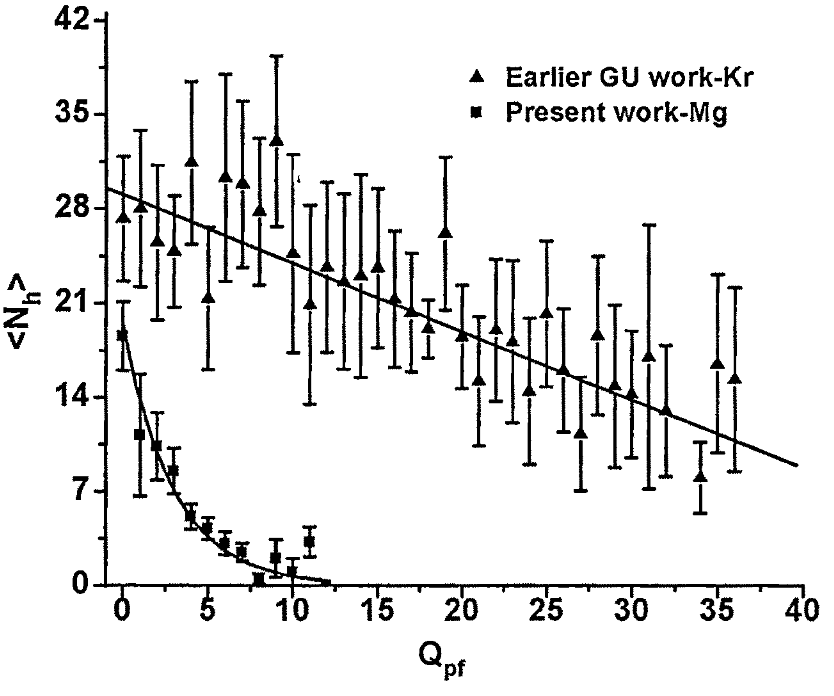

Fig. 3.9(b) Variation of <N_h> with Q_{pf} for Mg-Em and Kr-Em interactions.

3.2.3 Influence of mass of the fragmenting system on projectile multifragmentation

In the study of projectile multifragmentation, Z_b is considered to be one of the important observables. It is the sum of all projectile fragments with charge $Z_{PF} \geq 2$, which is also known as bound charge and gives the measure of the mass of the fragmenting system. Correlation between mean number of intermediate mass fragments (IMFs) and Z_b is one of the most interesting aspects of studying projectile multifragmentation that has been studied by different workers for various systems at different energies [13].

The variation of $\langle N_{IMF} \rangle$ on the mass of the fragmenting system is shown in Fig. 3.10(a) for Mg-Em interactions. Fig. 3.10(b) represents the same plot comparing the result of the present investigation with the lightest projectile system with the results reported by other workers for other heavier projectiles. It can be readily seen that for the present Mg-Em work the maximum value of $\langle N_{IMF} \rangle$ corresponds to the value of Z_b = 6-7. The value of bound charge corresponding to the maximum value of average number of intermediate mass fragments systematically increases with the increase of mass of the projectile. Thus the result of present investigation on the dependence of $\langle N_{IMF} \rangle$ on Z_b is found to be consistent with the results reported by ALADIN and KLMM group [13, 15-16].

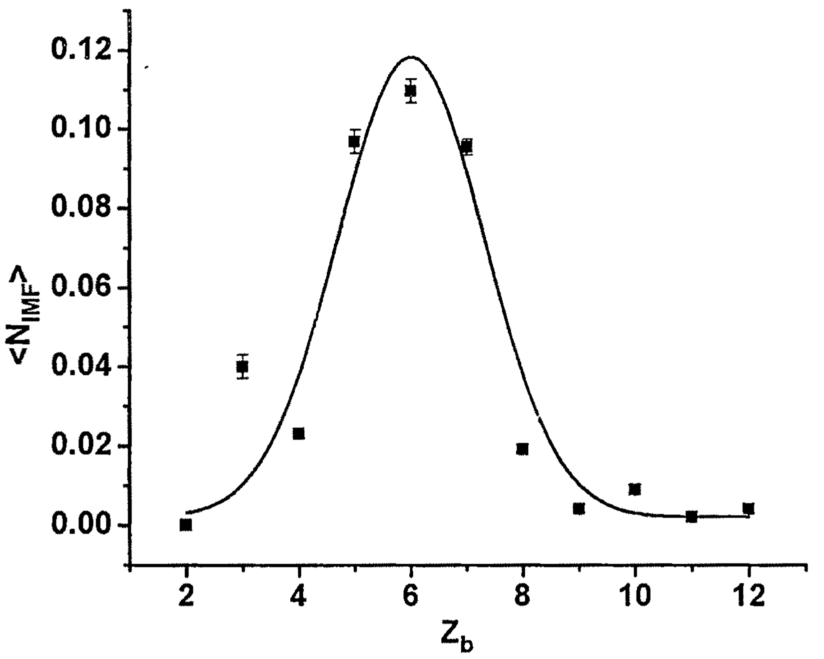

Fig. 3.10(a) Variation of $<N_{IMF}>$ with Z_b for Mg-Em interactions.

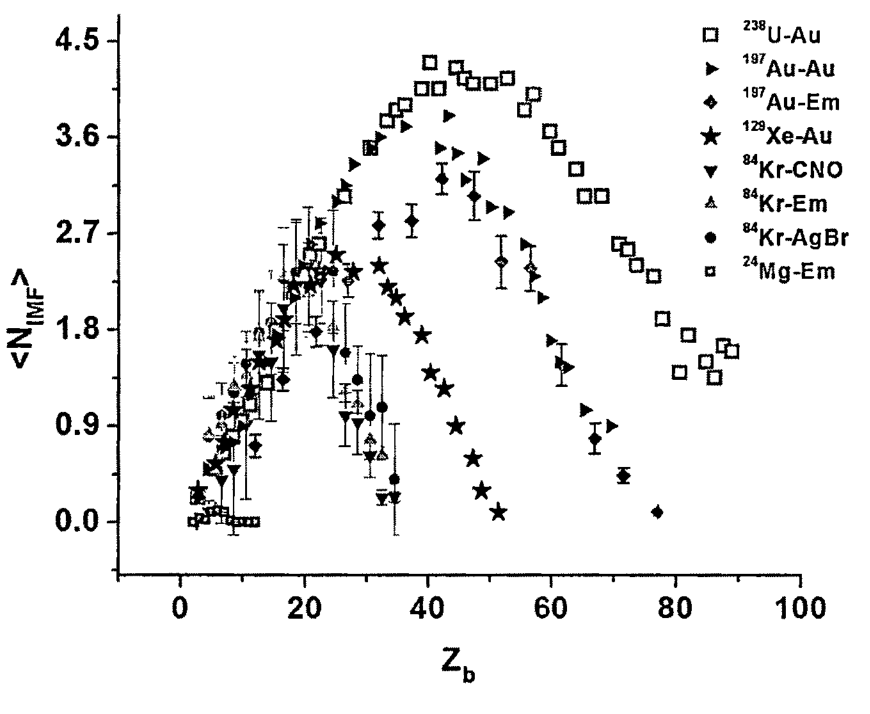

Fig. 3.10(b) Variation of $<N_{IMF}>$ with Z_b for the works of different groups.

To examine the size effect, the variation of <N_{IMF}> on Z_b normalized with the projectile charge Z_p, is plotted in the Fig. 3.10(c). The peaking behaviour of all the systems in the figure indicates a clear size effect for the studied system. It can be readily seen from this plot that for all the studied systems, the maximum value of <N_{IMF}> corresponds to the same Z_b / Z_p value indicating a clear evidence of system size effect on the average number of emitted intermediate mass fragments.

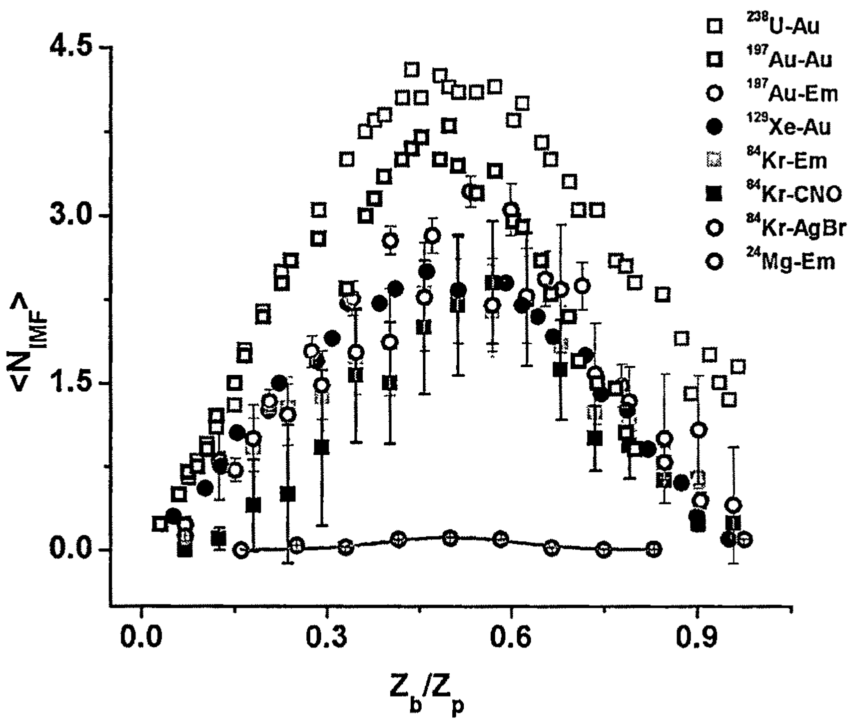

Fig. 3.10(c) Variation of <N_{IMF}> on Z_b normalized with the projectile charge Z_p.

3.2.4 Spatial distribution of projectile fragments

As mentioned earlier nuclear emulsion provide best spatial resolution than any other detector used in experimental high energy physics. Moreover it has the advantage of detecting charged secondaries that might have been emitted even in the extreme forward direction (0° acceptance). Because of these features of emulsion it has been found extremely useful to study the spatial distribution of those charged particle such as PFs that are emitted in the extreme forward angle.

3.2.4.1 Angular distribution of $Z_{PF} = 1$ projectile fragments

The normalized angular distribution of the $Z_{PF} = 1$ projectile fragments is shown in Fig. 3.11 and is fitted with a Gaussian function.

The centre and width at half maximum of the fitted Gaussian distribution are found to be 1.41 ± 0.06 and 1.30 ± 0.16 respectively. In case of ^{28}Si-Em interactions at 4.5 AGeV [47] it was reported that most of the singly charged projectile fragments were emitted in a narrow forward cone peaking at 0.9^{o}.

3.2.4.2 Angular distribution of $Z_{PF} = 2$ projectile fragments

Fig. 3.12 represents the angular distribution of ^{4}He projectile fragments and shows that most of the fast alpha fragments are emitted at an angle 1- 2^{o}. The peak of the fitted distribution is found to be at 1.10 ± 0.04 and the characteristic width is 0.815 ± 0.09.

The centre and characteristic width at half maximum of the fitted distribution as reported by V. Singh [54] for 0.95 AGeV ^{84}Kr-Em interactions were found to be $1.09^{o} \pm 0.18^{o}$ and 3.73 ± 0.33^{o} respectively. On the other hand, for ^{28}Si-Em interactions at 4.5 AGeV [47], it was reported that most of the doubly charged projectile fragments were emitted in a narrow forward cone peaking at 0.6^{o}. The results of R. Bhanja et al. [55] on ^{14}N-Em interactions at 2.1 AGeV reveal that the emission angle of most of the helium projectile fragments is 0^{o}. Clearly there lies inconsistency in the results of emission angles of fast projectile fragments with $Z_{PF} = 2$ and such discrepancy may be attributed to the inaccuracy of various measuring techniques.

3.2.4.3 Angular distribution of $Z_{PF} \geq 3$ projectile fragments

The angular distribution of $Z_{PF} \geq 3$ projectile fragments is plotted in Fig. 3.13 and the distribution is fitted with a Gaussian function.

It is observed that most of the heavier projectile fragments are confined to a narrow forward cone $0.973^{o} \pm 0.07^{o}$ and the characteristic width of the distribution at half maximum is found to be $0.703^{o} \pm 0.22^{o}$. In case of ^{84}Kr-Em interactions at

0.95 AGeV it was reported in ref. [54], that most of the heavier projectile fragments were confined to a narrow forward cone peaking at 0^o, having a characteristic width at half maximum of $\sim 1^o$. In case of ^{28}Si-Em interactions at 4.5 AGeV [47] it was observed that most of the heavy projectile fragments were emitted in a narrow forward cone peaking at 0.2^o.

From all the above discussions it may therefore be inferred that the width of the distribution at half maximum decreases with the increase of the charge of the projectile fragments. This result is found to be consistent with the result reported by A. El-Naghy et al. [47] for ^{28}Si-Em interactions at 4.5 AGeV.

It is further observed from these figures that with the increase of the charge of the PFs, the peaks of the fitted distributions shift towards lower θ_{PF} value indicating that most of the heavier PFs are emitted at narrow forward angle than that of lighter ones.

The standard deviations of projected angular distributions of all the projectile fragments for different systems in emulsion as discussed above is listed in table 3.2.

Table. 3.2 Standard deviations of projected angular distributions of projectile fragments for different systems in emulsion.

Reaction Channel	$Z_{PF}=1$	$Z_{PF}=2$	$Z_{PF}\geq 3$	Energy in AGeV	Reference
^{12}C-Em	1.3 ± 0.09	0.54 ± 0.02	0.33 ± 0.02	4.5	56
^{24}Mg-Em	1.41 ± 0.06	1.10 ± 0.04	0.97 ± 0.07	4.5	PW
^{28}Si-Em	1.26 ± 0.106	0.77 ± 0.024	0.29 ± 0.03	4.5	47
^{84}Kr-Em	1.73 ± 0.043	1.44 ± 0.14	0.71 ± 0.07	0.95	32

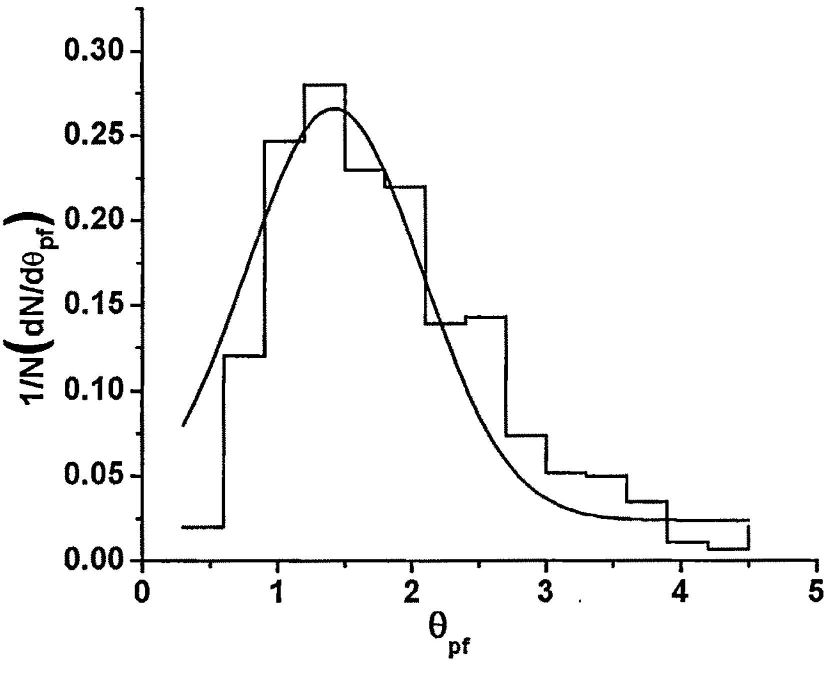

Fig. 3.11 Angular distribution of Z_{PF}=1.

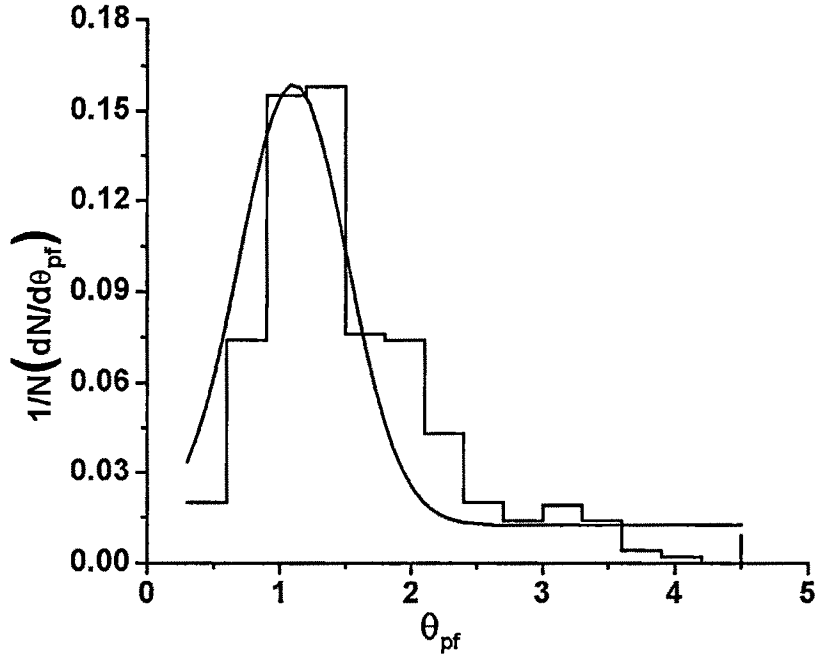

Fig. 3.12 Angular distribution of Z_{PF} =2.

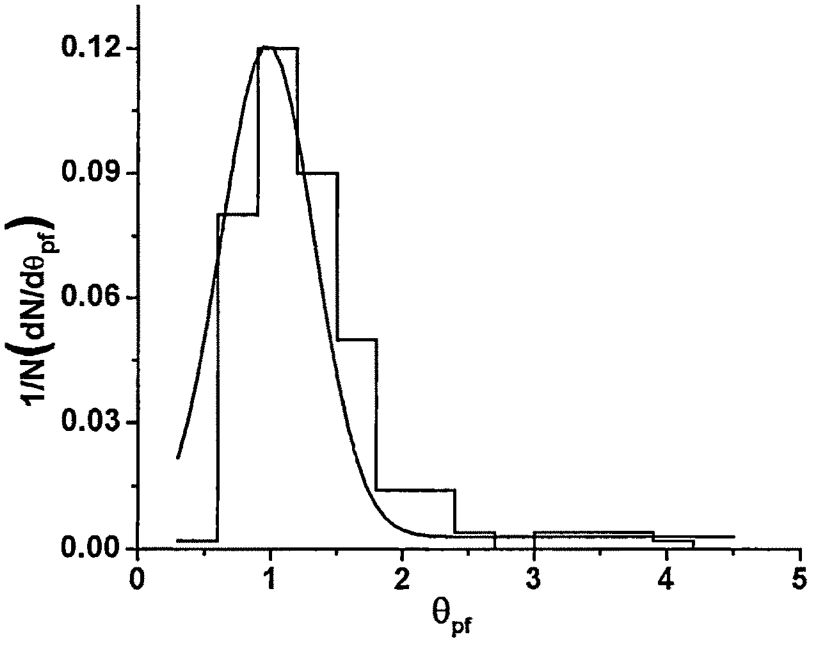

Fig. 3.13 Angular distribution of $Z_{PF} \geq 3$.

References

1. R. J. Glauber, *In Lectures of Theoretical Physics*, Vol.1 (1959) 315.
2. N. P. Andreeva et al., *Yad. Fiz.* **47** (1988) 157.
3. A. El-Naghy et al., *Nuovo Cimento* **A 71** (1982) 245.
4. A. El- Naghy et al., *Nuovo Cimento* **A 107** (1994) 279 and references therein.
5. J. Cugnon and D. L'Hote, *Nucl. Phys.* **A 397** (1983) 519.
6. M. A. Jilany, *Phys. Rev.* **C 70** (2004) 14901.
7. M. A. Jilany et al., *Int. J. Mod. Phys.* **4(4)** (1995) 815.
8. S. A. Keasnov et al., *Czechoslovak J. Phys.* **46 (6)** (1996) 513.
9. N. N. Abd Allah et al., *Int. J. Mod. Phys.* **E 10 (1)** (2001) 55.
10. I. Otterland, Proc. 4th High Energy Heavy Ion Summer Study Berkeley, LBL report, LBL **7766** (1978) 289.
11. R. R. Joseph et al., *Phys. Rev. Lett.* **54** (1985) 731.
12. A.C. Mueller, Proc. of the 3rd Int. Conf. on Radioactive Nuclear Beams, (East Lansing, USA, May, 1993), D.J. Morrisay, Ed. Edition Frontieres (Gif-sur-Yvette, France, 1993) 1.
13. J. Hubele et al., *Z. Phys.* **A 340** (1991) 263.
14. A. Dabrowska et al., *Acta Physica Polonica* **B 31(3)** (2000) 725.
15. M. L. Cherry et al., *Phys. Rev.* **C 52(5)** (1995) 2652.
16. A. Schuttauf et al., *Nucl. Phys.* **A 607** (1996) 457.
17. P. L. Jain et al., *Phys. Rev. Lett.* **74** (1995) 1534.
18. C. A. Ogilive et al., *Phys. Rev. Lett.* **67** (1991) 1214.
19. P. Kruetz et al., *Nucl. Phys.* **A 556** (1993) 672.
20. G. Shing and P.L Jain, *Phys. Rev.* **C 49** (1994) 3320.
21. J. Hubele et al., *Phys. Rev.* **C 46** (1992) R1577.

22. N. N. Abd-Allah, *J. Phys. Soc. Jap.* **69**(4) (2000) 1068.

23. R. Arora et al., *Z. Physik. A – Atomic Nuclei* **333** (1989) 373.

24. K. Sengupta et al., *Europhys. Lett.* **5**(2) (1988) 135..

25. M. M. Aggarwal, *Proceedings on 3rd International Conference on Physics and Astrophysics of Quark Gluon Plasma,* editors B. C. Sinha, D. K. Srivastava and Y. P. Vyogi (Narosa Publishing House, New Delhi, India, 1998).

26. Fu-Hu Liu et al., *Chin. J. Phys.* **44**(3) (2006) 202.

27. N. P. Andreeva et al., *Sov. J. Nucl. Phys.* **47** 102 (1988) 22

28. B. K. Singh and S. K. Tuli, *Nuovo Cimento* Soc. Ital. Fis. **A 112** 1093 (1999) 23.

29. S. Fakhraddin and M. Rahim, *Phys. Scr.* **78** (2008) 01501.

30. Cai-Rong Meng and Dong-Hai Zhang, *Chin. J. Phys.* **44**(1) (2006) 1.

31. P. L. Jain et al., *Phys. Rev. Lett.* **68**(11) (1992) 1656.

32. S. Sengupta, *Ph.D. Thesis* , Gauhati University, Guwahati, Inda.

33. Fu-Hu Liu, *Phys. Rev.* **C 62** (2000) 024613.

34. Fu-Hu Liu, *Chin. J. Phys.* **41**(5) (2003) 486.

35. Zhang Dong-Hai et al., *Chin. Phys. Soc.* **13**(8) (2004) 1239.

36. M. A. Jilany, *Eur. Phys. J.* **A 22** (2004) 471.

37. M. El-Nadi and S. M. Abdel-Halim, *J. Phys.* **G 28** (2002) 1251.

38. M. El-Nadi et al., *Int. J. Mod. Phys.* **E 2** (1993) 381.

39. M. I. Adamovich et al., (EMU-01 Collaboration), *Phys. Lett.* **B 338** (1994) 397.

40. B. Bhattacharjee and B. Debnath, *Journal of Physics: Conference Series* **110** (2008) 122003.

41. S. El-Sharkawy et al., *IL Nuovo Cimento* **A112** (9) (1999) 941.

42. N. N. Abd-Allah, *Nucl. Sci. J.* **30** (1993) 167.

43. N. N. Abd-Allah and M. Mohery, *Czech. J. Phys.* **51**(11) (2001) 1189.

44. G. M. Chernov et al., *Nucl. Phys.* **A 412** (1984) 534.

45. M. L. Cherry et al., *Eur. Phys. J.* **C 5** (1998) 641.

46. P. L. Jain and G. Singh, *Phys. Rev.* **C 47**(5) (1993) 2382.

47. A. El-Naghy et al., *Tr. J. of Physics* **23** (1999) 1051.

48. T. Ahmed and M. Irfan, *Mod. Phys. Lett.* **A 6**(36) (1991) 3313.

49. T. Ahmed, *Ph.D Thesis*, A.M.U., Aligarh (1991).

50. M El–Nadi et al., *J. Phys. G: Nucl. Part. Phys.* **25** (1995) 1169.

51. M. I. Adomovich et al., *Preprint JINR* **E1-92** (1992) 569.

52. Fu-Hu Liu, *Chin. J. Phys.* **40 (2)** (2002) 159.

53. M. E. Solite et al., *International Journal Physical Sciences* Vol **2** (12) (2007) 324.

54. V. Singh, *Ph.D. Thesis*, Banaras Hindu University, Varanasi, India (1998).

55. R. Bhanja et al., *Nucl. Phys.* **A 411** (1983) 507.

56. M. S. Ahmad et al., *Nucl. Phys.* **A 499** (1989) 821.

CHAPTER IV

INTERMITTENCY AND MULTIFRACTALITY IN THE FRAGMENTATION OF Mg PROJECTILE NUCLEI

4.1 Introduction

Nucleus-nucleus collisions at intermediate energy offer various possibilities to produce hot nuclei which often undergo break-up into smaller pieces having charges $Z_{PF} \geq 2$, resulting nuclear multifragmentation, where the excitation energy is near the binding energy. Within this region lies the possibility of seeing a phase transition and critical phenomena in the nuclear matter limit. One of the most important challenges of heavy ion physics is the identification and characterization of nuclear liquid-gas phase transition believed to be the underlying mechanism of nuclear multifragmentation process [1-2]. The striking characteristics of the systems undergoing continuous phase transition that might have taken place in the final stage of fragmentation of heavy ion collisions are believed to be the occurrences of fluctuations of the fragments charge (mass) distribution, that exist on all length scales in a small range of the control parameter. Such fluctuation may diverse or even tend to vanish near some critical value of the control parameter. A number of works on multifragmenting system at low energy ~ 1 AGeV [3-7] over all impact parameters exhibited large scale fluctuations. In the study of heavy ion collision, numerous techniques have been developed to analyze the fluctuations and the correlations for various physical quantities. In particular, one of the most powerful and promising possibilities seems to be the analysis of event-by-event data in terms of intermittency which is a statistical concept initially developed to study turbulent flows [8-9]. Intermittency in physical systems is studied by examining the scaling properties of the moments of the distributions of relevant variables over a range of scales. Białas and Peschanski first introduced the concept of intermittency to the study of dynamical fluctuations in the density distributions of particles produced in high energy collisions. To examine the intermittent pattern of fluctuations Bialas and Peschanski proposed the method of estimation of scaled factorial moments which has the advantage of quantifying dynamical fluctuations without the spurious influence of statistical fluctuations [8,10-12].

To understand the underlying physics of hadronization in QGP-hadron type phase transition, several works have been subsequently carried out to study the dynamical fluctuation of the prduced particles using SFM technique. There exists an abundant evidence of power law behaviour of produced particles in experimental data of e+e- annihilation [13-15], muon-hadron [16-17], hadron-nucleus [18-19], and nucleus-nucleus collision [18-22]. Later the technique of scaled factorial moment was also applied to study non-statistical fluctuations in the emission process of slow and fast target fragments. The investigations have been carried out with ^{16}O-AgBr (2.1 AGeV), ^{16}O-AgBr (60 AGeV), ^{32}S-AgBr (200 AGeV), ^{28}Si-AgBr (14.5 AGeV), ^{24}Mg-AgBr (4.5 AGeV) [23-27]. All these analyses show the presence of intermittent type of fluctuations in the emission of slow target fragments.

However, no such studies have been reported so far regarding the spatial distribution of projectile fragments. Projectile fragments have the momentum per nucleon almost equal to that of the parent nucleus and hence they are essentially emitted inside a narrow forward angle around the direction of the incident beam and remain relativistic. Hence unlike the target fragments, the heavy fragments of the projectile nucleus are very closely spaced having a very small angular separation. It has therefore always been a challenging task to study any such physical quantity that is related to the spatial distribution of the PFs. To understand thoroughly the complicated mechanism of heavy ion collision one has to take into account how the produced particles as well as the fragments of both TFs and PFs coming out of an interaction are distributed in phase space.

In general, the constituents of the spectator part of the projectile as well as the spectator part of the target can be well separated at energies like this work. But the experimental work on high energy A-A collisions carried out with electronic detectors to study PFs have limited coverage in the pseudo rapidity range. Nuclear emulsion on the other hand is a global 4π detector and has the best spatial resolution (0.1mrad) among all the detectors currently in use in experimental high energy physics [28-29]. Even the largest collaboration [30] that has been formed to study different characteristics of projectile fragments with active detectors has reported their limitation over the angular acceptance. Because of this advantage nuclear emulsion has been found to be a useful tool particularly to study those properties which are related to the spatial distribution of emitted particle. Intermittency in the high energy A- A collisions is one such property. In this work an attempt has been made to study the emission spectra of projectile fragments in the light of intermittency (self similarity).

The concept of intermittency is in turn intimately connected to the fractal geometry of the object under investigation and hence the dynamics of the underlying physical process [31]. Mandelbrot [32], the pioneer, showed a new way of looking into the world of apparent irregularities or fractals. Fractal geometry allows us to mathematically describe systems that are intrinsically irregular at all scales. A fractal structure has the property that, if one magnifies a small portion of it, it still shows the same complexity as the entire system. Such behaviour of fractals is called 'scale symmetry'. Usually the term fractal is used to characterize systems with properties of self-similarity in general. If these properties can be described by a single exponent, one has a simple or homogeneous fractal, a monofractal. In a more complex case, the term multi-fractality is used when discussing generalized scaling. The most notable property of fractals is their dimensions. A formalism for treating fractal dimension and its generalization had already been developed and has been applied effectively to the study of intermittent behavior in turbulent fluid. The intermittency exponent ϕ_q characterizes the fractal structure of the distribution via the anomalous fractal dimensions d_q as $d_q = \phi_q /(q - 1))$, where q is the order of the moment. The anomalous fractal dimensions describe how the distribution changes with increasing resolution and reflect the fractal and multifractal structure of particle emission.

As mentioned earlier, there are phenomenological hints for intermittent behavior in the emission pattern of charged secondaries emitted from high energy nuclear collisions. It was Carruthers and Ming [33] who, possibly for the first time, investigated the fractal dimension in hadronic multiparticle production. Later Dremin [34] suggested the study of correlation dimension; Lipa and Buschbeck [35] considered other generalized dimensions. Hwa [36-37] then pointed out that in none of the above mentioned investigations a formalism could be developed for a systematic study of the fractal properties that can provide an effective means of describing a highly non-uniform rapidity distribution of produced particles. He then identified a new set of moment, called generalized moment, G_q that can be determined from particle multiplicities in narrow rapidity windows and drew some important inference on the nature of the dimensions D_q that are generalizations of the fractal dimensions for multifractal sets. Hwa also discussed the general properties of the spectrum of scaling indices and indicated how it can provide an effective means of describing a highly non-uniform rapidity distribution.

Here in this chapter an attempt has been made to interpret the observed power law dependence of normalized factorial moments on the phase space bin size, which is a signature of the self similarity in fluctuation pattern of particle multiplicity, in terms of fractal geometry.

Meanwhile, Satz and coworkers [38-39] studied the moments of the distribution of the size of spin clusters in the two-dimensional Ising model and found that intermittency occurs around and can be associated with the critical point of that system. In particular, they point to the usefulness of the (factorial) moments as a method for studying fragmentation or decay mechanisms [40].

Later Płoszajczak and Tucholski first introduced the SFM analysis for the study of dynamical fluctuations in fragment size distributions [3, 41-43] in the break-up of high energy nuclei in the nuclear emulsion. They studied the break-up of ^{197}Au nuclei at around 1 GeV/nucleon, and showed that the factorial moments of the charge distribution of the fragments increased like a power law with the increasing charge resolution, thus exhibiting the property of self similarity or otherwise the intermittency and concluded that the study of intermittency in nuclear fragmentation is relevant in the search for critical phenomena. Thus, it has been believed that cluster size distributions are intermittent at the critical point. A similar analysis, confirming the existence of intermittency in nuclear fragmentation, was later applied to the break-up of ^{238}U and ^{131}Xe nuclei with energies a few GeV/nucleon [4-9]. In this work an attempt has also therefore been made to study the possible signature of non thermal phase transition in the light of intermittency and self similarity in spatial as well as in the fragments charge distribution for 4.5 AGeV minimum biased ^{24}Mg-Em interactions.

4.2 Mathematical formalism for intermittency analysis

Before presenting the details of the method of analysis related to the estimation of SFM one important technical difficulty in studying this parameter should be addressed.

In the study of the fluctuation in phase space variable, scaled factorial moments are estimated following two techniques - one, called horizontal averaging, takes into account the non-statistical part of fluctuation in spatial distribution of particles in an event while the other, called vertical averaging, characterizes dynamical fluctuation in event space. The technique of vertical averaging has the limitation of losing information about the fluctuation in spatial distribution in an event. The method of horizontal averaging though takes into account fluctuations in density distribution in phase space in an event, has the limitation of its dependence on the shape of the single particle density distribution spectrum and therefore needs to be corrected by a factor called Fialkowski factor [44] to make it shape independent [44-45]. However, the shape dependence of the horizontally averaged scaled factorial moments can also be eliminated by converting single particle density distribution spectrum from η (cos *θ)* space to a distribution in $\chi(\eta)$, where $\chi(\eta)$ is a new cumulative variable [35,45-47] defined as:

$$\chi(\eta) = \frac{\int_{\eta_{min}}^{\eta} \rho(\eta)\, d\eta}{\int_{\eta_{min}}^{\eta_{max}} \rho(\eta)\, d\eta} \qquad (4.1)$$

In the above equation, the numerator corresponds to the total number of PFs which have η values less than or equal to a particular value of η and the denominator corresponds to the total number of PFs in the entire sample of data. Obviously, the new variable $\chi(\eta)$ should vary from 0 to +1.

4.2.1 Horizontally scaled factorial moment

Following the technique of Bialas and Peschanski [8,10] in the study of intermittency, the pseudorapidity interval $\Delta\eta$ is divided into M bins of equal size, $\delta\eta = \Delta\eta/M$.

Let n_m be the number of particles in the m^{th} bin, where m can take the values from 1 to M.

For a single event, the q^{th} order scaled factorial moment is defined as [8,10]:

$$F_q = M^{q-1}\sum_{m=1}^{M}\frac{n_m(n_m-1)\ldots\ldots\ldots\ldots\ldots\ldots(n_m-q+1)}{n(n-1)\ldots\ldots\ldots\ldots\ldots(n-q+1)} \tag{4.2}$$

where n is the total number of particles in the event in the pseudorapidity interval , and M is the number of bins in which $\chi(\eta)$) space is divided into bins of equal size:

$$d\chi = \frac{\chi_{\max} - \chi_{\min}}{M} = \frac{1}{M} \tag{4.3}$$

Here, $n = \sum_{m=1}^{M} n_m$

For an ensemble of events having varying multiplicities, the expression for scaled factorial moment is modified as [48]:

$$F_q = M^{q-1}\sum_{m=1}^{M}\frac{n_m(n_m-1)\ldots\ldots\ldots(n_m-q+1)}{<n>^q} \tag{4.4}$$

Here, <n> represents the mean multiplicity of projectile fragments of the population in the full $\chi(\eta)$ space and is defined as:

$$<n> = \frac{1}{N_{eV}}\sum_{i=1}^{N_{eV}} n \tag{4.5}$$

On averaging over the number of events in the data sample, the horizontally averaged normalized or scaled factorial moments is expressed by the following relation:

$$<F>_q = \frac{1}{<n>^q} < \frac{1}{M}\sum_{m=1}^{M} n_m(n_m - 1) --- (n_m - q - 1) > \tag{4.6}$$

where

$$n = \frac{1}{M}\sum_{m=1}^{M} n_m$$

Now dividing $\chi(\eta)$ space into M bins one can find out the values of $<F_q>$ and plot them for different values of M.

4.2.2 Vertical scaled factorial moments

The vertical scaled factorial moments are defined by the relation:

$$F_q^v = \frac{1}{M}\sum_{m=1}^{M} \frac{n_m(n_m - 1).......(n_m - q + 1)}{<n_m>^q} \tag{4.7}$$

On averaging over all the events in the data sample we get the vertically averaged normalized or scaled factorial moment of q^{th} order which is given by:

$$<F_q^v> = \frac{1}{M}\sum_{m=1}^{M}\frac{1}{N_{eV}}\sum_{i=1}^{N_{eV}} \frac{n_m(n_m - 1).......(n_m - q + 1)}{<n_m>^q} \tag{4.8}$$

where, $<n_m> = \frac{1}{N_{eV}} \sum_{i=1}^{N_{eV}} n_m$

is the average multiplicity of the m^{th} bin over the whole data sample comprising the number of events, N_{ev}.

It has been shown by Bialas and Peshanski that for purely statistical fluctuations $<F_q>$ is essentially independent of the bin size or the number of bins

M. However for the presence of any dynamical contribution to the fluctuation, the scaled factorial moment should follow a power law of the form $F_q \propto M^{\phi_q}$.

Thus a linear plot of $\ln < F_q >$ against ln M with positive slope confirms self similar pattern in the emission spectra of the projectile fragments. The positive exponents, ϕ_q, referred to as intermittency indices, characterize the strength of the intermittency signal.

The intermittency indices can be obtained from the asymptotic behaviour represented by:

$$\phi_q = -\frac{\Delta \ln < F_q >}{\Delta \ln M} \tag{4.9}$$

The power law behavior of the scaled factorial moments is envisaged [48-49] to be due to the fractal nature of the multi-particle spectra. Lipa and Buschbeck [35] have correlated the scaling behaviour of the factorial moments to the physics of fractal and multifractal objects through the relation:

$$d_q = \frac{\phi_q}{(q-1)} \tag{4.10}$$

where d_q is called the anomalous dimension. It is used for the description of the fractal objects. Thus, using the above relation, the anomalous dimension d_q, can be calculated directly from the intermittency index ϕ_q. The order independence of d_q indicates monofractal behaviour of multiparticle spectra, whereas an increase of d_q with q indicates the presence of multifractality in the emission spectrum.

4.3 Mathematical formalism for fractal and multifractal analysis

The self similarity observed in the power law dependence of scaled factorial moments reveals a connection between intermittency and fractality. The particle number density in each phase space bin depends on whether the resolution of the binning is larger or smaller than the angular separation between neighboring particles [50]. It has been found that if the resolution is of the order of the average separation of two neighboring particles in the phase space, then the binning of the phase space with that resolution may result in some empty bins. Considering the empty bins in the distribution are analogous to the holes then the set of non-empty bins would form a fractal set [50].

In fractal approach, it has been suggested that the nuclear interactions can be treated as geometrical objects with non-integer dimensions. Out of various methods that have been proposed to investigate the fractal structure, Hwa [36] was the first to provide the idea of the generalized multifractal moments G_q to study the multifractality and self-similarity in multiparticle production. If the particle production process exhibits self-similar behavior, then a modified form of G_q moment in terms of step function [37] shows the remarkable power law dependence on phase space bin size.

With this concept of fractality, the fractal moments G_q have been defined to evaluate parameters which characterize the fractal properties.

In this approach, as mentioned earlier, a given pseudorapidity interval in an event, $\Delta\chi = \chi_{\max} - \chi_{\min}$ is divided into 'M' bins of equal size:

$$d\chi = \frac{\Delta\chi}{M} \tag{4.11}$$

If n_m denotes the number of particles in the m^{th} bin, and if non empty bins are also included, then 'm' would run from 1 to M. The total number of particles in an event is calculated using the following relation:

$$n = \sum_{m=1}^{M} n_m \tag{4.12}$$

The fraction of particles in the m^{th} bin is given by, $p_m = n_m / n$. The quantity p_m is a small number and fluctuates distinctly from bin to bin. The multifractal moment G_q introduced by Hwa is now defined [36, 50] as:

$$G_q = \sum_{m=1}^{M} (p_m)^q \tag{4.13}$$

where the summation is carried out over all the non empty bins only which constitute a fractal set and q is the order of the moment. Because of the very nature of the formulation of G_q, i.e., summation over non empty bins only, the fractal moments can be calculated for any positive or negative integral or non integral order (value of q) and thus may take a dominant role over other multiplicity moments in revealing the dynamics of multiparticle production through the study of fluctuations in the density of produced particles. When averaged over all the events in a data sample in which the total number of events is N_{eV} , $<G_q>$ is expressed as:

$$< G_q > = \frac{1}{N_{eV}} \sum_{i=1}^{N_{eV}} G_q \tag{4.14}$$

A given rapidity distribution is said to exhibit self-similar behaviour and hence of fractal nature if $<G_q>$ exhibits a power law behaviour [50-51] over a range of small $d\chi$ in the following manner:

$$< G_q > \propto (d\chi)^{\tau_q} \tag{4.15}$$

The exponent τ_q may be determined from the observed linear dependence of ln $<G_q>$ on ln χ using the relation:

$$\tau_q = \lim_{d\chi \to 0} \frac{\Delta \ln < G_q >}{\Delta \ln d\chi} \tag{4.16}$$

One of the most basic properties of the fractals which describe the scaling behaviour is the generalized dimension D_q, introduced by Hentschel and Procaccia [52]. τ_q is related to D_q for all values of q, by the following relation:

$$D_q = \frac{\tau_q}{q-1} \tag{4.17}$$

Here, D_0 is the fractal dimension, D_1 is the information dimension and D_2 is the correlation dimension [36, 53-54]. If D_q decreases with the increase of q, the emission pattern is said to be multifractal. On the other hand, if D_q remains constant, then the emission pattern is referred to as monofractal [52,55].

Later by introducing a step function to suppress the low multiplicity events for which the statistical fluctuation is large, Hwa and Pan [37] proposed a modified G_q moment to investigate the fractal properties of the emission spectra of different charged secondaries. In this investigation, the generalized moments G_q is first estimated in χ (cosθ) space using [24, 56] the relation:

$$G_q = \sum_{m=1}^{M} \left(\frac{n_m}{N_{eV}} \right)^q \theta\,(n_m - q) \tag{4.18}$$

Here $\theta(n_m - q)$ is a step function such that $\theta(n_m - q) = 1$ for $n_m >> q$, and $\theta(n_m - q) = 0$ for $n_m < q$.

The vertically averaged horizontal moment, $<G_q>$, is then calculated as:

$$<G_q> = \frac{1}{N_{eV}} \sum_{i=1}^{N_{eV}} G_q \tag{4.19}$$

A power law dependence of $<G_q>$ on the phase space bin size, or on the number of phase space bins M, of the form represented by the equation $<G_q> \propto M^{-\tau_q}$ indicates self similarity in the emission pattern [24,37,56]. The exponent τ_q, called the fractal index, can be obtained from the asymptotic behavior.

It is worthwhile to mention here that up to this stage of analysis of multifractality, no technique has so far been adopted to filter out the statistical part of the fluctuation. Since $<G_q>$ of Eq.(4.19) contains contribution from both statistical as well as dynamical components, it is therefore necessary to extract the dynamical information from the mixture of the two.

To calculate the statistical contribution to $<G_q>$, n particles are distributed randomly in the specified phase space. For each event, fractal moment is calculated with redistributed particles and the $<G_q^{st}>$ is obtained by averaging the statistical G_q's. The dynamical component of $<G_q>$ is then estimated by using the following formula given by Chiu [57]:

$$<G_q^{dyn}> = \left(\frac{<G_q>}{<G_q^{st}>}\right) M^{1-q} \tag{4.20}$$

If $<G_q>$ contains purely statistical information, then

$$<G_q^{dyn}> = M^{1-q} \tag{4.21}$$

Under such condition:

$$\tau_q^{dyn} = q - 1 \tag{4.22}$$

Thus, any deviation of τ_q^{dyn} from $q - 1$ indicates that $<G_q>$ contains dynamical information.

The self-similarity of a fractal object is characterized by the generalized dimension D_q which is now defined by the relation:

$$D_q = \frac{\tau_q^{dyn}}{q-1} \tag{4.23}$$

4.4 Non-thermal phase transition for spatial and size distribution of projectile fragments

In heavy ion collision a type of transition in which the new phase may not exhibit thermodynamical behavior often referred to as non-thermal phase transition. It is already shown in ref. [58-59] the intermittent behavior in the final state of multiparticle production in a heavy-ion collision may be a projection of non-thermal phase transition believed to occur during the evolution of the collision which in turn would be responsible for the occurrence of anomalous events. It is convenient and better to find a suitable observable which can be measured experimentally and can provide information about phase transition (thermal or nonthermal). It has been assumed that a self similar cascade of multiparticle system is not consistent with the creation of particle during one phase, but instead requires a non-thermal phase transition [13, 60-61]. The intermittency exponent ϕ_q is related to a parameter λ_q which provides the signature of non-thermal phase transition. We can study the non-thermal phase transition with the help of the parameter,

$$\lambda_q = (\phi_q + 1)/q, \qquad (4.24)$$

where ϕ_q is the intermittency index. The condition that such non-thermal phase transition may occur is that the function λ_q, is predicted to have a minimum value at $q = q_c$, where q_c need not necessarily be an integer. Among the two different regions $q < q_c$ and $q > q_c$, the numerous small fluctuation dominates the region $q < q_c$ but in the region $q > q_c$ dominance of small number of very large fluctuations occurs. There is a co-existence of the liquid phase of the many small fluctuation and the dust phase of a few grains of very high density fluctuation, depending on whether we probe the system by a moment of order $q < q_c$ or $q > q_c$ respectively.

4.5 Results and discussion

Part A: On the spatial distribution of PFs

4.5.1 Angular distribution of charged projectile fragments

The measurements on angular distribution of various charged secondaries emitted from each interaction were carried out according to the procedure already mentioned in section 2.7.3.

In the study of the relativistic heavy ion collision, the spatial distribution of emitted charged secondaries are often defined in terms of what is called 'pseudorapidity' η that is related with the emission angle θ through the relation:

$$\eta = -\ln \{\tan (\theta/2)\} \qquad (4.25)$$

The angular distribution of various charge projectile fragments in the pseudorapidity space is plotted in Fig. 4.1. It can readily be seen from this plot that, as expected, the PFs are emitted in the extreme forward angle following a Gaussian distribution.

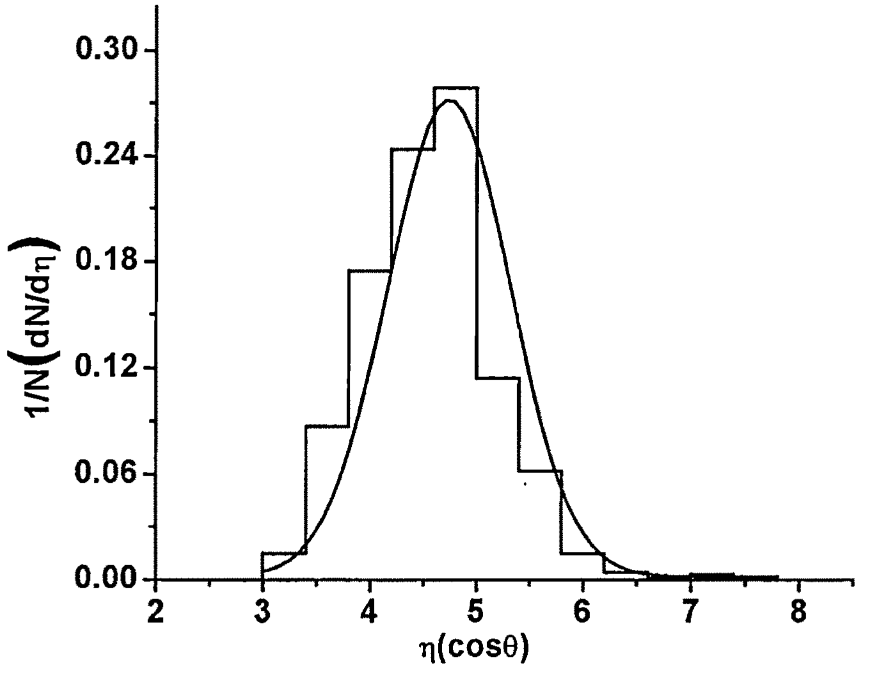

Fig. 4.1 Angular distribution of projectile fragments in η(cosθ) space.

As is evident from the very definition, the shape of the single particle density distribution spectrum in $\chi(\eta)$ space should be flat in nature. In Fig. 4.2, we present the frequency distribution of emitted projectile fragments of the work in $\chi(\eta)$ space. As expected, the best fitted lines for the data points are found to be flat in nature, with slope m = 0 and correlation coefficient R = 1.

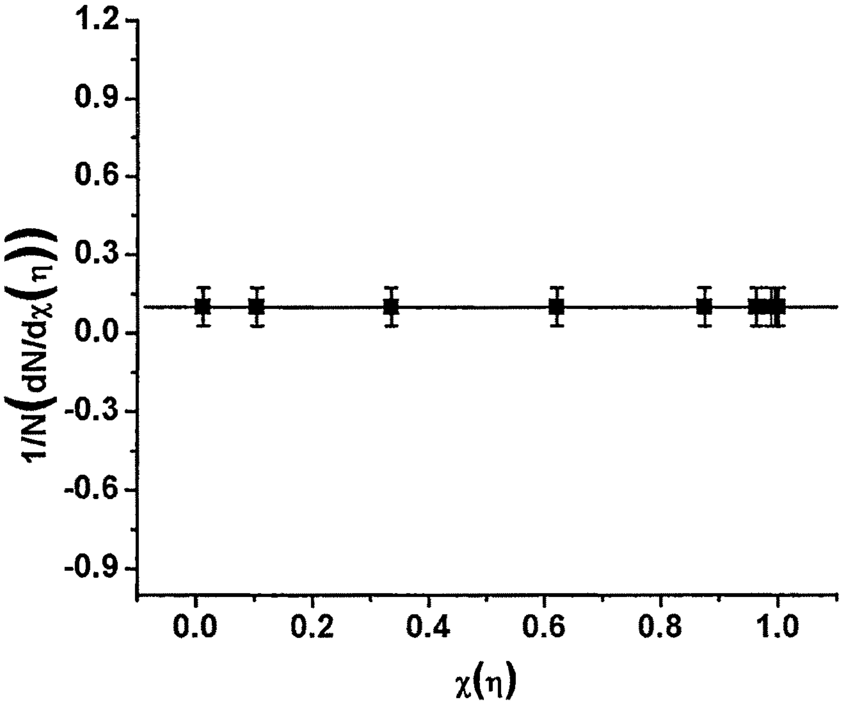

Fig. 4.2 Frequency distribution of projectile fragments in $\chi(\eta)$ space.

4.5.2 Scaled Factorial Moment Analysis for spatial distribution of projectile fragments

4.5.2.1 Variation of ln $\langle F_q \rangle$ with ln M

Fig. 4.3 shows a plot of ln $\langle F_q \rangle$ against ln M in $\chi(\eta)$ space for different order of moments q = 2–5 for all the projectile fragments with $Z_{PF} \geq 1$ for 4.5 AGeV ^{24}Mg projectile with emulsion targets. The straight lines drawn are the least square fit to experimental data points with Pearson correlation coefficients R equal to 0.875, 0.917, 0.952 and 0.954 for q = 2,3,4, and 5 respectively. From this figure, the SFM is observed to increase linearly with decreasing bin widths, indicating thereby the presence of intermittent behavior in the emission spectrum.

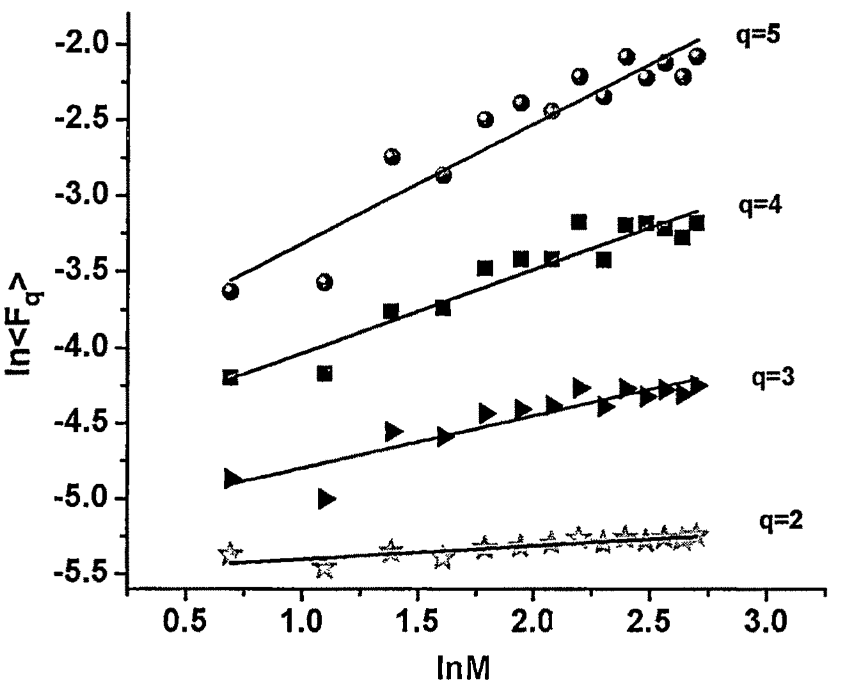

Fig. 4.3 Variation of ln $<F_q>$ with ln M for the spatial distribution of various PFs for Mg-Em interactions at 4.5 AGeV.

4.5.2.2 Variation of ϕ_q with q

The intermittency indices ϕ_q which characterize the strength of intermittency effect have been obtained for the linear dependence of ln $<F_q>$ on ln M. The values of slope parameter ϕ_q obtained for the interactions of 4.5 AGeV ^{24}Mg nuclei with emulsion target are listed in table 4.1. Fig. 4.4 shows ϕ_q versus q plot. The errors indicated in the plot are the statistical errors only. The slopes are observed to increase with the order of the moments.

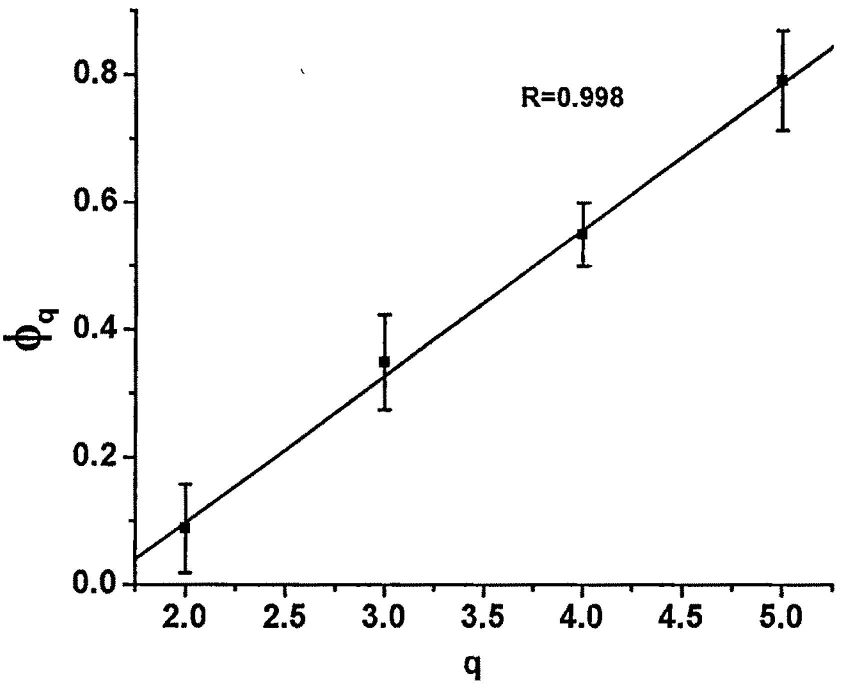

Fig. 4.4 Variation of the exponent ϕ_q with the order of the moments q for Mg -Em interactions at 4.5 AGeV.

4.5.2.3 Variation of anomalous dimension d_q with q

As stated earlier, Lipa and Buschbeck [35] for the first time had correlated the scaling behavior of factorial moments to the physics of fractal and multifractal objects. They pointed out that the intermittency index ϕ_q has a special significance from the point of view that the anomalous dimension, d_q, which is used for the description of the fractal objects, can be directly computed from the intermittency index ϕ_q using the Eq. (4.10).

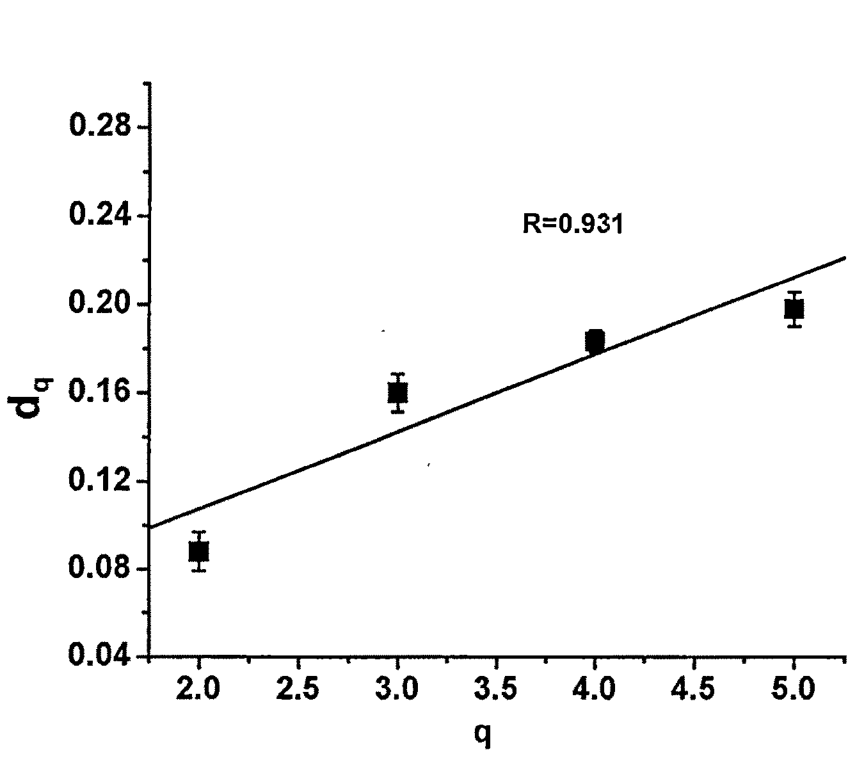

Fig. 4.5 Variation of anomalous dimension d_q with q for Mg-Em interactions at 4.5 AGeV.

As mentioned earlier, the order independence of d_q is associated with the monofractal behavior of multiparticle spectra whereas an increase will indicate multifractality. In Fig. 4.5, the variations of anomalous dimension d_q with the orders of the moment q are shown for the emission spectra of PFs. From this figure it can be readily seen that d_q increases linearly with q thereby indicating multifractal pattern of the emission spectra of the projectile fragments.

Table. 4.1 Values of the slope parameters ϕ_q for the collisions of 4.5 AGeV Mg nuclei with emulsion targets.

q	ϕ_q	R
2	0.088 ± 0.07	0.986
3	0.349 ± 0.074	0.977
4	0.550 ± 0.05	0.966
5	0.792 ± 0.078	0.967

4.5.2.4 Variation of λ_q with q

The variation of λ_q, estimated from the values of ϕ_q of the table 4.1, with q is shown in Fig. 4.6. From this plot no observed minimum at $q = q_c$ could be seen indicating no evidence of non thermal phase transition in the spatial distribution of projectile fragments.

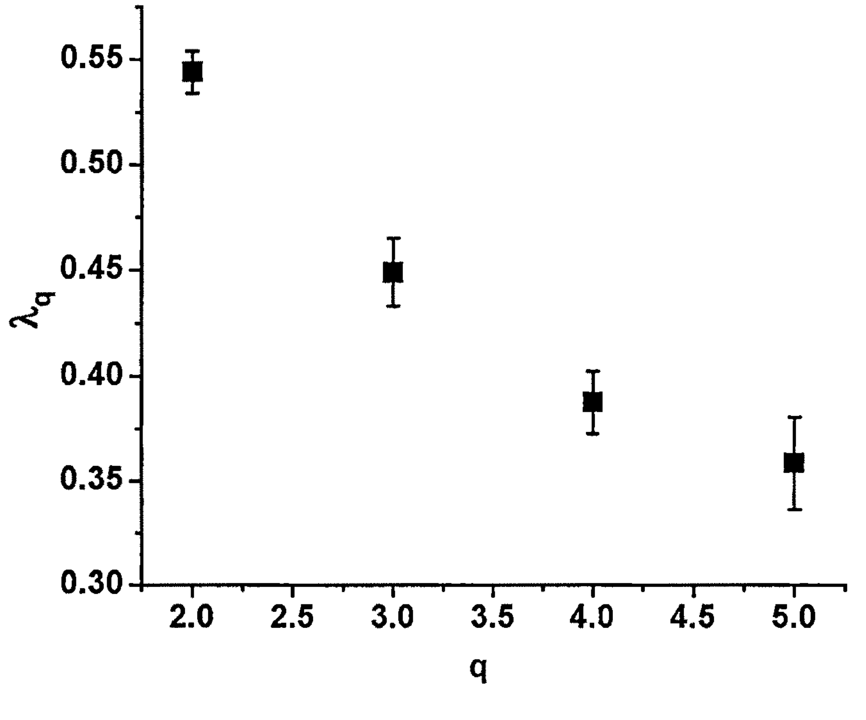

Fig. 4.6 Variation of λ_q with the order of the moment q for Mg-Em interactions at 4.5 AGeV.

4.5.3 Fractal Analysis in the spatial distribution of projectile fragments

4.5.3.1 Variation of $\ln <G_q>$ with $\ln M$

To calculate the statistical contribution to $<G_q>$, equal number of events are generated in cosθ space by a random number generator with cosθ values lying between -1 and +1. The cosθ values are then converted into $\chi(\eta)$ values using Eq. (4.1). $<G_q^{st}>$ is then estimated using Eqs. (4.18) and (4.19). The variation of $\ln <G_q>$ with $\ln M$ for q = 2, 3 and 4 for experimental data as well as for random number generated events are shown in Fig. 4.7. The solid lines are for the experimental data points and the dotted lines are for the equal number of generated events.

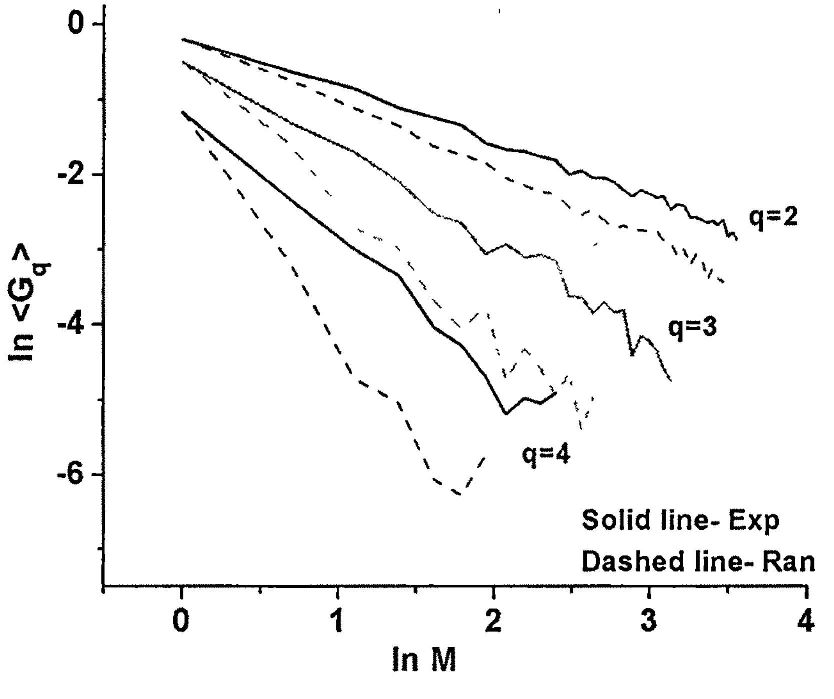

Fig. 4.7 Variation of $\ln <G_q>$ with $\ln M$ for experimental and random number generated events.

4.5.3.2 Variation of τ_q^{exp} with q

The exponents τ_q^{exp}, obtained from the portion of linear dependence of $\ln <G_q>$ with ln M as a function of the order of the moment q, for experimental data are plotted in the Fig. 4.8. The values of the exponents are found to increase with q.

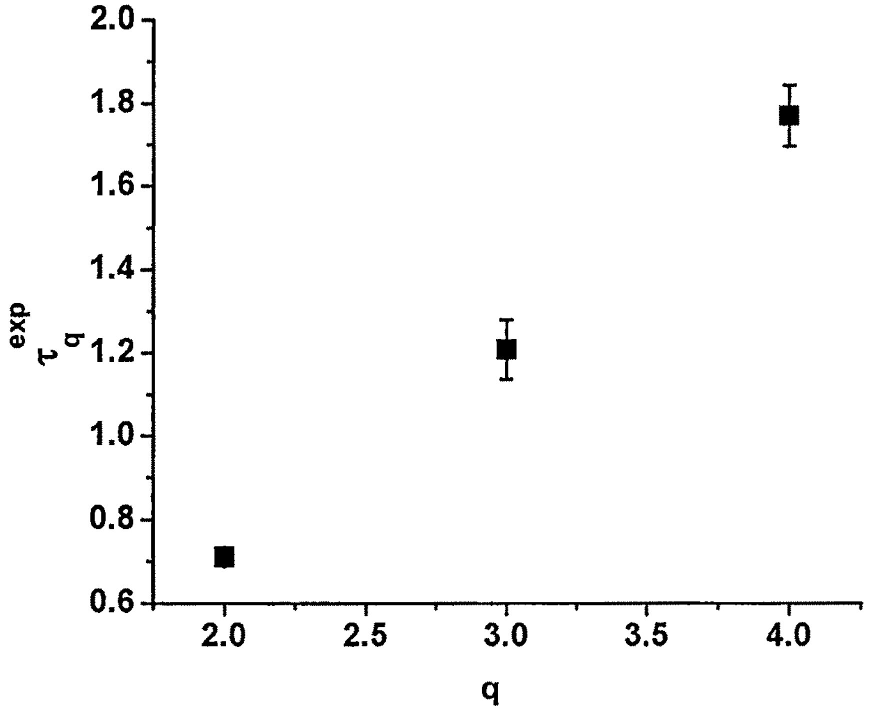

Fig. 4.8 Variation of τ_q^{exp} with q for Mg-Em interactions at 4.5 AGeV.

4.5.3.3 Deviation of exponents from q-1

Since the exponent τ_q^{exp} as obtained above, are estimated from the experimental data set, it contains statistical component also. The dynamical component of exponent τ_q is then estimated using the relation:

$$\tau_q^{dyn} = \tau_q^{exp} - \tau_q^{st} + q\text{-}1 \tag{4.26}$$

where τ_q^{st} represents the slopes of randomly generated data obtained from $\ln < G_q >$ vs ln M plot. Fig. 4.9 shows the deviation of τ_q^{dyn} from q-1.

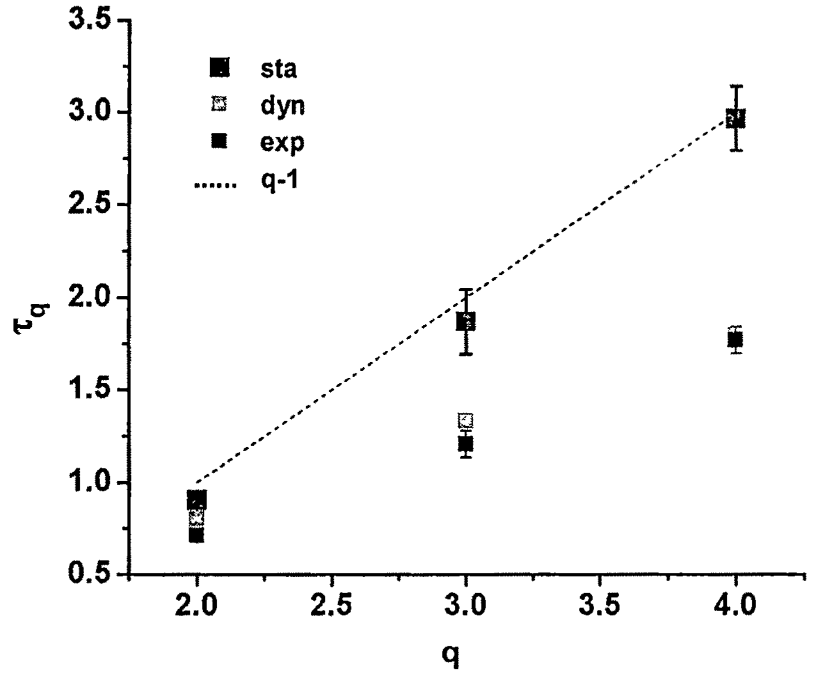

Fig. 4.9 Deviation of exponents from q-1.

4.5.3.4 Variation of D_q^{dyn} with q

The value of generalized dimensions D_q for various values of q have been estimated using Eq. (4.23) for the emission spectrum of projectile fragments with $\chi(\eta)$ as phase space variable in ^{24}Mg-Em interactions at 4.5 AGeV and their variations with different order of moments q = 2 - 4 are shown in Fig. 4.10. It is observed from the figure that the generalized dimensions D_q decreases linearly with q, indicating multifractality in the emission spectra of projectile fragments.

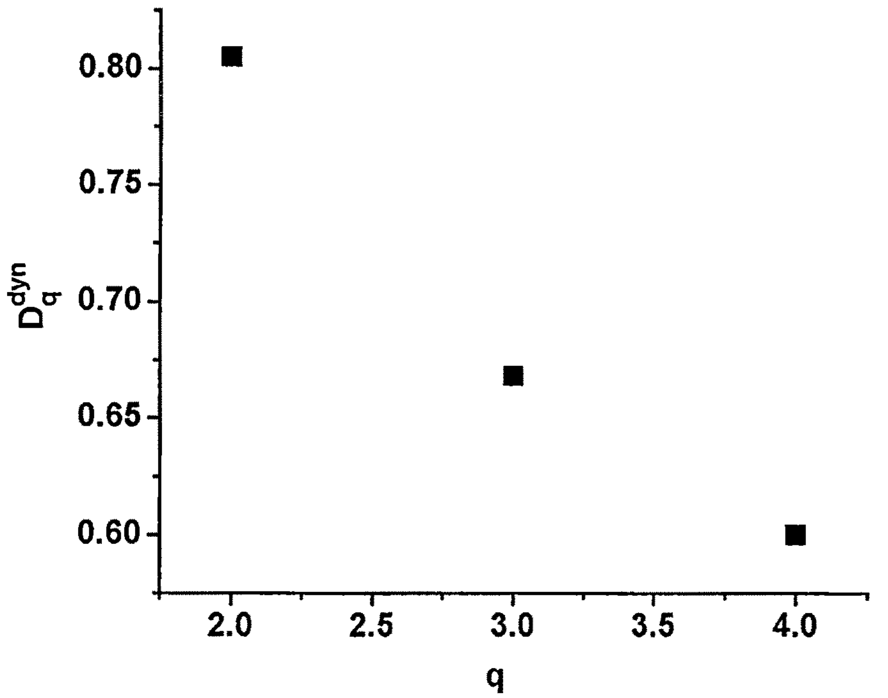

Fig. 4.10 Variation of D_q^{dyn} with q for Mg-Em interactions at 4.5 AGeV.

The values of τ_q^{exp} for experimental data points, τ_q^{st} for generated events, obtained from the slopes of the best fitted lines, τ_q^{dyn}, $q - 1 - \tau_q^{dyn}$ and D_q^{dyn} for different orders of moment are listed in table 4.2.

Table. 4.2 Values of τ_q for spatial distribution of projectile fragments.

q	τ_q^{exp} (R)	τ_q^{st} (R)	τ_q^{dyn}	q-1- τ_q^{dyn}	D_q^{dyn}
2	0.711 ± 0.018 (0.991)	0.905 ± 0.017 (0.995)	0.805 ± 0.035	0.19415	0.805
3	1.207 ± 0.072 (0.985)	1.87 ± 0.175 (0.974)	1.337 ± 0.247	0.6625	0.668
4	1.77 ± 0.073 (0.989)	2.97 ± 0.174 (0.986)	1.8 ± 0.247	1.2	0.6

The deviation of τ_q^{dyn} from q – 1 is clear from this table and this deviation is more as we go to the higher order of moments. This indicates that G_q contains information about dynamical contribution to the fluctuations.

Part B: On the charge distribution of Projectile Fragments

4.5.4 The Fragments multiplicity distribution

The multiplicity distribution of all the charged fragments with Z_{PF} = 1-12 is shown in the Fig. 4.11.

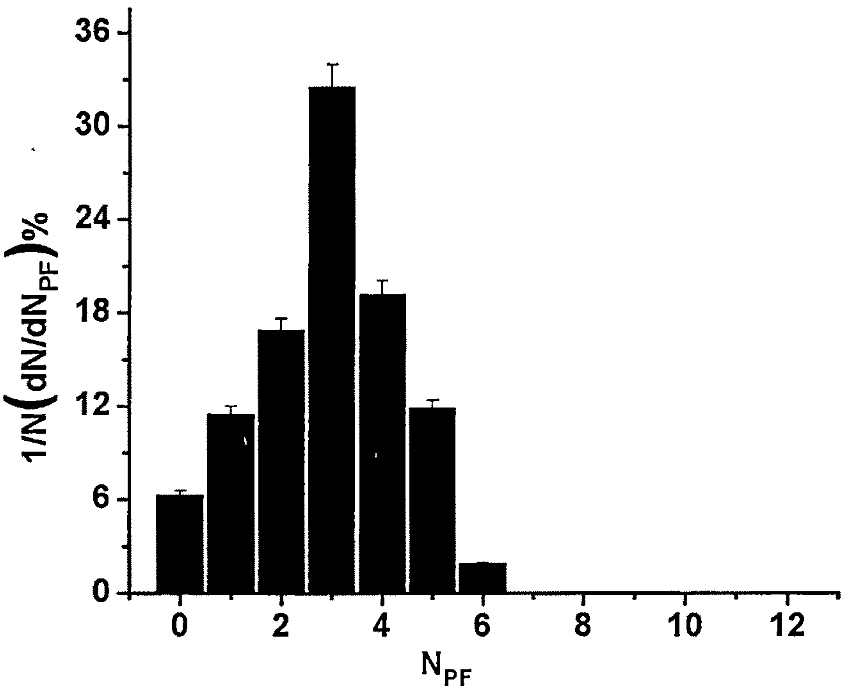

Fig. 4.11 Multiplicity distribution of projectile fragments.

4.5.5 Scaled Factorial Moment Analysis for fragments charge (mass) distribution.

Following Eq.(4.6) the scaled factorial moment analysis has been performed for searching intermittency signal for fragments charge distribution with the experimental data of this work. Here M is the total number of bins as the fragment charge interval Δs (1-12) is divided into bins of equal width δs = Δs / M. n is the fragment multiplicity in the interval Δs. For non flat fragment multiplicity distribution varying within a finite bin of width δs introduces an extra M-dependent correction factor R_q which is given by:

$$R_q = \frac{1}{M}\sum_{m=1}^{M}\frac{M^q < n_m >}{< n >^q} \tag{4.27}$$

Thus, $<F_q>/R_q = <F_q>_c$ measures the contribution of dynamical fluctuations. In doing so, one must be careful in selecting the smallest bin, which must not be smaller than the charge resolution of the detector [62]. If self-similar fluctuations exist at all scales of δs, the corrected factorial moment of the order q is given by $<F_q>_c = (\Delta s/\ \delta s)^{\phi_q}$. The exponent ϕ_q is the slope characterizing a linear rise of $\ln<F_q>_c$ with -ln δs for all bins of δs, which increases with the increasing order q of the moment.

4.5.5.1 Variation of $\ln <F_q>_c$ with -ln δs

Plots of $\ln<F_q>_c$ against -ln δs for different orders of moments are shown in Fig. 4.12. It can be readily seen from this plot that the moment for the fragment multiplicity distribution continue to increase according to power law with the decreasing bin width δs variable, thereby indicating the intermittent pattern. The errors shown in this plot are standard deviation and the straight lines drawn are the best fitted lines for the respective data points. The different values of intermittency indices, ϕ_q along with the correlation coefficient R values for the present work and the values reported earlier are shown in table 4.3.

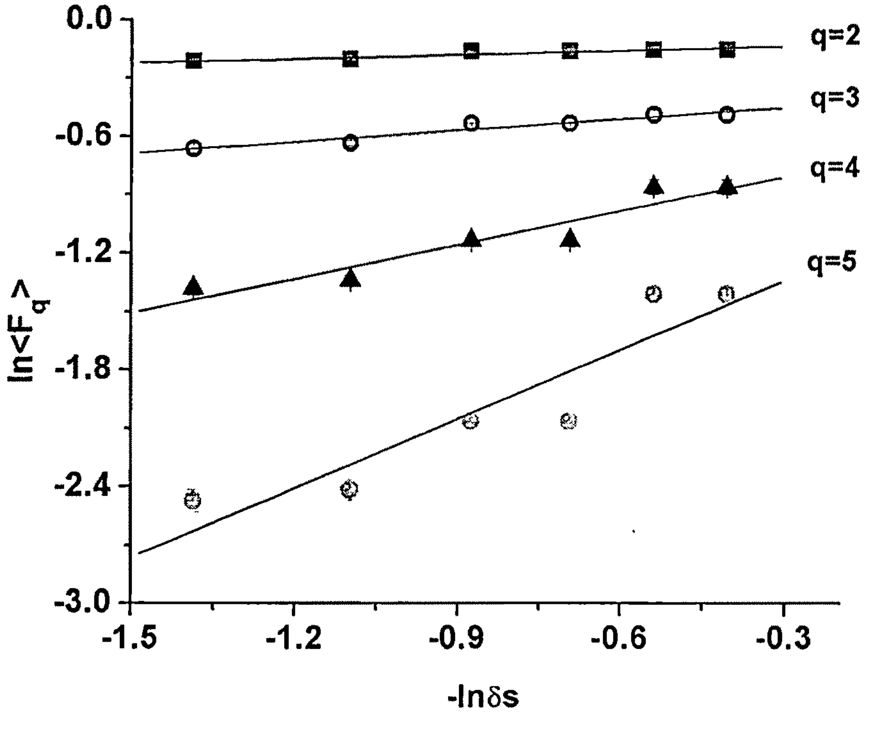

Fig. 4.12 Variation of of ln $<F_q>_c$ with -ln δs for charge distribution in the interactions of Mg nuclei with emulsion targets at 4.5 AGeV.

Table. 4.3 Values of the slope parameters ϕ_q for charge distribution of projectile fragments in Mg-Em interaction at 4.5 AGeV.

System	Energy	ϕ_q for q=2 (R)	ϕ_q for q=3 (R)	ϕ_q for q=4 (R)	ϕ_q for q=5 (R)	ϕ_q for q=6 (R)	Reference
Mg-Em	4.5	0.080± 0.017 (0.940)	0.216± 0.035 (0.963)	0.571± 0.137 (0.924)	1.121± 0.334 (0.888)	–	PW
Kr-Em	0.95	0.011± 0.002 (0.892)	0.038± 0.004 (0.949)	0.081± 0.007 (0.968)	0.134± 0.010 (0.974)	0.196± 0.014 (0.976)	63
Au-Em	0.1-1	0.010± 0.011	0.027± 0.017	0.049± 0.023	0.073± 0.030	–	64
Au-Em	10.6	0.005± 0.004	0.015± 0.005	0.026± 0.007	0.039± 0.009	–	64
U-Em	0.96	0.0068± 0.0002	0.010± 0.0003	0.013± 0.0004	0.0163± 0.0006	0.0191± 0.0006	4

4.5.5.2 Variation of ϕ_q with q

Variation of the intermittency exponent ϕ_q with q is plotted in the Fig. 4.13 and is found to increase exponentially with the order of the moment q following the relation:

$$y = A_1 * \exp(-x/t_1) + y_0 \tag{4.28}$$

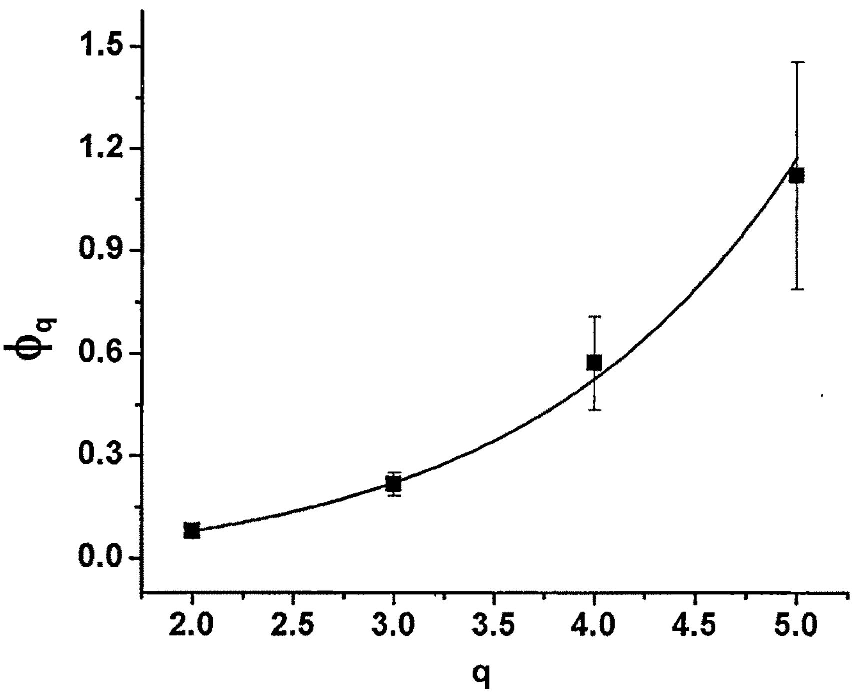

Fig. 4.13 Variation of ϕ_q with q in the charge distribution of projectile fragments for Mg-Em interactions at 4.5 AGeV.

The solid line represents the best fit to the data points with the values of the different parameters as, A_1= 0.27±0.013, y_0 = -0.046±0.039, t_1= -1.31 ± 0.191 and R^2 = 0.985 respectively. Such an exponential increase of ϕ_q clearly indicates strong intermittency in the fragments charge distribution of Mg-Em interaction.

4.5.5.3 Variation of anomalous dimension d_q with q

Following equation (4.10) the variation of anomalous dimension d_q with q is plotted in Fig. 4.14. for fragments charge distribution for the present set of experimental data. From this figure it can be readily seen that d_q increases exponentially with q thereby indicating multifractal pattern in the size (charge) of the projectile fragments as well. The R^2 value for the fitted parameter is found to be 0.978.

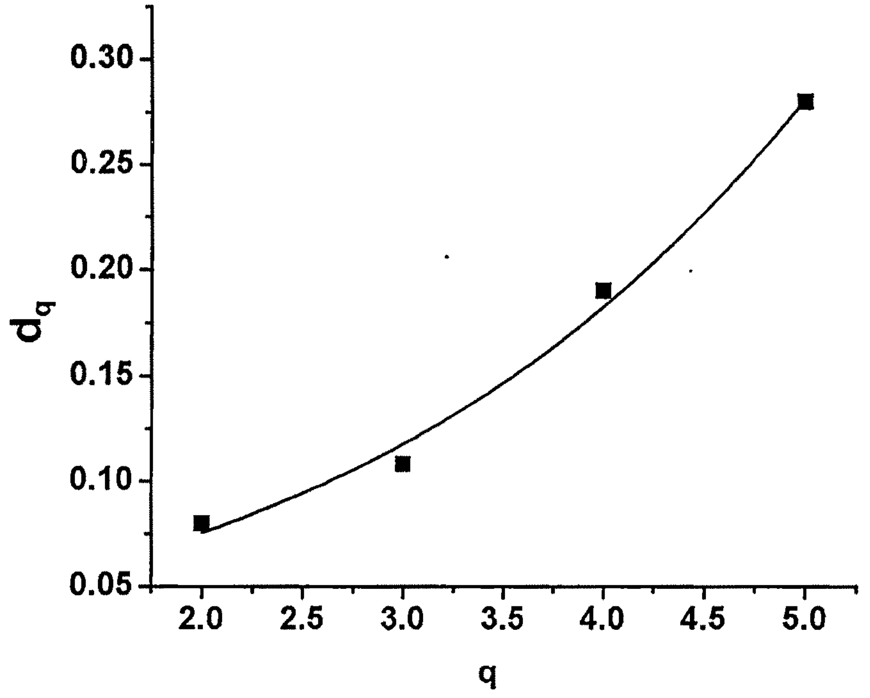

Fig. 4.14 Variation of anomalous dimension d_q with q for Mg-Em interactions at 4.5 AGeV.

4.5.5.4 Variation λ_q with q

Fig. 4.15 shows the variation of λ_q with q for the size (charge) distribution of projectile fragments in the interactions of Mg nuclei with emulsion targets at 4.5 AGeV. It is interesting to note that a distinct minimum at q~3.5 is observed; the observed minimum in the variation of λ_q with q may be an indication for the occurrence of non-thermal phase transition in the size distribution of projectile fragments.

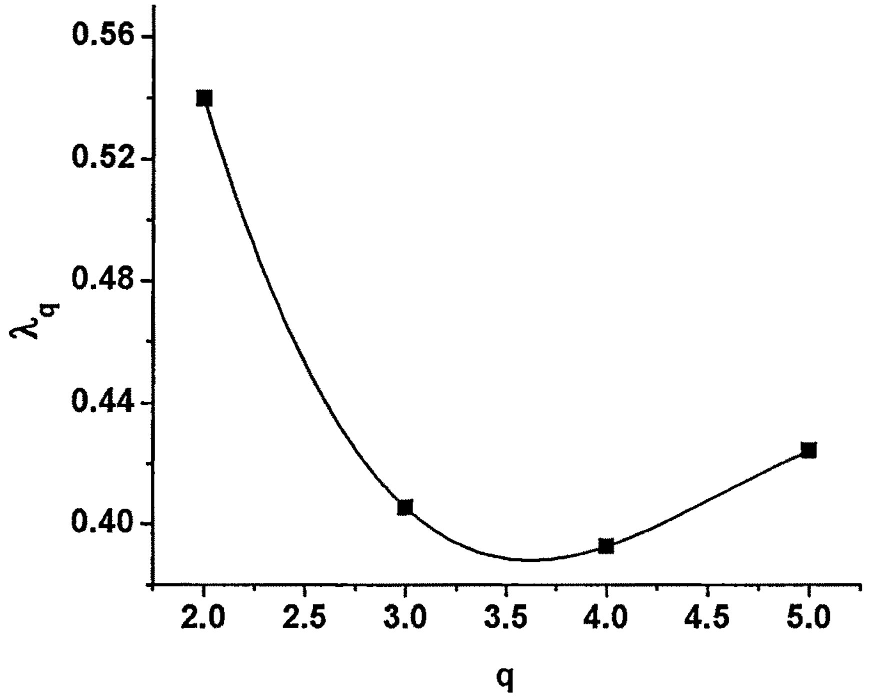

Fig. 4.15 Variation of λ_q with q for size distribution of projectile fragments for Mg-Em interactions at 4.5 AGeV.

4.5.6 Fractal Analysis of the charge distribution of projectile fragments

4.5.6.1 Variation of ln $<G_q>$ with -ln δs

The data set for the various charges of projectile fragments has been analyzed further, applying the same concept of section 4.3 for evaluating G_q moments. Here also if the charge distributions have the fractal structure, then the G_q moment should follow a power law i.e.,

$$<G_q> \propto (\delta s)^{\tau_q} \qquad (4.29)$$

where τ_q is fractal index or mass (charge) exponent. From the linear dependence of ln $<G_q>$ on ln δs, τ_q can be calculated as:

$$\tau_q = \frac{\Delta \ln\langle G_q \rangle}{\Delta \ln(\delta s)} \tag{4.30}$$

To calculate the statistical contribution to $<G_q>$, equal number of events are also generated by random number generator with charge of the PFs lying between 1 to 12 for Mg projectile beams. $<G_q^{st}>$ is then calculated for uncorrelated projectile fragments in randomly generated events. From Fig. 4.16, a significant difference could easily be seen between the experimental and random data for the fragments of Mg projectile. The dynamical part of $<G_q>$ can be determined from [57]:

$$< G_q^{dyn} > = \frac{< G_q >}{< G_q^{st} >} (\delta s)^{q-1} \tag{4.31}$$

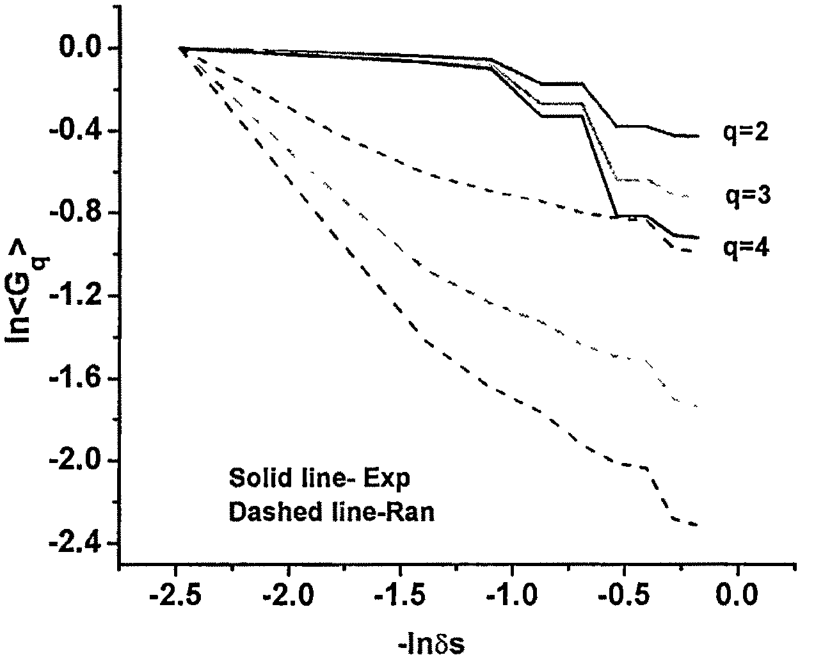

Fig. 4.16 Variation of ln $<G_q>$ with -ln δs for fragments charge distribution in 4.5 AGeV Mg nuclei with emulsion target.

4.5.6.2 Variation of τ_q(exp) with q

The exponents τ_q^{exp}, obtained for the portion of linear dependence of $\ln <G_q>$ with $- \ln \delta s$ is plotted in Fig. 4.17 as a function of the order of the moment q. The values of the exponents are found to increase linearly with q.

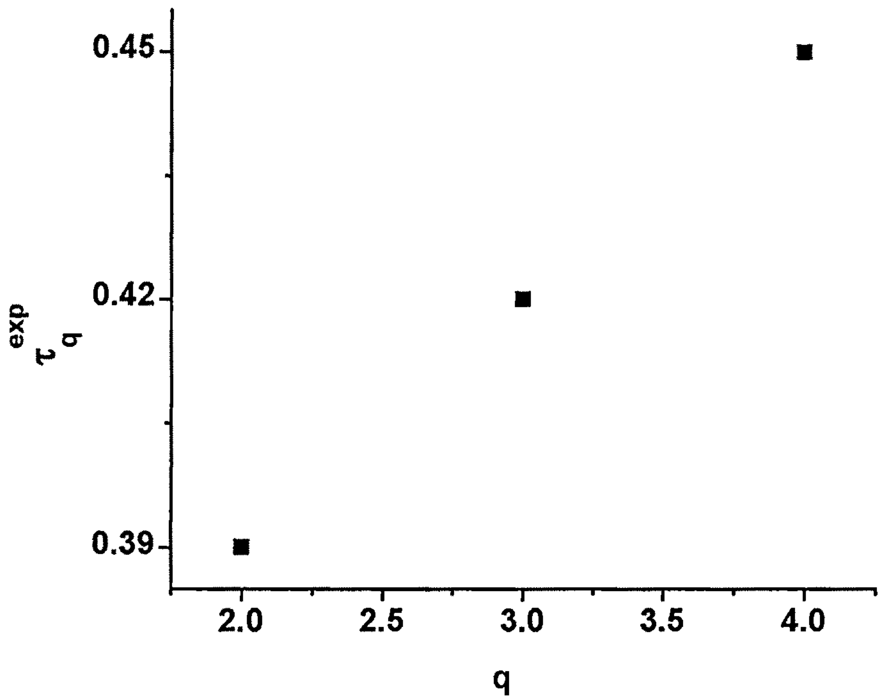

Fig. 4.17 Variation of τ_q (exp) with q for fragments charge distribution in 4.5 AGeV Mg nuclei with emulsion target.

4.5.6.3 Daviation of mass exponens from q-1

The dynamical component of exponent τ_q^{dyn} is calculated in a similar way as done in section 4.5.3.3. In the present calculation, τ_q^{st} represents the slopes of randomly generated data obtained from $\ln <G_q>$ vs $-\ln \delta s$ plot. Fig. 4.18 shows the deviation of τ_q^{dyn} from q-1.

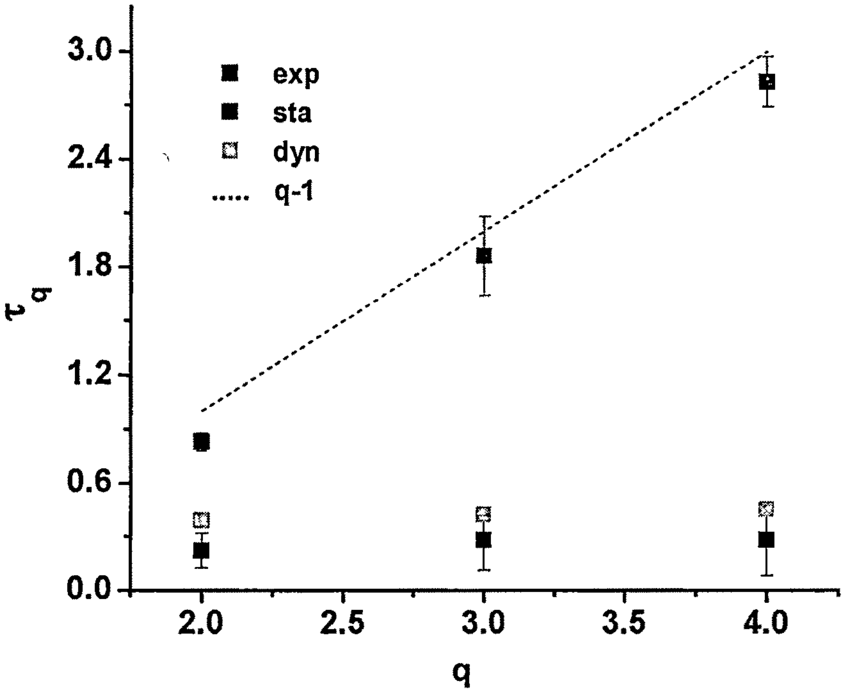

Fig. 4.18 Deviation of mass exponents from q-1.

4.5.6.4 Variation of D_q^{dyn} with q

The value of generalized dimensions D_q for various values of q have been estimated using Eq. (4.23) for the charge distribution of projectile nuclei with emulsion target , and their variations with different order of moments q = 2 - 4 are shown in Fig. 4.19. It is observed from the figure that the generalized dimensions D_q decreases linearly with q for the present set of data. Thus it is evident that there is a signature of multifractality in the charge distribution of projectile fragments.

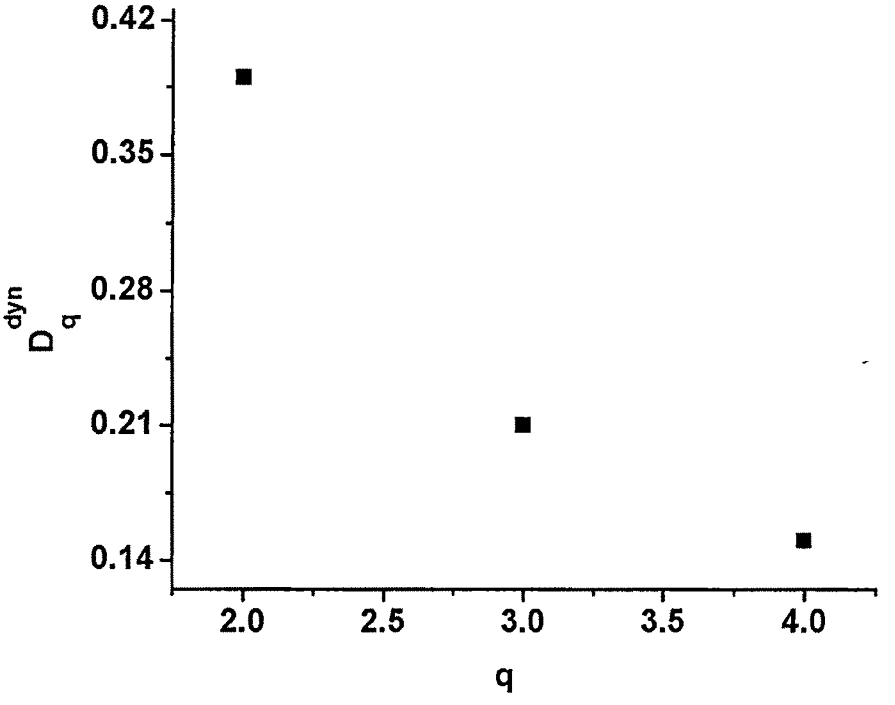

Fig. 4.19 Variation of D_q^{dyn} with q for fragments charge distribution in 4.5 AGeV Mg nuclei with emulsion target.

Table. 4.4 Values of τ_q for charge distribution of projectile fragments.

q	τ_q^{exp} (R)	τ_q^{st} (R)	τ_q^{dyn}	$q-1-\tau_q^{dyn}$	D_q^{dyn}
2	0.22 ± 0.097 (0.954)	0.83 ± 0.05 (0.987)	0.39 ± 0.035	0.61	0.39
3	0.28 ± 0.17 (0.948)	1.86 ± 0.22 (0.947)	0.42 ± 0.247	1.58	0.21
4	0.28 ± 0.2 (0.968)	2.83 ± 0.14 (0.958)	0.45 ± 0.247	2.55	0.15

The values of τ_q^{exp}, τ_q^{st}, τ_q^{dyn}, $q - 1 - \tau_q^{dyn}$ and D_q^{dyn} for different orders of moment as obtained from the charge distribution of various projectile fragments are listed in table 4.4. It is observed from this table that the value of τ_q^{dyn} deviates from $q - 1$ and this deviation is more as we go to the higher order of moments. This indicates that G_q contains information about dynamical contribution to the fluctuations in the charge (mass) distribution of the fragments of projectile spectator.

References

1. R.T. de Souza et al., *Phys. Lett.* **B 268** (1991) 6.
2. D. R. Bowman et al., *Phys. Rev. Lett.* **67** (1991) 1527.
3. M. Ploszajczak and A. Tucholski, *Phys. Rev. Lett.* **65** (1990) 1539.
4. P.L. Jain et al., *Phys. Rev. Lett.* **68** (1992) 1656.
5. P.L. Jain and G. Singh, *Phys. Rev.* **C 46** (1992) R 10.
6. G. Singh et al., *Euro. Phys. Lett.* **21** (1993) 527 and references therein.
7. G. Singh et al., *Mod. Phys. Lett.* **A 7** (1992) 1113.
8. A. Bialas and R. Peschanski, *Nucl. Phys.* **B 273** (1986) 703.
9. P.L. Jain et al., *Phys. Rev.* **C 47** (1993) 342.
10. A. Bialas and R. Peschanski, *Nucl. Phys.* **B 308** (1988) 857.
11. A. Bialas et al., *Euro. Phys. Lett.* **7** (1988) 125.
12. R. Peschanski, *New Results in hadronic interaction. Proc. of the 24th Rencontre de Moriond.* Les Ares. Savoie, French, March 12-18, ed. J. Tran Thanh Van (Editions Frontiesse) (1989) 247.
13. B. Buschbeck et al., *Phys. Lett.* **B 215** (1988) 788.
14. W. Braunschweig et al., *Phys. Lett.* **B 231** (1989) 548.
15. P. Abreu et al., *Phys. Lett.* **B 247** (1990) 137.
16. W. Shaoshun et al., *Phys. Rev.* **D 49** (1994) 5787.
17. I. Derado et al., *Z. Phys.* **C 47** (1990) 23.
18. R. Holynski et al., (KLM Collaboration), *Phys. Rev. Lett.* **62** (1989) 733.
19. R. Holynski et al., (KLM Collaboration), *Phys. Rev.* **C 40** (1989) R2449.
20. M.I. Adamovich et al., (EMU01 Collaboration), *Phys. Rev. Lett.* **65** (1990) 412.
21. T. Akensson et al., (HELIOS Collaboration) *Phys. Rev. Lett.* **B 252** (1990) 303.
22. K. Sengupta et al., *Phys. Lett.* **B 236** (1990) 219.

23. D. Ghosh et al., *Phys. Rev.* **C 49** (1994) R1747.

24. D. Ghosh et al., *Phys. Rev.* **C 58** (1998) 3553.

25. D. Ghosh et al., *Z. Phys.* **C 73** (1996) 269.

26. D. Ghosh et al., *Int. J. Mod. Phys.* **E 12** (2003) 407.

27. D. Ghosh et al., *J. Phys. G: Nucl. Part. Phys.* **29** (2003) 983.

28. V. Bradnova et al., JINR-LHE-0983-2.

29. M. Aggarwal, Physics and Astrophysics of Quark–Gluon Plasma, Narosa Publishing House, New Delhi.

30. A. SchÄuttauf et al., *Nucl. Phys.* **A 607** (1996) 457.

31. B. Chiu and R. C. Hwa, *Phys. Rev.* **D 45** (1992) 2276.

32. B. Mandelbrot, The Fractal Geometry of Nature (Freeman, New York,1982).

33. P. Carruthers and Ming Duong-Van, *Los Alamos Report No.* **LA-UR-83-2419.**

34. I. M. Dremin, *Mod. Phys. Lett.* **A 3** (1998) 1333.

35. P. Lipa and B. Buschbeck, *Phys. Lett.* **B 223** (1998) 465.

36. R. C. Hwa, *Phys. Rev.* **D 41** (1990) 1456.

37. R. C. Hwa and J. Pan, *Phys. Rev.* **D 45** (1992) 1476.

38. H . Satz, *Nucl. Phys.* **B 326** (1989) 613.

39. B. Bambah et al., *Nucl. Phys.* **B 332** (1990) 629.

40. A. R. DeANGELIS et al., *Nucl. Phys.* **A 537** (1992) 606.

41. M. PloszaJczak et al., *Phys. Lett.* **B 262** (1991) 383.

42. M. PloszaJczak and A. Tucholski, *Nucl. Phys.* **A 523** (1991) 651.

43. P. Bozek et al., *Nucl. Phys.* **A 539** (1992) 693.

44. K. Fialkowski et al., *Acta Phys. Pol.* **B 20**, (1989) 639.

45. M. K. Ghosh and A. Mukhopadhyay, *Phys. Rev.* **C 68** (2003) 34907.

46. M. Bialas and M. Gradzicki, *Phys. Lett.* **B 252** (1990) 483.

47. W. Shaoshun and W. Zhaomin, *Phys. Rev.* **D 57** (5) (1998) 3036.

48. A. Bialas and R. Peschanski, *Jagellonion University Report* **JPJU/4/88**.

49. M. Adamus et al., NA22 Collaboration, *Phys. Lett.* **B 185** (1987) 200.

50. C. B. Chiu and R. C. Hwa, *Phys. Rev.* **D 43**(1) (1991) 100.

51. E. A. De Wolf et al., *Phys. Rep.* **270** (1996).

52. H. G. E. Hentschel and I. Procaccia, *Physica* **8 D** (1983) 435

53. G. Paladin and A. Valpiani, *Phys. Rep.* **156** (1987) 147

54. P. Grassberger and I. Procaccia, *Physica* **13 D** (1984) 34.

55. N. Prashar, *IL Nuovo Cim.* **A 108** (1995) 489.

56. B. Bhattacharjee & S. Sengupta, *Int. J. Mod. Phys.* **E 14** (2005) 1223.

57. C. B. Chiu et al., *Mod. Phys. Lett.* **A 5** (1990) 2651.

58. A. Bialas and K.Zalewski, *Phys. Lett.* **B 238** (1990) 413.

59. A. Bialas and K.Zalewski , *Nucl. Phys.* **B 237** (1989) 65.

60. R. Peschanski, *Int. J. Mod. Phys.* **A 6** (1991) 3681.

61. R. Peschanski, *Nucl. Phys.* **B 327** (1989) 144.

62. P.L. Jain and G. Singh, *Phys. Rev.* **C 44** (1991) 854 and references therein.

63. B. Debnath, *Ph.D thesis*, Department of Physics, Gauhati University (2011).

64. M. L. Cherry et al., *Phys. Rev.* **C 53**(4) (1992) 1532.

CHAPTER V

SYSTEM SIZE EFFECT
AND
CRITICAL BEHAVIOUR IN NUCLEAR MULTIFRAGMENTATION

5.1 Introduction

Studies on intermediate energy A+A collision are of special significance from the point of view that such collisions are associated with abundant multifragment production [1]. The connection between the multifragmenation (MF) as decay mechanism of excited nuclei and a possible liquid gas phase transition taking place in the nuclear matter has been a subject of hot debate during the last two decades or so [2-4]. From the presence of the power law in fragment mass distribution and from the observation of the values of the exponents of various charge moments close to those of ordinary fluid, coupled with the strong similarity of the nuclear and Van-der-Waals potentials, it was inferred that multifragmentation of nuclei might be analogous to a continuous phase transition from liquid to a gas [5-7].

Campi [8-9] and Bauer et al. [10-11] showed that the methods of estimation of various moments of cluster size as used in percolation can be applied to analyze multifragmentation data to realize the possible association of criticality with such processes. Subsequently a large number of workers [8-23] have applied the technique of cluster approximation in analyzing projectile fragmentation data for various systems at different energies. From all such studies a number of important information about the possible liquid-gas phase transition in nuclear matter could be gathered. A few of these are: tentative estimation of critical temperature, estimation of various exponents and their scaling behaviour [16-18, 24], system size dependence of the position and height of critical singularity [18], role of Coulomb and surface energies [25] on MF process etc.

Finite size effect [26-33] has been found to have considerable influence on MF mechanism. This is due to the fact that the hot piece of nuclear matter produced in any nuclear collision has at most a few hundreds of nucleons and so is not adequately described by the properties of infinite nuclear matter. As stated earlier surface and Coulomb effects can play a significant role in finite nuclear system. These effects have been evaluated and lead to a sizable reduction of the critical temperature [28]. Finite size effects have been found to reduce the temperature by 2-6 MeV depending on the size of nuclei while the Coulomb force is responsible for a further reduction of 1-3 MeV. However large reductions due to small sizes are associated with small reductions from Coulomb effect. Consequently , in the range A=50-400 a total reductions of about 7 MeV is calculated leading to a "critical" temperature of about 10 MeV for nuclei or hot pieces of nuclear matter produced in collisions between very heavy nuclei. The authors of reference [28] indicate that, due to some approximation the derived values can be regarded as upper limits. Finally we can recall that in infinite nuclear matter, the binding energy per particle is 16 MeV whereas it is about 8 MeV in a finite nucleus. A finite system like a nucleus with its limited number of constituents does not exhibit, in the neighborhood of critical point, a sharp singularity in the traditionally accepted signatures of critical behavior. It rather shows a rounded finite peak [18] at a temperature $T = T'$ where T' is a temperature dependent on the system size. This temperature T' is regarded as the critical temperature of the finite system at and above which the distinction between the phases vanishes; T' corresponds to T_c, the critical temperature for an infinite system, as the system size approaches infinity. The effect of finite size thus not only lowers the peak value, but also lowers the critical point [34-35] thereby influencing even the order of phase transition.

EOS collaboration [18-19, 27] has analyzed the fragments mass distribution resulting from the interactions of 1 AGeV Au, La and Kr on carbon and observed that while for larger systems like Au and La the fragment yield distribution follows a power law with exponent values greater than 2; for Kr, the mass yield distribution is exponential with exponent value 1.88. They reported that there is a systematic variation in the peak value of the reduced variance, σ^2 for Au, La and Kr. For Au and La, the peak values of γ_2 are reported to be greater than 2 and for Kr, the smallest of the three, the value is found to be less than 2. Such variation in the peak value of γ_2 was attributed to system size effect ruling out the possible phase transition in Kr to be a continuous one. It has been argued by EOS group that a change in the size of the fragmenting nuclei changes the Coulomb energy [25] of the system which in turn shifts the critical point. In contrast to percolation [36], Ising [37] or microcanonical Monte Carlo (MMMC) [38] model predictions, they reported a decrease in the critical temperature with the increase of system size. Such observation was explained in the light of statistical multifragmentation model (SMM) [39] and attributed to the dominant role played by the Coulomb energy over surface energy in the multifragmentation mechanism. In other studies, it was found that finite size effect and Coulomb force lead to a considerable reduction in the critical temperature [17,19,28] and the critical temperature decreases with the decrease of system size. Thus there exists clear contradictions, both in theory and observation, about the roles played by charge and finite size of the nuclei in nuclear multifragmentation processes and till date it is not very clear which of these two effects plays the more dominant role in MF mechanism.

In chapter IV, to realize the signature of phase transition, the data of this work on Mg-Em interaction at 4.5 AGeV has been analyzed using scaled factorial moment technique and a clear evidence of non thermal liquid gas phase transition is observed for the charge distribution of the projectile fragments. In this chapter an attempt has been made, by using cluster approximation technique, to examine the influence of system size on the critical behavior of nuclear matter in the fragmentation of Mg nuclei at 4.5 AGeV.

5.2 Mathematical formalism

The distance ε of a given event from the critical point is generally measured by taking a difference between the total charged fragment multiplicity, m and the multiplicity at the critical point, m_c. Thus:

$$\varepsilon = | m_c - m | \qquad (5.1)$$

The total charged fragment multiplicity m as defined in ref. [8-10, 17], is:

$$m = N_f + N_\alpha + N_{prot} \qquad (5.2)$$

where N_f, N_α and N_{prot} denote the number of heavy PFs with charge $Z_{PF} \geq 3$, alpha particles with $Z_{PF} = 2$ and the number of emitted protons with $Z_{PF} = 1$ respectively. Here N_{prot} is determined by using charge balance of the PFs, m is a parameter which is considered to be linearly related with the temperature T of the system.

Thus, $\varepsilon = m_c - m$ gives a measure of the distance of a given event from the critical point [16, 41-43].

5.3 Charge moments and Conditional moments

In order to extract relevant information from experimental data we need exclusive experiments in which the sizes (generally the charges) of almost all fragments are measured event by event. The method of single event moments is used here, following campi.

For a single event, Campi [8-10] has defined the k^{th} moment of charge distribution as:

$$M_k(\varepsilon) = \sum n_{Z_{PF}}(\varepsilon) Z_{PF}^k \tag{5.3}$$

and for a collection of data, $<M_k(\varepsilon)>$ in the small bins of multiplicity m as:

$$< M_k(\varepsilon) >= \frac{1}{N}\sum M_k^{(i)}(\varepsilon) = \frac{1}{N}\sum_i \left(\sum_{Z_{PF}} n^i_{Z_{PF}}(\varepsilon) Z_{PF}^k \right) \tag{5.4}$$

Here $n_{Z_{PF}}$ is the normalized charge distribution and is defined as $n_{Z_{PF}} = N_{Z_{PF}} / Q_{PF}$, Q_{PF} is the sum of charges of all the projectile spectator protons, fast alpha particles and heavy projectile fragments with charges $Z_{PF} \geq 3$. N denotes the total number of events in a given small range of ε, and $M_k^{(i)}$ is the k^{th} order charge distribution moment for i^{th} event.

These moments are related to the basic physical quantities. For example, $M_0^{(i)}$ is the number of fragments (minus one) present in the event i. $M_1^{(i)}$ is the mass (or charge) of these $M_0^{(i)}$ fragments,

$$M_1^{(i)} = Z_0 - Z_{max}(i) \tag{5.5}$$

and $M_1^{(i)} / M_0^{(i)}$ is the mean size of these fragments. Moments with $k < 0$ are mainly sensitive to the distribution of very light fragments.

The variance of the distribution is given by:

$$\sigma^{(i)^2} = \frac{M_2^{(i)}}{M_0^i} - \left(\frac{M_1^{(i)}}{M_0^{(i)}}\right)^2 \tag{5.6}$$

Which is related to a quantity γ_2 defined as:

$$\gamma_2^{(i)} = \frac{\sigma^{(i)^2}}{< Z^{(i)} >^2} + 1 = \frac{M_2^{(i)} M_0^{(i)}}{M_1^{(i)2}} \tag{5.7}$$

This quantity is known as reduced variance.

5.4 Results and discussion

5.4.1 Frequency distribution of charged projectile fragments

Frequency distribution of various charged projectile fragments with $Z_{PF} \geq 1$ emitted from Mg-Em interactions is plotted in Fig. 1(a). Similar distribution fitted with a power law has also been reported in projectile fragmentation of ^{238}U at 0.96 AGeV, ^{84}Kr at 1.25 AGeV, ^{131}Xe at 1.22 AGeV and ^{84}Kr at 0.95 AGeV in nuclear emulsion [17,20-23,40]. For the experimental data of the present investigation, considering total number of system constituents as 12, yields of the fragments charge distribution, lying between 1-6, have been re-plotted in log-log scale in Fig.1(b) and compared with the results of GU [17] works on Kr-Em interactions at 0.95 AGeV. A straight line fit using least square approach to the respective data points gives the values of the exponent τ, 2.54 ± 0.417 and 2.12 ± 0.15 respectively for Mg-Em and Kr-Em [17] interactions.

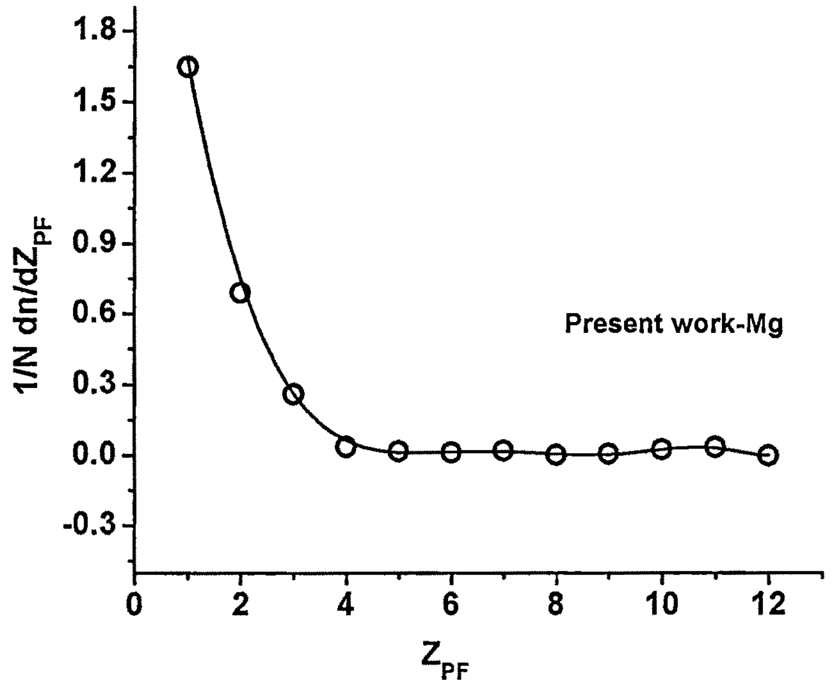

Fig. 5.1(a) Frequency distribution of various charged projectile fragments with $Z_{PF} \geq 1$ for Mg- Em interactions at 4.5 AGeV.

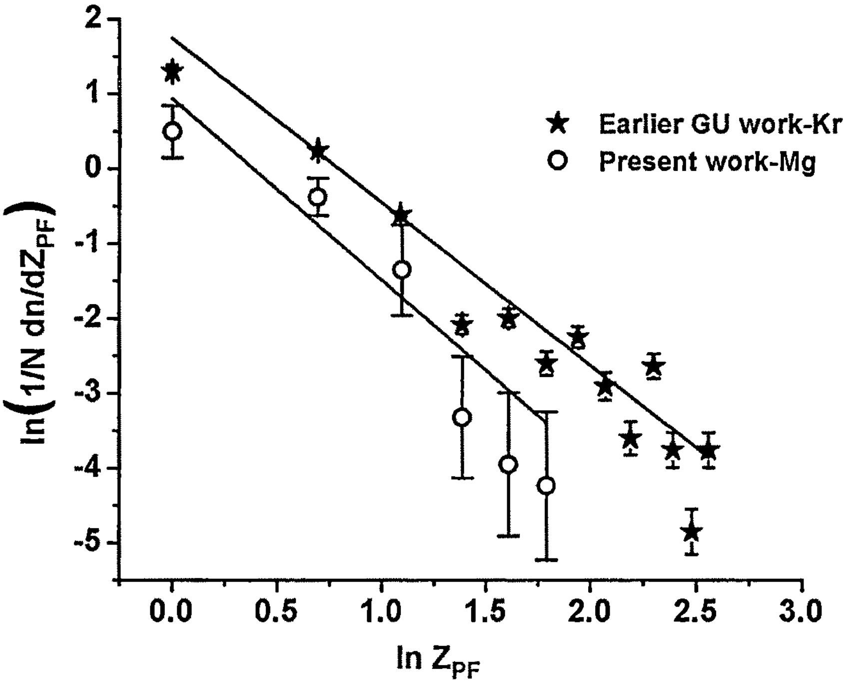

Fig. 5.1(b) Frequency distribution in log-log scale upto Z_{PF} = 1-6 for Mg and 1-13 for Kr-Em interactions.

5.4.2 Size effects on fluctuation in Z_{max}

It is known that a system exhibits significant fluctuations in the neighborhood of the critical point in a small range of the control parameter and appears at increasingly large scale as $\varepsilon - 0$. Elliott et al. [18] have pointed out that in the study of the critical behavior of the nuclear system using cluster approximation technique; the most readily observed fluctuations in the cluster distribution are those in the size of the largest cluster.

In Fig. 5.2, the standard deviations of Z_{max} normalized with respect to the charge of the projectile are shown as a function of multiplicity for both Mg and Kr-Em interactions. While for Kr large fluctuations in the multiplicity range between 11-19 are readily seen from this plot with a peak at m = 17 ± 1, for Mg, such fluctuation is observed in the range of 4-9 with a peak at m = 5 ± 1. The distinct differences in the heights and positions of the two peaks as seen in Fig. 2 is believed to be due to different system size of the fragmenting nuclei [17-19,26,40].

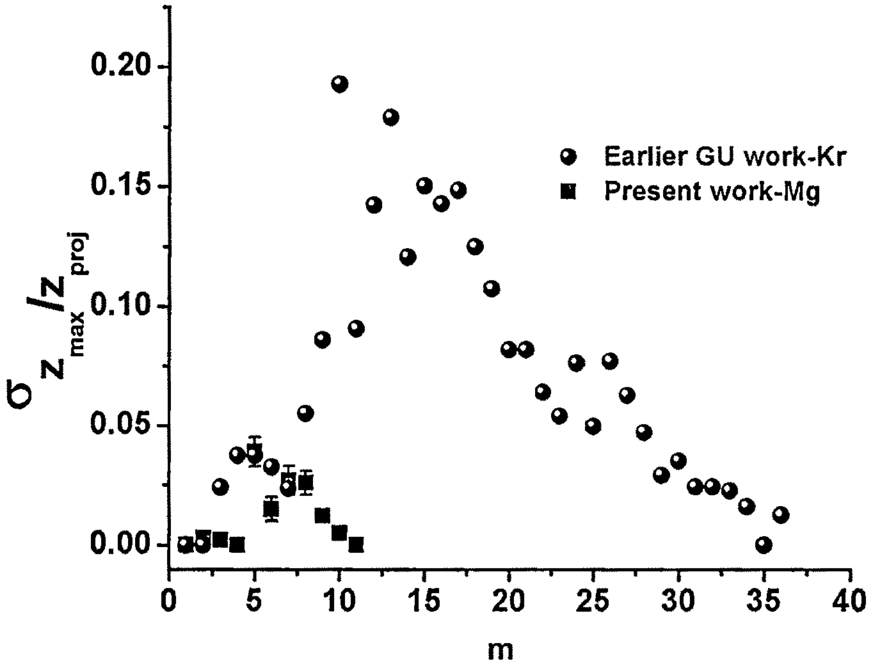

Fig. 5.2 Standard deviation of normalized Z_{max} as a function of multiplicity m for Mg-Em and Kr-Em interactions.

5.4.3 Fluctuation in γ_2

The γ_2 values have been calculated event by event as a function of total charge multiplicity for Mg and compared the results with the results of the earlier works on Kr-Em [17] and are presented in Fig. 5.3(a). The error estimations are made considering these to be independent statistical errors only. It can readily be seen from this plot that a considerable change in the height and position of γ_2 values take place as one goes from Kr to Mg projectile system. While the peak height is almost 5 times more in case of Kr than that of Mg, the position of the peak is 4.5 times less in Mg than that of the other one. In Fig. 5.3(b), the results of the present investigation have been compared with the result of EOS [26-27] works. It is interesting to see that both the height and position of the peak values of γ_2 vary systematically as one varies the system size from Au down to Mg via La and Kr. In the table 5.1, the values of these quantities have been listed for different systems as obtained by earlier workers of GU group [17] and EOS collaboration independently.

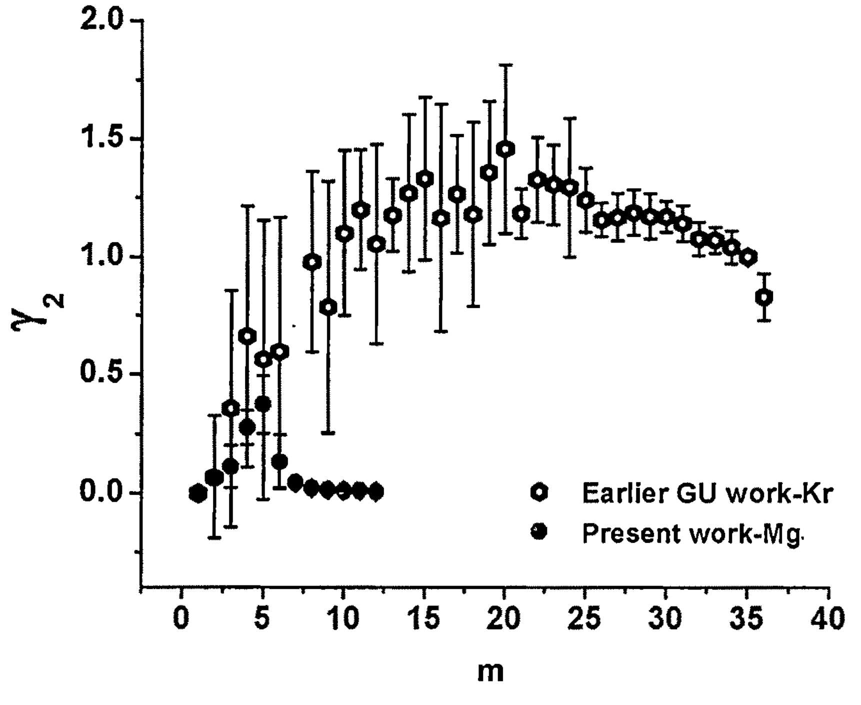

Fig. 5.3(a) Variation of γ_2 with total charged fragment multiplicity m for Mg-Em and Kr-Em interactions.

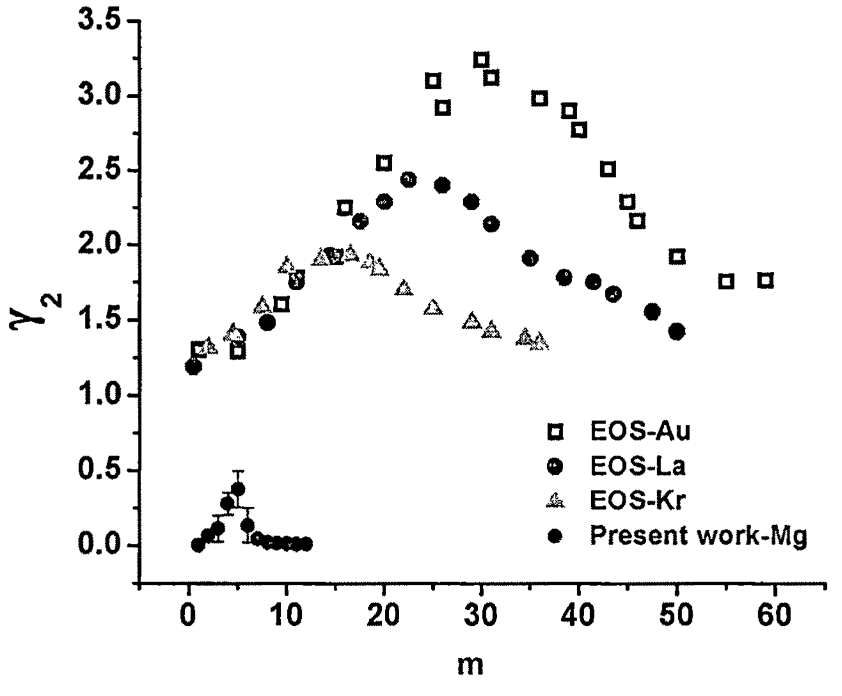

Fig. 5.3(b) Variation of γ_2 with total charged fragment multiplicity m for Mg-Em and Au, La and Kr on C.

To cross check the size effect, the variation of γ_2 is plotted against m / Z_{proj} in Fig. 5.3(c). From this plot it is readily evident that the transition is taking place almost at same normalized multiplicity (temperature) for various systems under consideration. Collapsing of transition temperature (multiplicity) to a particular value, when normalized by respective beam size (charge) rather confirms size effect only.

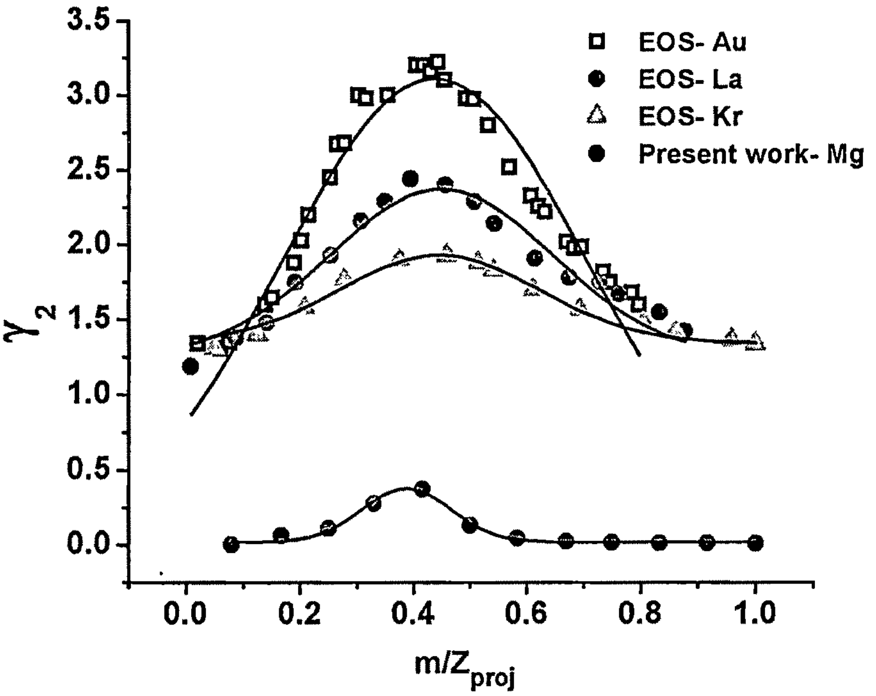

Fig. 5.3(c) Variation of γ_2 against m/ Zproj.

Table. 5.1 Variation of peak height and peak position in γ_2 with the system size.

Systems compared	Peak Height of γ_2	Peak Position of γ_2	Reference
Au-C at 1 AGeV	3.24	28 ± 3	EOS [26,27]
La-C at 1 AGeV	2.43	24 ± 3	EOS [26,27]
Kr-C at 1 AGeV	1.93	18 ± 2	EOS [26,27]
Kr-Em at 0.95 AGeV	1.5	18 ± 1	GU group [17]
Mg-Em at 4.5 AGeV	0.39	5 ± 1	Present work

Thus, unlike EOS findings of ref.[25] , the emulsion data of the present work for a smaller system like Mg confirms percolation, Ising and MMMC models prediction that the critical temperature should decrease with the decrease of size of the fragmenting nuclei [19,26-27] .

5.4.4 Fluctuation in M_2

Another traditional signature, often used in cluster approximation technique to realize critical behaviour, is the exhibition of a peaking behaviour in the mean value of second moment of charge distribution $< M_2>$ in a small bin of the control parameter. In the present investigation M_2 is calculated excluding the largest fragment which for the present work is considered to be 9. While excluding the largest fragment generally half of the size is considered. This is mainly because to exclude the contribution of fission fragments. Since in present case fission is not a possibility, it is therefore considered to be $Z_{PF} = 9$.

In Fig. 5.4(a), $< M_2 >$ for Mg-Em data is plotted against m and compared with the results of Kr-Em interactions [17]. Fig. 5.4(b) represents the same plot comparing present results on Mg-Em and earlier GU result on Kr-Em with EOS result on Au-C interactions. Clear evidence of size effect could be seen again with significant differences in the position and heights of the peaks.

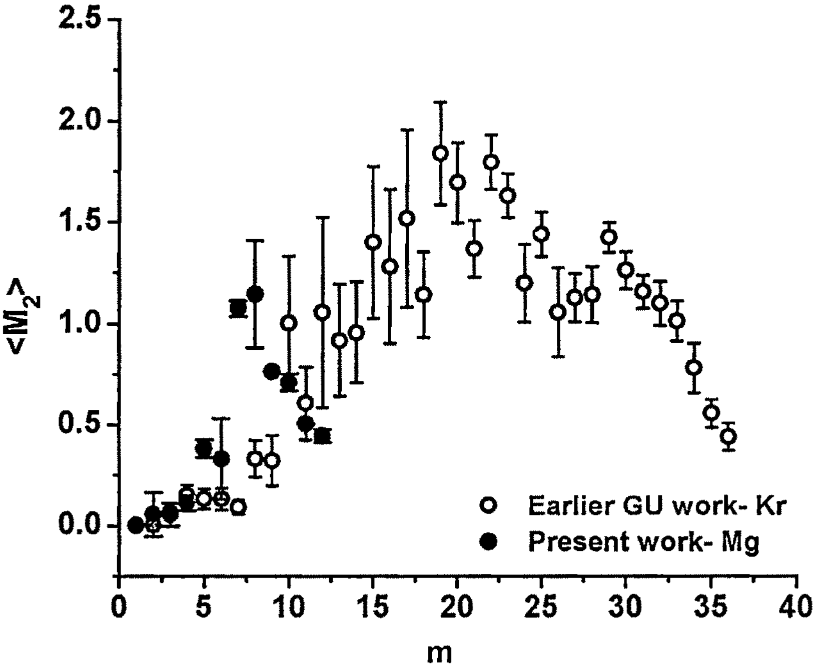

Fig. 5.4(a) Average of second charge moments as a function of multiplicity m for Mg-Em and Kr-Em interactions.

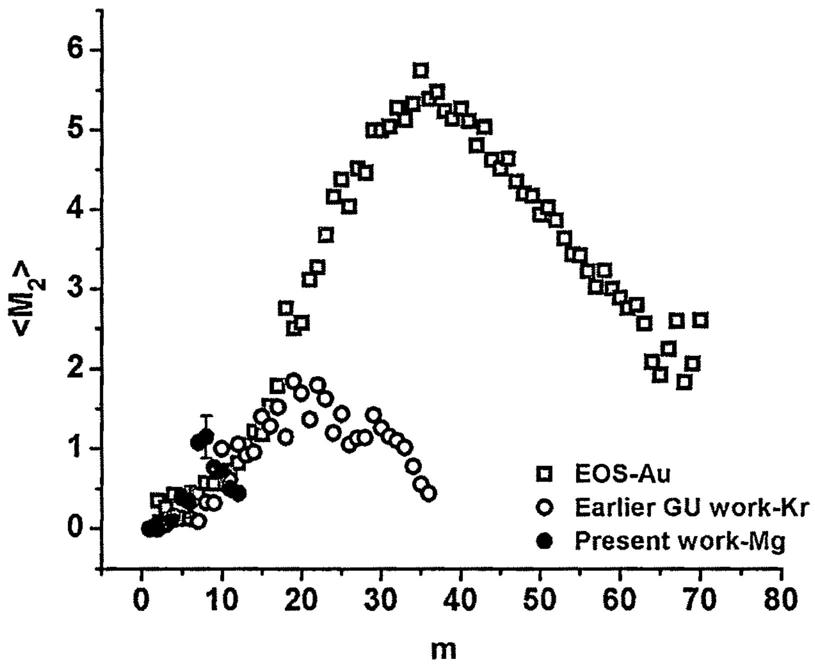

Fig. 5.4(b) Average of second charge moments as a function of multiplicity m for Mg-Em, Kr-Em and Au-C.

References

1. X. Campi and H. Krivine, *Nucl. Phys.* **A 545** (1992) 161.
2. R. T. de Souza et al., *Phys. Lett.* **B 268** (1991) 6.
3. D. R. Bowman et al., *Phys. Rev. Lett.* **67** (1991) 1527.
4. C.A. Ogilvie et al., *Phys. Rev. Lett.* **67** (1991) 1214.
5. M. E. Fisher, Physics N.Y. **3** (1967) 255, M. E. Fisher, *Rep. Prog. Phys.* **30** (1969) 615.
6. C. S. Kiang and D. Stauffer, *Z. Physik* **235** (1970) 130.
7. A. S. Hirsch et al., *Phys. Rev.* **C 29** (1984) 508.
8. X. Campi, *J. Phys.* **A 19** (1986) L917.
9. X. Campi, *Phys. Lett.* **B 208** (1988) 351.
10. W. Bauer et al., *Phys. Lett.* **B 150** (1985) 53.
11. W. Bauer et al., *Nucl. Phys.* **A 452** (1986) 699.
12. X. Campi, *Nucl. Phys.* **A 495** (1989) 259.
13. X. Campi and H.Krivine, *Z. Phys.* **A 344** (1992) 81.
14. X. Campi and H. Krivine, contribution to the International Workshop on Dynamical Features of Nuclei and Finite size Systems World Scientific, Singapore (1993).
15. J. Pochodzalla et al., *Phys. Rev. Lett.* **75** (1995) 1040.
16. D. Kudzia et al., *Phys. Rev.* **C 68** (2003) 054903-1.
17. B. Bhattacharjee and B. Debnath, *Nucl. Phys.* **A 829** (2009) 210.
18. J.B. Elliott et al., *Phys. Rev.* **C 62** (2000) 064603-1.
19. B. K. Srivastava et al., *Phys. Rev.* **C 65** (2002) 054617-1.
20. P. L. Jain et al., *Phys. Rev. Lett.* **68** (1992) 1656.
21. P. L. Jain and G. Singh, *Phys. Rev.* **C 46** (1992) R10-14.

22. P. L. Jain et al., *Phys. Rev. Lett.* **52** (1984) 2213.

23. G. Singh., *Mod. Phys. Lett.* **A 7** (1992) 1113.

24. D. Stauffer, *Phys. Rep.* **54** (1979) 11214.

25. S. Levit and P. Bonche, *Nucl. Phys.* **A 437** (1985) 426.

26. B. K. Srivastava (EOS Collaboration), *Pramana-J. Phys.* **57** (2001) 301.

27. B. K. Srivastava et al., *Phys. Rev.* **C 64** (2001) 041605(R)-1.

28. H. Jaqaman et al., *Phys. Rev.* **C 29** (1984) 2067 and ref. no.8 therein.

29. Y. Imry, *Phys. Rev.* **B 21** (1980) 2042.

30. P. Labastic and R. L. Whatten, *Phys. Rev. Lett.* **65** (1990) 1567.

31. D. H.Boal and J.N Glosli, *Phys. Rev.* **C 42** (1990) R502.

32. Wang Neng-ping et al., *J. Phys.* **G 20** (1994) 101.

33. G. T. Zheng, *Phys. Rev.* **C 50** (1994) 771.

34. L. Satpathy et al., *Phys. Rev.* **C 39** (1989) 162.

35. J. Bondorf et al., *Nucl. Phys.* **A 444** (1985) 460 .

36. D. H. E. Gross, *Rep. Prog. Phys.* **53** (1990) 605 .

37. J. M. Carmona et al., *Nucl.Phys.* **A 643** (1998) 115.

38. D. W. Heermann and D. Stauffer, *Z.Phys.B: Condens.Matter* **44** (1981) 339.

39. J. Bondorf et al., *Phys. Rep.* **257** (1995) 133.

40. F. Gulminelli and M.DAgostino, *Eur. Phys. J.* **A 30** (2006) 253.

41. W. Bauer and W.A. Friedman, *Phys. Rev. Lett.* **75** (1995) 767.

42. W. Bauer and A. Botvina, *Phys. Rev.* **C 52** (1995) R1760.

43. J. A. Hauger et al., *Phys. Rev. Lett.* **77** (1995) 235.

CHAPTER VI

SUMMARY AND CONCLUDING REMARKS

Summary and Concluding Remarks

The prime objective of the present investigation was to study the fluctuation, both in spatial as well as charge distribution of projectile fragments to realize the signature of liquid-gas phase transition.

The nuclear multifragmentation phenomenon was predicted and studied since the early 80's. It is however only with the advent of powerful 4π detectors that real advances had been achieved only recently. Such arrays of detectors allow the detection of a large amount of fragments and light particles produced in nuclear collisions at intermediate and high energies. The Equation of State describing nuclear matter, similar to the Van der Waals equation for classical fluids, foresees the existence of a liquid-gas type phase transition; multifragmentation was long-assimilated to this transition. The dominant role played by surface and Coulomb energy on multifragmentation mechanism has extensively been studied in the recent past. In this work an attempt was made to show the system size dependences on multifragmentation data, due to the interplay of surface and Coulomb free energies of the fragmenting system.

The fragmentation of relativistic nuclei is a source of information about their structure. Both the participant and spectator are relevant for studying the nuclear collision dynamics. Since nuclear emulsion is a global 4π detector and has the best spatial resolution (about 0.1 m rad) among all the detectors currently in use in high energy physics, this technique has been found to be an important tool particularly to study those properties which are related to the spatial distribution of the emitted particles. Intermittency in the emission spectra of high energy A+A collision is one such property. Until now, no result has so far been reported on the studies of fluctuation in the spatial distribution of PFs due to the difficulties of the measurement of PF angle. In the present investigation an attempt was made to study the fluctuations in the emission spectra of projectile fragments in terms of Scaled Factorial Moments (SFM) and generalized moments. Multiplicity characteristics of various charged projectile fragments has also been studied for the present multifragmentation data of 4.5 AGeV ^{24}Mg-Em interaction.

From this experimental work the mean multiplicity of all the projectile fragments for the entire data sample of present investigation on ^{24}Mg-Em interactions at 4.5 AGeV is found to be 2.76 ± 0.37. The mean multiplicities of projectile fragments with $Z_{PF} = 1$, $Z_{PF} = 2$ and $Z_{PF} \geq 3$ are found to be 1.57 ± 0.1, 0.89 ± 0.09 and 0.47 ± 0.11 respectively. The normalized multiplicity distribution of projectile fragments reveals that the number of events with no $Z_{PF} = q$ where q=1, 2, 3…is more than the number of events with a particular $Z_{PF.}$ Such observations are found to consistent with the results reported by other workers for lighter projectile like ^{28}Si, but inconsistent with the results reported for heavier system like ^{197}Au and ^{238}U.

The projectile mass is found to have strong influence on the mean multiplicities of various charged secondaries emitted from high energy A+A collisions. However, a more strong correlation could be observed for smaller systems.

The average number of produced particles, fast protons and evaporated particles as well as the heavily ionizing fragments are found to decrease exponentially with Q_{pf}, that is, as one goes from central to peripheral collisions.

Correlation between average number of IMFs and the mass of the fragmenting system is one of the most interesting aspects of studying projectile fragmentation. For a given colliding system, the magnitude of Z_b is independent of the beam energy and is also taken as a measure of the degree of centrality of the collision. It is found that the production of heavy and intermediate mass fragments is a function of the size of the fragmenting system., Light, intermediate and heavy charge projectile fragments such as Z_{PF} =1 & 2 and ≥3 show strong dependence on mass number of projectiles of similar energies. A systematic decrease in the system size has also been observed for the present multifragmentation data when compared with the results of other workers.

The horizontally averaged scaled factorial moment (SFM) analysis for spatial distribution of projectile fragments exhibits a power law behaviour with decreasing phase space bin size of the type $\langle F_q \rangle \propto M^{\phi_q}$, where M is the number of bins in which a given pseudorapidity interval is divided. This thereby indicates an intermittent pattern in the emission of projectile fragments. Similar investigation of SFM on the size of the projectile fragments reveals a power law growth of $< F_q >$ on bin width δs, of PF charge(mass).

The different values of the exponents ϕ_q, called intermittency indices, representing the strength of the intermittency signal, are found to increase with the order of moments for both the spatial and charge distributions of projectile fragments.

The anomalous dimension $d_q = \phi_q /(q-1)$ is found to increase linearly with the order of the moments 'q' for both the analyses, thereby indicating the multifractal structure for single particle density spectrum.

To study the fractal behaviour of the multiplicity fluctuation, ^{24}Mg - Em interactions data are investigated using the multifractal moments, G_q as a function of phase space bin size M for the emission spectra of the projectile fragments. $<G_q>$ shows a power law dependence on the phase space bin size of the form $<G_q> \propto M^{-\tau_q}$, thereby indicating fractal nature of the emission spectra of projectile fragments. Similarly for the charge distribution of projectile fragments, the G_q moment have been found to follow a power law of the form $<G_q> \infty (\delta s)^{\tau_q}$

The fractal indices τ_q or the experimental data points and τ_q^{st} for the generated events are obtained from the slopes of the best fitted lines of the respective analyses. A clear deviation of τ_q^{dyn} from q-1 as obtained for the present experimental data points for single particle density and charge distribution clearly indicates that $<G_q>$ contains dynamical information.

The generalized dimension D_q characterizing the extent of disorderness of the fractal object have been estimated for different order of moments for the emission spectra as well as for the charge distribution of projectile fragments with $\chi(\eta)$ and Z_{PF} as phase space variable. The variation of D_q with $q = 2 - 4$ show that D_q decreases linearly with q in either cases. This is considered to be a signature of the association of multifractality in both the emission spectra of projectile fragments from ^{24}Mg - Em interactions at energy of 4.5 AGeV.

The intermittent behaviour in the final state of multiparticle production in relativistic nuclear collisions may be a projection of the occurrence of a non thermal phase transition. This aspect is investigated in terms of behaviour of $\lambda_q = (\phi_q + 1)/q$. In the present study, for the interactions of ^{24}Mg nuclei with emulsion, no distinct minimum has been observed for λ_q versus q plot for the spatial distribution of projectile fragments, whereas for the charge distribution of projectile fragments, a distinct minimum has been observed. The observed minimum may be an indication for the occurrence of a non-thermal phase transition in the charge distribution of projectile fragments for the collisions.

The occurrence of non- thermal phase transition in the charge distribution of projectile fragments indicated the relevance of further analysing the gathered data in the light of criticality and possible liquid to gas phase transition.

From the cluster approximation technique analysis of the data of present investigation, a clear rise and fall pattern could be observed in the size of the largest cluster and the second moment of charge distribution. Such rise and fall pattern of these observables have been traditionally accepted as the signature of critical behaviour in nuclear matter. A comparison of the results of this work with the results of earlier works of GU group on Kr-Em and EOS data on Kr, La and Au interactions with C reveal clear evidences of system size dependences on multifragmentation mechanism.

List of publication

A. List of Publication in Journal

1. "System size effect on the critical behaviour in nuclear multifragmentation", B. Bhattacharejee and **R. Talukdar,** ***Nuclear Physics A*** **Vol. 864** Issue 1 (2011) 167.

2. "Effect of system size on the traditional signatures of critical behavior in projectile multifragmentation", B.Bhattacharejee and **R. Talukdar,** ***Journal of Physics: Conference Series*** **312** (2011) 082014.

3. "Variation of multiplicities of the secondary charged particles on the geometry of collision", **R. Talukdar**, S. Sengupta, B.Debnath and B. Bhattacharjee, ***Indian J. of Physics*** **Vol. 84(6)** (2010) 757.

4. "Emission characteristics of intermediate mass fragments on the residual part of the projectile nucleus", B. Debnath, **R. Talukdar** and B. Bhattacharjee, ***Indian J. of Physics*** **Vol. 82** (2008) 633.

B. List of Publication in Proceedings of Conference/Symposium

1. "Evidences of system size effect on the traditionally accepted signatures of critical behavior in projectile multifragmentation", B. Bhattacharjee and **R. Talukdar, Proceedings of the DAE Symposium on Nuclear Physics,** held at BITS, Pilani, during 20-24 December, 2010.

2. "Multifractal analysis of fragments charge distribution in ^{24}Mg-Em interactions at 4.5 AGeV", **R. Talukdar** and B.Bhattacharjee, To be published in the **Proceedings of Seventeenth National Symposium on Solid State Nuclear Track Detectors and Their Applications (SSNTD-17),** held at the Department of Physics, Faculty of Science, The M. S. University of Baroda, Vadodara, during 17-19, October, 2011

3. "Strong intermittent behavior in the emission spectra of ^{24}Mg-Em interactions at 4.5A GeV", **R. Talukdar** and B. Bhattacharjee, To be published in the **Proceedings of Seventeenth National Symposium on Solid State Nuclear Track Detectors and Their Applications (SSNTD-17),** held at the Department of Physics, Faculty of Science, The M. S. University of Baroda, Vadodara, during 17-19, October, 2011.

4. "Variation of intermediate mass fragments with the mass of the fragmenting system", B. Bhattacharjee and **R. Talukdar, Proceedings of DAE Symposium on Nuclear Physics** held at the Department of Nuclear Physics, Andhra University, Visakhapatnam, A. P., India ,during December 26-30, 2011. Available online at www.sympnp.org/proceedings.

5. "Study of nonthermal phase transition in the emission spectra of projectile fragments", **R. Talukdar** and B. Bhattacharjee, **Proceedings of DAE Symposium on Nuclear Physics** held at the Department of Nuclear Physics, Andhra University, Visakhapatnam, A. P., India ,during December 26-30, 2011. Available online at www.sympnp.org/proceedings.

6. "Multifractality in the emission spectra of projectile fragments in ^{24}Mg-Em interactions at 4.5 AGeV" , **R. Talukdar** and B. Bhattacharjee, **Proceedings of DAE Symposium on Nuclear Physics** held at the Department of Nuclear Physics, Andhra University, Visakhapatnam, A. P., India ,during December 26-30, 2011. **Available online at www.sympnp.org/proceedings.**

School/Conference/Symposium attended

1. Vth National Conference of the Physics Academy of the North-East (PANE) held at Gauhati University, Guwahati, during 1-3rd March ,2007.
2. QGP winter school held at Jaipur during 1-3rd February, 2008.
3. 20th International Quark Matter Conference held at Jaipur during 4th -10th February, 2008.
4. SERC school on Computational Statistical Physics held at IIT, Guwahati during December 01- 21, 2008.
5. National Workshop on Simulation and Data Analysis techniques for High Energy Cosmic ray experiments, held at Gauhati University, Guwahati, during 23-25 March, 2009.
6. VIth National Conference of the Physics Academy of the North-East (PANE) held at Tripura University, during April 2-4, 2009.
7. 6th International Conference on Physics and Astrophysics of Quark Gluon Plasma (ICPAQGP 2010) held at National Institute of Oceanography, Dona Paulo, Goa, India, during 5-10 December, 2010.
8. XIX DAE-BRNS High Energy Physics Symposium held at LNM institute of Information technology, Jaipur, during13-18 December, 2010.

9. DAE Symposium on Nuclear Physics held at BITS, Pilani, during 20-24 December, 2010.

10. Seventeenth National Symposium On Solid State Nuclear Track Detectors and their Applications (SSNTD-17), held at the Department of Physics, Faculty of Science, M. S. University of Baroda, Vadodara, during 17-19, October, 2011.

ELSEVIER

Available online at www.sciencedirect.com

ScienceDirect

Nuclear Physics A 864 (2011) 167–175

NUCLEAR PHYSICS A

www.elsevier.com/locate/nuclphysa

System size effect on the critical behavior in nuclear multifragmentation

B. Bhattacharjee *, R. Talukdar

Department of Physics, Gauhati University, Guwahati-781014, India

Received 6 February 2011; received in revised form 2 June 2011; accepted 4 June 2011

Available online 7 June 2011

Abstract

Attempt has been made to examine the role of system size on the traditional signatures of critical behavior from a comparative study of Mg–Em at 4.5 A GeV and Kr–Em at 0.95 A GeV interactions. A number of relevant observables such as fluctuation in the sizes of the largest cluster, reduced variance and the mean value of second moment of charge distribution were estimated with the experimental data. From a comparison of our results with that of EOS collaboration for Au, La and Kr on carbon at 1 A GeV, a definite systematic variation in the heights and positions of the peaks could be observed with the change of fragmenting nuclei thereby confirming the effect of system size on MF mechanism.

Keywords: Nucleus–nucleus collision; Multi-fragmentation; Power law; Phase transition; Charge moment; Critical behavior

1. Introduction

Studies on intermediate energy A + A collision are of special significance from the point of view that such collisions are associated with abundant multifragment production [1]. The connection between the multifragmentation (MF) as decay mechanism of excited nuclei and a possible liquid–gas phase transition taking place in the nuclear matter has been a subject of hot debate during the last two decades or so [2–4]. From the presence of the power law in fragment mass distribution and from the observation of the values of the exponents of various charge

* Corresponding author. Tel.: +91 361 2670968; fax: +91 361 2700133.
E-mail address: bb_22@rediffmail.com (B. Bhattacharjee).

0375-9474/$ – see front matter
doi:10.1016/j.nuclphysa.2011.06.019

Effect of system size on the traditional signatures of critical behavior in projectile multifragmentation

B Bhattacharjee[1] and R Talukdar

Department of Physics, Gauhati University, Guwahati- 781014, India

E-mail: bb_22@rediffmail.com

Abstract. The effect of the system size on a number of traditionally accepted signatures of cluster approximation technique of critical behavior have been examined for projectile multifragmenting systems like Mg at 4.5 AGeV and Kr at 0.95 AGeV. The results obtained from analyzing our experimental data on the fluctuation of size of the largest fragments, reduced variance and the mean value of the second moments of charge distribution provide clear evidences of size effect in terms of the height and position of the peaks of the studied parameters.

1. Introduction

Nucleus-nucleus collisions at intermediate energies offer various possibilities to produce hot nuclei which may break up into smaller pieces having charges $Z_{pf} \geq 3$, resulting multifragmentation (MF). The measured fragment properties are expected to reveal information about a possible phase transition which was earlier theoretically predicted for nuclear matter [1-3]. The connection between MF as decay mechanism of excited nuclei and a possible liquid-gas phase transition taking place in nuclear matter was initially motivated by the strong resemblance between van-der-waals potential and nucleon-nucleon potential [4,5]. The presence of the power law in the mass yield distribution of the fragments along with the values of the exponents close to that of an ordinary fluid led Purdue [6] group to suggest that multifragmentation of nuclei might be analogous to a fluid undergoing a continuous phase transition from liquid to a gas.

Although a considerable amount of work in understanding the statistical aspects of multifragmentation have been carried out by several groups [7-19], the mechanism of nuclear multifragmentation is not yet completely understood. One of the most complicated questions related to the liquid-gas phase transition in nuclear matter which is yet to be answered is the order of the phase transition. EOS collaboration, from analyzing the results of interactions of 1 AGeV Au on C using cluster approximation technique, has suggested that, MF of Au can be understood as due to a continuous phase transition. Similar results have also been reported for 1 AGeV La on carbon [20-22].

A continuous phase transition in nuclear matter is generally characterized by the presence of some characteristic signatures. One of the most striking characteristics of the systems undergoing continuous phase transition that might have taken place in the final stage of fragmentation of heavy ion collisions is that certain experimentally observed quantities might undergo fluctuations that exist on all length scales in a small range of the control parameter. These observables

[1] Corresponding author.

Indian J. Phys. **84** (6), 757-761 (2010)

Variation of multiplicities of the secondary charged particles on the geometry of collision

R Talukdar, S Sengupta, B Debnath and B Bhattacharjee*

Department of Physics, Gauhati University, Guwahati- 781 014, Assam, India

E-mail: bb_22@rediffmail.com

Abstract · The total charge of the projectile spectator fragments, Q_{pf} is taken as a measure of the degree of centrality of collision thus defining the collision geometry. In this paper the mean multiplicities of the different charged secondaries emitted in the interaction of ^{24}Mg-Em at 4.5A GeV have been investigated as a function of the total charge Q_{pf} of the projectile spectator fragments. It has been observed that the average number of the produced particles, $\langle N^s \rangle$ and the heavily ionizing particles, $\langle N_h \rangle$ decreases exponentially with the increase of Q_{pf} showing strong correlation with the geometry of the collision. An attempt has also been made to compare these results with ^{84}Kr-Em interaction at 0.95A GeV.

Keywords: Nucleus-Nucleus collision, Collision geometry, multiplicity

PACS Nos.: 25.75.-q, 25.70.Pq, 13.85.Hd

1. Introduction

According to participant spectator model [1] the interacting system in high energy nucleus-nucleus collision can be divided into three parts: a target spectator, a participant and a projectile spectator. The overlapping part of the two colliding nuclei is called the participant, and the non-overlapping portion of target and projectile nuclei are respectively called the target and projectile spectators. The model predicts that violent nucleon-nucleon collision takes place in the participant region and weak excitations and cascade collision takes place in the spectator parts. The participants produce many mesons, nucleons, photons, lepton pairs etc., and the spectators break into many nucleons and nuclei. There are relations between the participants and the spectators.

Relativistic nucleus-nucleus collisions are the unique tool to produce and study dense nuclear matter in the laboratory [2-4]. From straightforward geometrical considerations,

*Corresponding Author

Indian J. Phys. 82 (5), 633-638 (2008)

Emission characteristics of intermediate mass fragments on the residual part of the projectile nucleus

B Debnath, R Talukdar and B Bhattacharjee*

Department of Physics, Gauhati University,
Guwahati-781 014, Assam, India

E-mail : bb_22@rediffmail.com

Abstract : In the study of projectile multifragmentation, a number of properties such as multiplicities, energy of fragments etc. of the emitted intermediate mass fragments (IMFs) are found to vary significantly with Z_b, where Z_b is a measure of the mass of the fragmenting system. In this work we report the variation of $<N_{IMF}>$ with Z_b for 950 MeV/A ^{84}Kr interactions with different targets of photonuclear emulsion. The maximum value of $<N_{IMF}>$ has been found to vary systematically with the target mass. Further, from this study it has been observed that $<Z_b>$ is linearly correlated with the number of emitted projectile protons (N_p) for the studied interactions.

Keywords : Nucleus-nucleus collision, multifragmentation, intermediate mass fragments.

PACS Nos. : 25.75.-q; 25.70.Pq ; 13.85.Hd

1. Introduction

In projectile multifragmentation process, a projectile spectator, on excitation, splits into several pieces of intermediate mass fragments (IMFs) which span the mass-range between alpha particle and fission fragments. It is believed that studies on the decay of such excited nuclear systems may provide information about the nuclear collision dynamics. The sum of all projectile fragments (PFs) with charge $Z = 2$, which is also known as bound charge Z_b, gives the measure of the mass of the fragmenting system [1]. Correlation between average number of IMFs and the mass of the fragmenting system is one of the most interesting aspects of studying projectile multifragmentation. For a given collision system, the magnitude of Z_b is independent of the beam energy and is also taken as a measure of the degree of centrality of the collision [2,3]. On the other hand, when the variation of $<N_{IMF}>$ is studied with Z_b for a given projectile, in reactions with the lighter targets, the maximum value of the mean multiplicities of IMFs depend on the bombarding

* Corresponding Author